

**ANALYSIS OF THE ELECTROMAGNETIC  
SCATTERING FROM FLAT PLATES BY USING  
DIFFERENT SINC-TYPE BASIS FUNCTIONS IN  
METHOD OF MOMENTS**

**A Thesis Submitted to  
the Graduate School of Engineering and Sciences of  
İzmir Institute of Technology  
in Partial Fulfillment of the Requirements for the Degree of**

**DOCTOR OF PHILOSOPHY**

**in Electronics and Communication Engineering**

**by  
Başak ÖZBAKIŞ**

**May 2012  
İZMİR**

We approve the thesis of **Başak ÖZBAKIŞ**

**Examining Committee Members:**

---

**Assoc. Prof. Dr. Alp KUŞTEPELİ**

Department of Electrical-Electronics Engineering,  
Izmir Institute of Technology

---

**Prof. Dr. Taner OĞUZER**

Department of Electrical-Electronics Engineering,  
Dokuz Eylül University

---

**Assist. Prof. Dr. Sevinç Aydınlık BECHTELER**

Department of Electrical-Electronics Engineering,  
Izmir Institute of Technology

---

**Prof. Dr. A. Arif ERGİN**

Department of Electronics Engineering,  
Gebze Institute of Technology

---

**Assoc. Prof. Dr. Thomas BECHTELER**

Department of Electrical-Electronics Engineering,  
Izmir University

**24 May 2012**

---

**Assoc. Prof. Dr. Alp KUŞTEPELİ**

Supervisor, Department of Electrical-Electronics  
Engineering, Izmir Institute of Technology

---

**Prof. Dr. F. Acar SAVACI**

Head of the Department of Electrical and  
Electronics Engineering

---

**Prof. Dr. R. Tuğrul SENER**

Dean of the Graduate School of  
Engineering and Sciences

## **ACKNOWLEDGEMENTS**

I would like to express my gratitude to my committee member Prof. Dr. Taner Oğuzer for his guidance and inspiration during the course of my Ph.D. I would also like to thank to my advisor, Assoc.Prof.Dr. Alp Kuştepe for his support and encouragement during my Ph.D. studies. Their patience and kindness are greatly appreciated. I have been fortunate to have both of them who are studying professionally. I consider it an honor working with them.

I also thank Prof. Dr. A. Arif Ergin for his useful suggestions and commenting on this thesis.

I also thank Assoc. Prof. Dr. Thomas Bechteler and Assist. Prof. Dr. Sevinç Aydınlık Bechteler for their reading and commenting on this thesis.

## **ABSTRACT**

### **ANALYSIS OF THE ELECTROMAGNETIC SCATTERING FROM FLAT PLATES BY USING DIFFERENT SINC-TYPE BASIS FUNCTIONS IN METHOD OF MOMENTS**

Electromagnetic scattering from three dimensional arbitrary flat surfaces illuminated by a plane wave is investigated by using sinc-type basis functions in the method of moments (MoM) in this study. Sinc-sinc based Galerkin MoM formulation is obtained and its fortran program is developed firstly. The number of integrals to be computed is decreased by using analytical properties of the sinc function in the formulation. Therefore, the CPU time for obtaining the coefficient matrix is decreased appreciably. The relative error during the generation of the main matrix elements is obtained between 0.058% and 0.095% for considerably large matrices. Rooftop based MoM formulation is developed and it is coded with a similar approach used in sinc based program. The accuracy and CPU time of the sinc based bistatic scattering results are compared with those of rooftop. The MoM formulation of the sinc-pulse (sinctop) basis functions with non-Galerkin case is developed to reduce the overflow problem at the edges. Induced surface currents and far-field results of the sinc-sinc and sinc-pulse based formulations are compared with those of the rooftop basis functions and with the ones obtained from SuperNEC. Both sinc-sinc and sinc-pulse based simulation results are in good agreement with the results of rooftop based and SuperNEC simulation results. The main purpose in this study is to obtain accurate bistatic scattering results by using different sinc-type basis functions in MoM procedure while filling the main matrix in less CPU time when compared with the well-known methods.



## ÖZET

### DÜZLEMSEL YAPILARDAN ELEKTROMANYETİK SAÇILIMIN MOMENTLER YÖNTEMİNDE FARKLI SINC TİPİ BAZ FONKSİYONLARI KULLANILARAK ANALİZİ

Bu çalışmada, düzlemsel dalga ile uyarılmış üç boyut rasgele düzlemsel yüzeylerden saçılan elektromanyetik alan momentler yönteminde (MoM) sinc tipinde baz fonksiyonları kullanılarak incelenmiştir. İlk önce sinc-sinc tabanlı Galerkin MoM formülasyonu elde edilmiş ve onun fortran programı geliştirilmiştir. Formülasyonda sinc fonksiyonunun analitik özellikleri kullanılarak integrallerin sayısı azaltılmıştır. Buna ek olarak katsayılar matrisinin hesaplanma süresi düşürülmüştür. Ana matris elemanlarının hesaplanmasında ortaya çıkan bağıl hata oldukça büyük matrisler için %0.058 ve % 0.095 arasındadır. Rooftop tabanlı MoM formülasyonu geliştirilmiş, sinc tabanlı programda kullanılabenzer yaklaşımla programlanmıştır. Sinc tabanlı bistatik saçılım sonuçlarının doğruluğu ve hızı rooftop ile karşılaştırılmıştır. Sinc-pulse (sinctop) baz fonksiyonlarının Galerkin olmayan MoM formülasyonu, kenarlardaki taşma problemini önlemek için geliştirilmiştir. Sinc-sinc ve sinc-pulse tabanlı formülasyonlardan elde edilen akım ve uzak alan sonuçları rooftop ve SuperNEC sonuçlarıyla karşılaştırılmıştır. Sinc-sinc ve sinc-pulse sonuçlarının her ikisi birden rooftop ve SuperNEC ile uyumlu sonuçlar vermiştir. Bu çalışmanın asıl amacı MoM prosedüründe sinc tipinde baz fonksiyonlarını kullanarak diğer bilinen yöntemlere göre ana matrisi daha hızlı doldurmak ve doğru saçılım sonuçları elde etmektir.

# TABLE OF CONTENTS

LIST OF TABLES.....	viii
LIST OF FIGURES.....	ix
CHAPTER 1. INTRODUCTION .....	1
1.1. Literature Review.....	1
1.2. Motivation of the Study.....	6
CHAPTER 2. MOM FORMULATION.....	7
2.1. Method of Moments (MoM).....	7
2.1.1. Basis Functions.....	10
2.1.1.1. Subdomain Functions.....	10
2.1.1.2. Entire Domain Functions.....	13
2.1.2. Linear Solvers.....	15
CHAPTER 3. RADAR CROSS SECTION (RCS).....	17
3.1. Radar Cross Section Computation of Flat Plate.....	17
CHAPTER 4. METHOD OF MOMENTS BY ROOFTOP BASIS FUNCTIONS.....	24
4.1. Rooftop Basis Function.....	24
CHAPTER 5. METHOD OF MOMENTS BY SINC-SINC BASIS FUNCTIONS.....	33
5.1. Sinc Function.....	33
5.2. Sinc-Sinc Basis Functions.....	35
CHAPTER 6. METHOD OF MOMENTS BY SINC-PULSE BASIS FUNCTIONS...	44
6.1. Overflow Problem.....	44
6.2. Sinc-Pulse Basis Functions.....	44
6.2.1. Sinc-Pulse Formulation with Galerkin Procedure.....	48

6.2.2. Sinc-Pulse Formulation with non Galerkin Procedure.....	61
CHAPTER 7. NUMERICAL RESULTS.....	73
7.1. Square Flat Plate.....	73
7.2. Error Analysis in the MoM Matrix Elements.....	86
7.3. Arbitrary Flat Plate Geometries.....	88
CHAPTER 8. CONCLUSION.....	96
REFERENCES.....	98
APPENDICES	
APPENDIX A. NUMERICAL DIFFERENTIATION.....	103
APPENDIX B. SINC FUNCTION.....	105
APPENDIX C. SUBROUTINES.....	106

# LIST OF TABLES

<b><u>Table</u></b>	<b><u>Page</u></b>
Table 4.1. Location of the basis functions.....	25
Table 4.2. Definitions of the functions and vectors.....	26
Table 7.1. CPU time comparisons of the MoM based formulations in seconds.....	85
Table 7.2. Matrix dimensions of the problems $((N + K) \times (N + K))$ .....	86
Table 7.3. Relative error in the computed matrix elements (%).....	87

# LIST OF FIGURES

<b><u>Figure</u></b>		<b><u>Page</u></b>
Figure 2.1.	Subdomain basis function and functional approximation, (a) subintervals and points, (b) Pulse basis, (c) Step approximation.....	11
Figure 2.2.	Subdomain basis function and functional approximation, (a) subintervals and points, (b) Triangular basis, (c) Piecewise linear approximation.....	12
Figure 2.3.	Subsectional basis function and approximated function. (a) Spline function, (b) approximated function.....	13
Figure 2.4.	Entire domain basis function for $n=1, 2, 3$ . (a) $\cos\left(\frac{(2n-1)\pi x}{l}\right)$ , $n=1, 2, 3$ . (b) sum of the functions, continuous linear approximation .....	14
Figure 3.1.	Field representation of the flat plate.....	19
Figure 3.2.	Far field radiation field for a geometry.....	20
Figure 4.1.	Rooftop basis functions.....	24
Figure 4.2.	Location of the rooftop basis functions within the rectangular cell Mesh $m_1\left(p(s)a, q(s)b - \frac{b}{2}\right)$ , $m_2\left(\bar{p}(s)a - \frac{a}{2}, \bar{q}(s)b\right)$ .....	25
Figure 5.1.	Subsectional sinc basis for $W_x = 500$ , $N = 5$ . (a) points and subintervals $n$ , (b) $\text{sinc}(2W_x x - n)$ for $n = 1$ , (c) approximated function.....	34
Figure 5.2.	3D plot of the sinc-sinc basis functions.....	36
Figure 5.3.	Location of the sinc-sinc basis functions within the rectangular cell mesh $m_1(p(s)t_x, q(s)t_y)$ , $m_2(\bar{p}(s)t_x, \bar{q}(s)t_y)$ .....	36
Figure 5.4.	Pseudocode of determining the coefficients $hx_{d,r}^{f,n}$ , $hy_{\bar{d},\bar{r}}^{\bar{f},\bar{n}}$ .....	40
Figure 5.5.	Obtaining the MoM matrix elements for the IE (5.24).....	42
Figure 5.6.	Obtaining the MoM matrix elements for the IE (5.25).....	43
Figure 5.7.	Pseudocode of obtaining current coefficients for vertical polarization .....	43
Figure 5.8.	Pseudocode of obtaining current coefficients for horizontal polarization .....	43

Figure 6.1.	Overflow of the sinc function on the interval $x \in (-3, 3)$ . (a) subintervals, (b) ycut overflow for $\text{sinc}(x + 2)$ , (c) xcut overflow.....	46
Figure 6.2.	3D plot of the sinc-pulse basis functions.....	47
Figure 6.3.	Location of the sinc-pulse basis functions within the rectangular cell mesh $m_1(p(s)t_x, q(s)t_y - t_y/2)$ and $m_2(\bar{p}(s)t_x - t_x/2, \bar{q}(s)t_y)$ .....	48
Figure 6.4.	Pseudocode of determining the coefficients $\tilde{h}_{d,r}^{f,n}$ .....	55
Figure 6.5.	Pseudocode of obtaining only the integrals for the third term.....	56
Figure 6.6.	Pseudocode of determining the coefficients $\tilde{h}_{\bar{d},\bar{r}}^{\bar{f},\bar{n}}$ .....	57
Figure 6.7.	Obtaining the MoM matrix elements for the Galerkin MoM obtained in (6.38).....	60
Figure 6.8.	Obtaining the MoM matrix elements for the Galerkin MoM obtained in (6.39).....	61
Figure 6.9.	Pseudocode of determining the coefficients $h_{d,r}^{f,n}$ .....	64
Figure 6.10.	Obtaining the MoM matrix elements for the IE's (6.72) and (6.73).....	72
Figure 7.1.	Flat plate illuminated with a plane wave.....	74
Figure 7.2.	x directed current densities at the vertical polarization for $1\lambda \times 1\lambda$ square flat plate with $\theta_i = 45^\circ$ , $\varphi_{in} = 0^\circ$ .....	75
Figure 7.3.	Compare of the current densities at $\theta_i = 45^\circ$ , $\varphi_{in} = 0^\circ$ . (a) ycut, (b) xcut.....	76
Figure 7.4.	X directed current densities at the vertical polarization for $2\lambda \times 2\lambda$ square flat plate with $\theta_i = 45^\circ$ , $\varphi_{in} = 0^\circ$ .....	77
Figure 7.5.	Compare of the current densities at $\theta_i = 45^\circ$ , $\varphi_{in} = 0^\circ$ for $2\lambda \times 2\lambda$ square flat plates. (a) ycut, (b) xcut.....	78
Figure 7.6.	Vertically polarized <b>y</b> directed current densities at $\theta_i = 45^\circ$ , $\varphi_{in} = 0^\circ$ for $2\lambda \times 2\lambda$ square flat plates. (a) rooftop, (b) sinc-sinc, (c)sinc-pulse.....	79
Figure 7.7.	Compare of the vertically polarized <b>y</b> directed current densities at $\theta_i = 45^\circ$ , $\varphi_{in} = 0^\circ$ for $2\lambda \times 2\lambda$ square flat plates. (a) ycut, (b) xcut.....	80
Figure 7.8.	The vertically polarized <b>x</b> directed current densities of square flat	

	plates at $\theta_i = 45^\circ$ , $\varphi_{in} = 0^\circ$ : $4\lambda \times 4\lambda$ , $5\lambda \times 5\lambda$ , $6\lambda \times 6\lambda$ .....	81
Figure 7.9.	Bistatic scattering solutions of the $4\lambda \times 4\lambda$ square flat plate ( $g_1$ ) at $\varphi_{in} = 60^\circ$ and $\theta_i = 45^\circ$ , $\varphi_s = 60^\circ$ while $\theta_s = 0^\circ : 360^\circ$ . (a) co-polarized (vertical-vertical), (b) cross-polarized case (vertical-horizontal).....	83
Figure 7.10.	Bistatic scattering solutions of the $4\lambda \times 4\lambda$ square flat plate ( $g_1$ ) at $\varphi_{in} = 60^\circ$ and $\theta_i = 45^\circ$ , $\varphi_s = 60^\circ$ while $\theta_s = 0^\circ : 360^\circ$ . (a) cross-polarized (horizontal-vertical), (b) co-polarized case (horizontal-horizontal).....	84
Figure 7.11.	Arbitrary flat plate geometries. (a) $g_2$ , (b) $g_3$ , (c) $g_4$ .....	88
Figure 7.12.	Bistatic scattering of the arbitrary geometry $g_2$ for $\varphi_{in} = 30^\circ$ and $\theta_i = 45^\circ$ , $\varphi_s = 30^\circ$ while $\theta_s = 0^\circ : 360^\circ$ . (a) co-polarized (vertical-vertical) results, (b) cross-polarized (vertical-horizontal) results.....	89
Figure 7.13.	Bistatic scattering of the arbitrary geometry $g_2$ for $\varphi_{in} = 30^\circ$ and $\theta_i = 45^\circ$ , $\varphi_s = 30^\circ$ while $\theta_s = 0^\circ : 360^\circ$ . (a) co-polarized (horizontal-horizontal) results, (b) cross-polarized (horizontal-vertical) results.....	90
Figure 7.14.	Compare of the RCS results for arbitrary geometry $g_3$ for $\varphi_{in} = 60^\circ$ , $\theta_i = 45^\circ$ while $\theta_s = 0^\circ : 360^\circ$ . (a) RCS VV co-polarized case $\varphi_s = 30^\circ$ , (b) RCS VH cross-polarized case $\varphi_s = 30^\circ$ .....	91
Figure 7.15.	Compare of the RCS results for arbitrary geometry $g_3$ for $\varphi_{in} = 60^\circ$ , $\theta_i = 45^\circ$ while $\theta_s = 0^\circ : 360^\circ$ . (a) RCS HH co-polarized case $\varphi_s = 30^\circ$ , (b) RCS HV cross-polarized case $\varphi_s = 30^\circ$ .....	92
Figure 7.16.	Compare of the RCS results for arbitrary geometry $g_3$ for $\varphi_{in} = 60^\circ$ , $\theta_i = 45^\circ$ while $\theta_s = 0^\circ : 360^\circ$ . (a) RCS VV co-polarized case $\varphi_s = 60^\circ$ , (b) RCS VH cross-polarized case $\varphi_s = 60^\circ$ .....	93
Figure 7.17.	Compare of the RCS results for arbitrary geometry $g_3$ for $\varphi_{in} = 60^\circ$ , $\theta_i = 45^\circ$ , $\theta_s = 0^\circ : 360^\circ$ . (a) RCS HH co-polarized case $\varphi_s = 60^\circ$ , (b) RCS HV cross-polarized case $\varphi_s = 60^\circ$ .....	94
Figure 7.18.	Bistatic scattering results of the arbitrary geometry $g_4$	

$\varphi_{in} = 0^\circ, \theta_i = 45^\circ, \theta_s = 0^\circ:360^\circ$  (a) co-polarized (vertical-vertical)  
at specular reflection direction  $\varphi_s = 0^\circ$ , (b) co-polarized (vertical-vertical)  
at nonspecular reflection direction  $\varphi_s = 30^\circ$  .....95



# CHAPTER 1

## INTRODUCTION

### 1.1. Literature Review

Near and far radiation fields of electromagnetic problems are investigated in [1] in detail. Electromagnetic scattering problem can be solved with the MoM technique by using different types of basis and testing functions [2-4]. In this technique, an integral equation (IE) is obtained to satisfy the boundary conditions on the scattering surface in terms of the induced surface current density. Then, the unknown current density is expanded approximately in MoM with different types of basis functions. Linear matrix system that includes impedance matrix mentioned in [5] is solved to obtain current density coefficients. The rooftop basis functions are used as a subdomain type basis in solving 3D scattering problems. In the main study [6], Rao, Wilton and Glisson (RWG) type basis functions are developed and used for obtaining unknown currents for arbitrary shaped surfaces. Also, the entire domain basis functions can be used for large antenna problems in order to reduce the number of the basis functions [7-8]. For example, Chebyshev type basis functions are used in MoM with Galerkin procedure to solve electromagnetic scattering problem by using parallelization technique [8]. Galerkin or non-Galerkin procedures can be applied in MoM. Spline functions are employed with different orders as basis and testing functions in [9]. Furthermore, a type of second-order accuracy is obtained in the backscattered far field results regardless of whether or not Galerkin's method is utilized.

Large electromagnetic scattering problems can be solved by using various iterative techniques with preconditioning techniques mentioned in the studies [10-21]. One of the iterative methods is BiCG (biconjugate gradient) method which requires to calculated within each iteration the multiplication between the transpose of the system matrix and a vector in addition to that between the system matrix and a vector [14]. Furthermore, the multiplication between the transpose of the system matrix and a vector is found to be more complicated than that between the system matrix and a vector. Therefore, the algorithm can stagnate and fail to produce the solution. Algorithm

termination is more complicated because the residuals produced at each step by the BiCG approach do not have a monotonically decreasing norm. TFQMR (Transpose free quasi-minimal residual) based on the quasi-minimal version of the CGS (Conjugate Gradient Squared) algorithm called TFQMR method [15-19] that smooths its convergence without involving  $A^T$  vector products. It is employed to avoid the complicated multiplication between the transpose of the system matrix and a vector. Iterative techniques with preconditioning, especially ILU (incomplete LU) preconditioning in the iterative algorithms are used in solving large complex valued dense linear systems in less CPU (computer processing unit) time [20-23]. ILU preconditioning can be used with the Multilevel Fast Multipole Algorithm (MLFMA) to solve large electromagnetic scattering problems efficiently for open and closed geometries as an alternative way. Different effective preconditioners again with MLFMA are used in solving large open and closed surfaces with efficient parallelization. Furthermore, iterative algorithm with a preconditioning can be used with parallelization in order to solve very large electromagnetic problems obtained by IE (integral equation) formulation for conducting surfaces in the study. Improved iterative algorithms are developed in the study [24] in order to solve large electromagnetic problems involving open surfaces with a fast convergence rate.

The usage of different types of basis functions for solving EM (electromagnetic scattering) scattering problems is important for decreasing the computation time. For example, wavelet functions are used as expansion and testing functions in MoM for the efficient solution of the electromagnetic scattering from the two dimensional conducting geometries [25]. The effectiveness of the wavelet functions in terms of the radiation and receiving characteristics are analyzed again in the study [25]. Wavelet functions are used as expansions in MoM in solving an electromagnetic coupling problem in [26]. Spatio-temporal wavelet functions are used in order to solve the transient analysis of wire antennas by compressing impedance matrix in implicit MoM [27].

Sinc functions are used with other functions as bases for approximations in numerical analysis in [28]. The approximate solution of the differential and integral equations, approximate evaluation of transforms and interpolation, and approximate evaluation of functions based on sinc functions are given in this study. All sinc based methods converge at an optimal rate if the singularities on the boundary are ignored. The theory of the inverse scattering problem are given in [29] for an inhomogeneous body in a homogeneous surrounded media by the use of data collected from multiple

detectors and multiple sources. Sinc functions are used as basis in MoM in this problem. The implementation and numerical evaluation of this theory is given in [30]. A test object is used to generate simulated scattering data. Simulated noise is added and this new data and the sum is used to solve the inverse scattering problem by using sinc basis in MoM to recover the original test object. Fast algorithm based on FFT convolution is developed in [31] to solve the inverse scattering problem in less CPU time than in [30]. The method is suggested for interpolating measurements from one detector geometry to a new perturbed detector geometry. An alternative algorithm is developed in [32] for the previous studies [29-31]. The improved algorithm reconstructs circular cylinders equally well when given exact scattered field data. These studies are important for the medical imaging, for example solving inverse scattering problems of the type encountered in ultrasonic computed tomography. In the literature, the sinc functions are also used to solve IE's, ordinary and partial differential equations that characterize the initial and boundary value problems [33]. The sinc functions are classified as the quasi-localized band-limited functions in the study [34]. They are easily implemented in the problems having singularities and a good accuracy is obtained by their usage. Therefore, sinc functions are effectively used in engineering and applied physics. For example in [35], the Hallen's integral equation and the corresponding one dimensional dipole antenna problem with feed is solved by the sinc-collocation method. The computational burden is reduced by the application of the sinc function in some linear algebraic equations in this study. Two dimensional scattering problem for rough surfaces is solved in [36] by applying the sinc-type Galerkin to a simple 2D problem as a sampling approach. The simulated results show good agreement with the well-known solutions, even it can be seen for a very low-level discretization.

Bistatic and monostatic scattering measurement results for the flat geometries are compared with the geometrical theory of diffraction solutions as a function of aspect angle in the studies [37-40]. Monostatic scattering calculations based on geometrical theory of diffraction is in good agreement with the measured results except at edge-on aspects for the flat rectangular plate [37]. Bistatic scattering for a frustum is calculated with the geometrical theory of diffraction again and the results obtained from that are compared with those of the measurement results in the study [38]. The GTD (geometrical theory of diffraction) is developed for the 3-7 wavelengths square plates illuminated with vertical polarization as a function of aspect angle and the solutions are compared with the MoM numerical results [39]. Both empirical and UTD formulas are

developed for circular disks and square plates and compared again with MoM in the study [40]. Accuracy of the formulas degrades while the ratio of height to width becomes much less than one. In the studies [37-38] the GTD solutions agree well with the experimental data away from grazing incidence. GTD and PO/PTD equivalent currents are used to predict the far field monostatic scattering from perfectly conducting, flat, rectangular plates in non principal plane in the study [41]. High frequency models are used in [42] for verification and to illustrate weaknesses that still exist in high frequency modeling technique for the RCS measurements of plate geometries.

In the two dimensional scattering problem given in [43-46], the sinc functions and some of their mathematical properties were applied to the multi strip grating scattering which have been obtained by the plane wave excitation. It is used to obtain the approximate surface current densities and the far field patterns of the finite strip grating. Then, these studies are extended to simulate the multilayered structures [47] and so the two dimensional micro-strip geometries are successfully solved. In these two studies mentioned above, it is considered that the expansion of the unknown current density with the sinc functions includes sampling it at the peak positions on the scattering surface. In the study [48], the scattering from flat plates are solved by using Shannon's sampling theorem in MoM with entire basis functions. Shannon's sampling is applied in spectral domain, but the number of the basis functions is not much less than the RWG functions used in MoM, because degrees of freedom do not incorporate edge singular behaviors [48].

MoM in conjunction with the asymptotic waveform evaluation (AWE) technique is applied to obtain the RCS of an arbitrarily shaped three-dimensional perfect electric conductor body over a frequency band in the study [49]. AWE results are compared with model based parameter estimation (MBPE). AWE is found to be superior in terms of CPU time to obtain the frequency response. However, the accuracy of AWE is not proved in this study. On the other side, AWE based on characteristic basis function method is investigated in [50-51] to analyze wideband electromagnetic scattering from multiple two dimensional PEC objects. CPU time is decreased with high accuracy compared with the conventional MoM.

In this study, three dimensional electromagnetic scattering problem will be solved for arbitrary flat geometries using sinc-based Galerkin and non-Galerkin procedures. Additionally, in this 3D version of the sinc-based formulation, the

mathematical properties of the sinc functions are again used in the ordinary MoM solution. By the usage of these properties, no integrals are evaluated numerically and approximate analytical expressions are used under certain relative error limit. Only a few integrals are numerically computed for the region close to the Green's function singularity. In MoM, the filling time of the main matrix is reduced appreciably but higher discretization is required, so the matrix size increases. This causes an increase in the CPU time of the solution of the matrix equation. Also, it can be said that the main matrix inversion is performed directly by LU decomposition method. Therefore, mainly we can say that the MoM matrix can be filled quickly and much of the time is spent in the numerical solution of the algebraic main matrix equation. TFQMR method is used in order to reduce the overall CPU time.

In the sinc-sinc based MoM procedure, the multiplication of the two sinc functions in x and y directions are chosen [53]. Also the discretization is performed as the pointwise manner and it is so much easier than the complex basis functions. Our geometries that are studied here are arbitrary flat plates with the 90° connections at the corners of the plate. The ordinary rooftop formulation and its numerical solution were also performed. This well-known solution is used in comparison with the sinc basis results. SuperNEC [54] is also included in the study and used for comparison. The simulation results based on sinc-sinc based formulation are compared with the RCS calculations in the studies [55,56]. They are in good agreement. However, in the sinc-based MoM formulation, some types of errors possibly cause incorrect results. Firstly, the overflow can occur near the edges close to the singularity region of surface current density. Therefore, new types of basis functions called sinc-pulse type are chosen [56]. Here the pulse function is chosen such that the surface current density brings the singularity parallel to the edges and the sinc functions are chosen as an approximation perpendicular to the edges. By this way, the surface current density is approximated better and overflow problem is reduced. On the other hand, the errors occurred by using finite difference derivative and the sinc function integral approximations are the other error possibilities. The finite difference derivative error can be reduced by decreasing the mesh size, but the error coming from the sinc function integrals are numerically determined as the maximum 0.0005 relative level.

In this study, the numerical results are obtained from sinc type basis functions and these results are compared with the ordinary rooftop MoM and SuperNEC ones. However, matrix is filled with the numerical evaluation of the functions in rooftop

based formulations differently than in [57]. It is shown that when the matrix inversion time of our codes is decreased by the iterative solver with preconditioning transpose free quasi minimal residual (TFQMR) method, then the overall code is obtained to a level comparable with SuperNEC.

All our codes are developed in Fortran [58] in a single desktop computer. Furthermore, in the numerical results section the accuracy of the program is verified by the comparison of the simulations. CPU time comparison is given for the matrix filling of different MoM based programs.

## **1.2. Motivation of the Study**

Sinc functions are used in the literature for the electromagnetic scattering, radiation and inverse problems. In this study, a different application of the sinc functions is performed in the numerical MoM solutions. Flat plate geometry is chosen as an example for electromagnetic scattering problem.

It is important to calculate accurately the power scattered in some other direction than back to the transmitter in order to detect an object. The main purpose in this study is to obtain accurate bistatic scattering results from arbitrary flat plates by using different sinc-type basis functions in MoM procedure with filling the main matrix in less CPU time when compared with the well-known methods and software in literature. Analytical and mathematical properties of the sinc functions will be used in order to obtain a compact formulation. Approximate functions will be used instead of integrals in MoM. Computer program will be developed in personal computer by using Fortran routines. It is shown that the overall CPU will be decreased by using iterative solvers in MoM when compared to SuperNEC and ordinary rooftop based formulation with direct solvers.

## CHAPTER 2

### MOM FORMULATION

The roots of the method of moments originate in the methods of Rayleigh, Ritz and Galerkin. This method involves discretization procedure such as finite element method, finite difference method which can be related with method of moments (MoM) [59- 61]. The discretization of a continuous equation by MoM involves the projection of the continuous linear operator onto finite-dimensional subspaces defined by the basis and testing functions. Almost any problem, analytical or numerical could be solved with method of moments such as deterministic and eigenvalue problems. Two and three dimensional electromagnetic field scattering and eigenvalue problems can be easily solved with this well-known method [2]. The main idea of this method is to reduce a functional equation to a matrix equation. The matrix equation is then solved by direct and iterative methods. The unknown current density is first expanded in terms of basis functions then tested by weighting functions in order to construct the main matrix elements in the linear system. By using the excitation vector the coefficient matrix is solved.

#### 2.1. Method of Moments (MoM)

The mathematical technique which reduces the functional equation to matrix equation is called the Method of Moments [3]. The inhomogeneous equation of the deterministic problem can be represented as

$$L(f(x)) = g(x) \quad (2.1)$$

where  $L$  is a linear operator,  $g$  is known,  $x \in (a, b)$  and  $f$  is to be determined. Let  $f$  be expanded in a series of linearly independent basis functions.

$$f(x) = \sum_{s=1}^N a_s B_s(x) + \underbrace{\gamma_N}_{\text{discretization error}} \quad (2.2)$$

where  $a_s \in \mathbb{C}$  and they are constants and  $B_s$  are called basis (expansion) functions. The solution of  $f$  in the equation (2.2) is obtained approximately, and  $B_s$  forms a complete set of functions. For approximate solutions, equation (2.2) is a finite summation and given

$$f(x) \cong \sum_{s=1}^N a_s B_s(x). \quad (2.3)$$

In this equation  $B_s$  represents entire domain or subdomain basis functions. From the linearity property of the  $L$  we can write

$$\sum_{s=1}^N a_s L(B_s(x)) = g(x). \quad (2.4)$$

After determining an inner product, a set of weighting functions, or testing functions are defined in the range of  $L$ . Both sides of the equation (2.4) is tested with testing function  $T_o(x)$ . The testing procedure is applied with an inner product given as

$$\langle T_o(x), g(x) \rangle = \int_a^b T_o^*(x) g(x) dx. \quad (2.5)$$

The inner product of the equation (2.5) must be taken with each testing functions  $T_o$  such that

$$\sum_{s=1}^N a_s \langle T_o(x), LB_s(x) \rangle = \langle T_o(x), g(x) \rangle \quad o = 1, 2, \dots, N. \quad (2.6)$$

The set of resulting equations can be written in matrix form such as

$$[l_{os}][a_s] = [g_o] \quad (2.7)$$

where  $[l_{os}]$  matrix is obtained with the same procedure given in [4]



$$\begin{aligned}
[l_{os}] &= \begin{bmatrix} \langle T_1, LB_1 \rangle & \langle T_1, LB_2 \rangle & \dots \\ \langle T_2, LB_1 \rangle & \langle T_2, LB_2 \rangle & \dots \end{bmatrix}_{o \times s} \\
[a_s] &= \begin{bmatrix} a_1 \\ a_2 \\ \cdot \\ \cdot \\ \cdot \end{bmatrix} & [g_o] &= \begin{bmatrix} \langle T_1, g \rangle \\ \langle T_2, g \rangle \\ \cdot \\ \cdot \\ \cdot \end{bmatrix} \\
[a_s] &= [l_{so}]^{-1} [g_o] \text{ if } [l_{os}] \text{ is nonsingular, } (\det(l_{os}) \neq 0).
\end{aligned} \tag{2.8}$$

The process given in (2.1)-(2.5) can be applied to a deterministic problem to produce approximate solution regardless of whether or not the basis and testing functions  $\{B_s\}$  and  $\{T_o\}$  form complete orthogonal sets. Generally, the basis and testing functions are often not orthogonal sets. If the  $\{T_o\}$  form an orthogonal set, the projection of the range space onto the testing function is orthogonal and a best approximated solution is obtained. Even if the basis function  $\{B_s\}$  is orthogonal, the projection of the domain space onto the basis functions is not guaranteed to be orthogonal. In any case, since  $N$  is necessarily finite for numerical calculations, the result obtained from (2.2) is always approximate.

Two different procedures can be applied in MoM. When the basis and testing functions are identical in the problem, it is called Galerkin. In the other procedure, basis and testing functions are not the same functions. This procedure is called non-Galerkin.

The choice of the basis and testing functions is the principle issue arising within a method of moments implementation [2]. The factors which affect the choice of  $B_s$  (basis) and  $T_o$  (testing) are:

- The accuracy of solution desired
- The ease of the evaluation of the matrix elements
- The size of the matrix that can be inverted
- Realization of a well-conditioned matrix [2].

The basis and testing functions should be linearly independent and able to accurately approximate  $B$  and  $LB$ , respectively.

### 2.1.1. Basis Functions

Basis functions should be chosen according to their ability to represent and resemble the unknown function. Two types of basis functions can be classified. The first one is the subdomain basis functions which are nonzero only over a part of the domain of the function. Secondly, entire domain basis functions exist over the entire domain of the unknown function. Entire domain basis function expansion is similar to the well-known Fourier series expansion method. Appropriate basis functions can be chosen in terms of the problem.

#### 2.1.1.1. Subdomain Functions

The subdomain approach involves subdivision of the geometry of the problem into  $N$  nonoverlapping segments [2]. The most common subdomain basis functions are piecewise constant and piecewise linear. They form complete sets.

Spline function, pulse function and triangular function are examples of the subsectional basis given below.  $N$  equispaced points on the interval  $-4 \leq x \leq 4$  are shown in Figure 2.1. In this figure, a subinterval is defined to be of width  $8/(N+1)$  centered on the  $x_n$  where  $x_n \in (-4, 4)$  and  $N=7$ . A function which exists over only one subinterval is the pulse function. The pulse basis and expanded function with pulse basis are given in Figure 2.1.

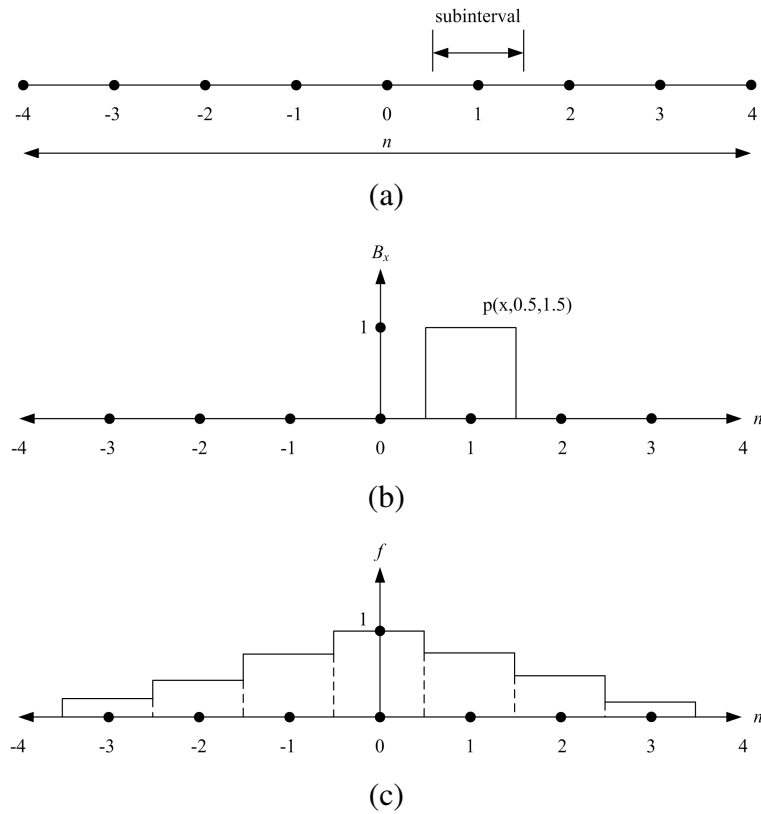


Figure 2.1. Subdomain basis function and functional approximation, (a) subintervals and points, (b) Pulse basis, (c) Step approximation.

Pulse function is given below

$$\text{pulse}(x, x_n - \frac{a}{2}, x_n + \frac{a}{2}) = \begin{cases} 1, & |x - x_n| < \frac{a}{2} \\ 0, & |x - x_n| > \frac{a}{2} \end{cases} \quad (2.7)$$

where  $a = l$  and it is the width of the subinterval centered at  $x_n$  in terms of the Figure 2.1.

Triangle basis function and its piecewise linear approximation are given in Figure 2.2.

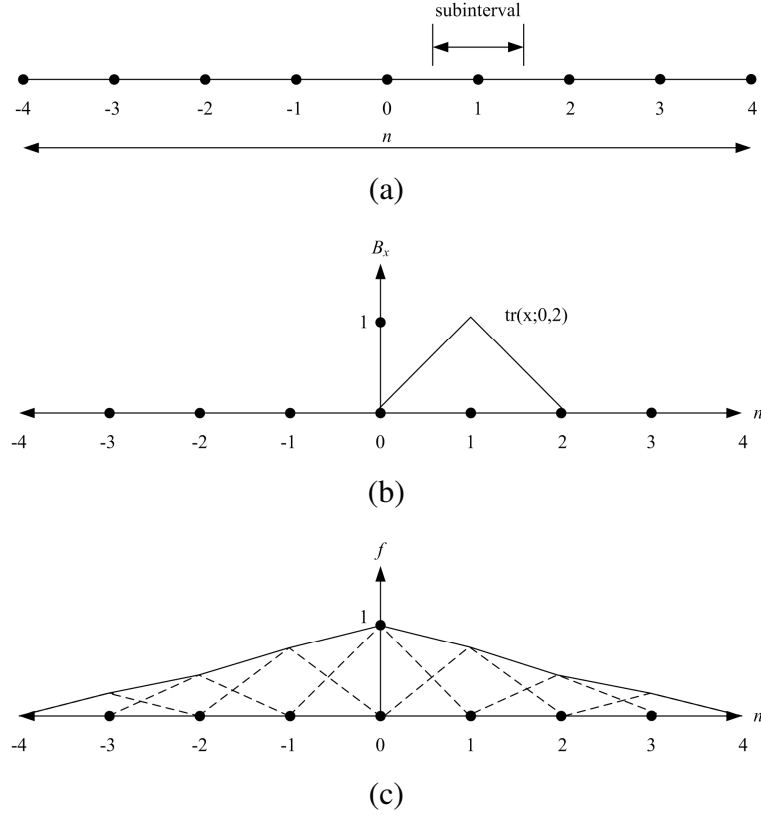


Figure 2.2. Subdomain basis function and functional approximation, (a) subintervals and points, (b) Triangular basis, (c) Piecewise linear approximation.

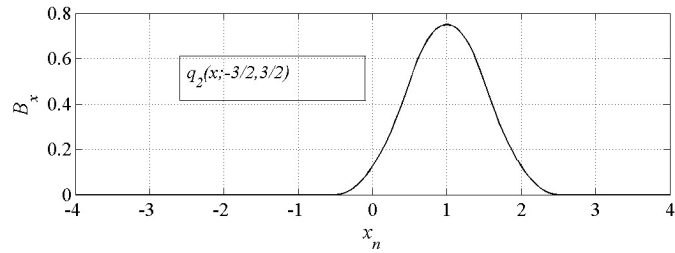
Triangle basis function is given as follows

$$tr(x; x_n - a, x_n + a) = \begin{cases} 1 - \frac{|x - x_n|}{a}, & |x - x_n| < a \\ 0 & , |x - x_n| > a \end{cases}. \quad (2.8)$$

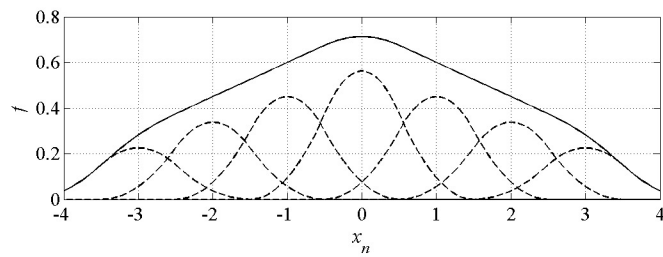
Another kind of subdomain basis functions are spline functions. The equation of the quadratic spline is given below

$$q_2\left(x; -\frac{3a}{2}, \frac{3a}{2}\right) = \begin{cases} 0, & x \leq -\frac{3a}{2} \\ \frac{9}{8}a + \frac{3xa}{2a} + \frac{x^2a}{2a^2}, & -\frac{3a}{2} < x \leq -\frac{a}{2} \\ \frac{3}{4}a - \frac{x^2a}{a^2}, & -\frac{a}{2} < x \leq \frac{a}{2} \\ \frac{9}{8}a - \frac{3xa}{2a} + \frac{x^2a}{2a^2}, & \frac{a}{2} < x \leq \frac{3a}{2} \\ 0, & x > \frac{3a}{2} \end{cases}. \quad (2.9)$$

The subsectional quadratic spline function is given in the Figure 2.3. The spline functions are again used in this study as subsectional basis functions.



(a)



(b)

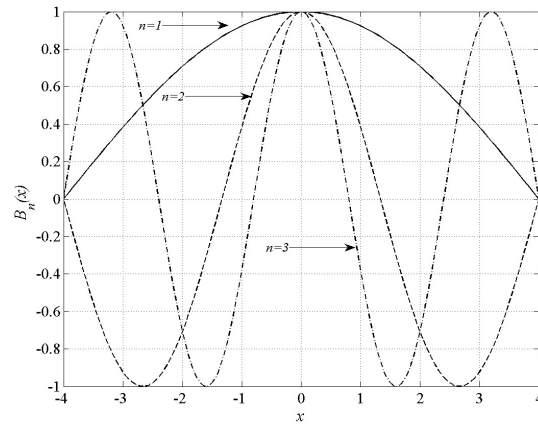
Figure 2.3. Subsectional basis function and approximated function. (a) Spline function, (b) approximated function.

### 2.1.1.2. Entire Domain Functions

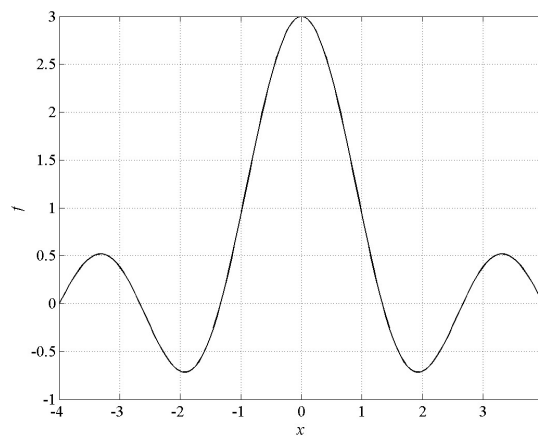
Entire domain basis functions are nonzero identically over the entire length of a chosen structure under investigation. No segmentation is involved in their use. The most common used entire domain basis set is the sinusoidal function, where

$$B_n(x) = \cos\left[\frac{(2n-1)\pi x}{l}\right] \quad \frac{-l}{2} \leq x \leq \frac{l}{2} \quad (2.10)$$

where  $l$  is the length of the structure. The basis functions for  $n = 1, 2, 3$  are given in Figure 2.4.



(a)



(b)

Figure 2.4. Entire domain basis function for  $n=1, 2, 3$ . (a)  $\cos\left(\frac{(2n-1)\pi x}{l}\right)$ ,  $n=1, 2, 3$ .

(b) sum of the functions, continuous linear approximation.

This basis function is useful to model the current on a wire dipole [3]. Entire domain cosine and sine functions are similar to the Fourier series expansion of arbitrary functions. Entire domain basis functions can be generated using Tschebyscheff, McLaurin, Legendre, and Hermite polynomials [2].

Wavelets are used in electromagnetic scattering problems as basis functions in the studies [25-27]. They represent the current density within integral equation formulations. Wavelets produce sparse matrices because of their oscillatory nature.

## 2.1.2. Linear Solvers

The inverse of the matrix  $[l_{os}]$  given in (2.7) can be evaluated by using different algorithms. One of the direct methods is LU factorization. In this study, LU factorization is used in solving linear matrix systems. This method divides the matrix into two parts which are lower triangular matrix and the upper triangular matrix. By using lower parts and upper parts of the matrix forward and backward substitutions are applied and the unknown coefficients are determined. An other similar algorithm is QR factorization. In QR factorization the system matrix can be solved by dividing the matrix into an orthogonal matrix and upper triangular matrix. Since QR decomposition involves almost twice as many operations as LU decomposition, it is not used for typical systems of linear equations.

Iterative solvers are applied in large electromagnetic scattering problems for solving linear matrix systems. The Conjugate Gradient and the Bi-Conjugate Gradient (BiCG) Algorithms are nonstationary iterative techniques [10-14] that are applied to general linear systems. Conjugate Gradient Method is an effective method for symmetric positive definite systems. The method proceeds by generating vector sequences of iterations and residuals in terms of iterations. At the end of each iteration the residual is compared with the desired error. If the convergence is satisfied, the algorithm stops and the result is obtained. The conjugate gradient method is not suitable for nonsymmetric systems. BiCGA does not minimize a residual [13-14]. BiCGA has significant features that make it an alternative to the standard CG algorithm [14]. Moreover, this algorithm cannot converge and it fails then breakdown situation (stagnation) occurs. QMR (quasi-minimal residual) method is used to overcome stagnation [15]. Quasi-minimal Residual method of Freund and Nachtigal solves the reduced tridiagonal system in a least squares sense [15]. The convergence behavior of QMR is typically much smoother than for BiCG. TFQMR is used in this study in order to reduce the overall CPU time. TFQMR is based on the quasi-minimal version of the CGS algorithm called TFQMR method [15-19] that smooths its convergence without involving  $A^T$  vector products. It is employed to avoid the complicated multiplication between the transpose of the system matrix and a vector.

Iterative solvers with a reasonable initial condition and a suitable preconditioning matrix are used in large electromagnetic scattering problems to make

the convergence of the solution as fast as possible [20-24]. Several integral equation solvers are given in the studies [20-24], which reduce computational complexity and memory requirements. Large electromagnetic scattering problems can be solved by using incomplete LU decomposition with threshold as a preconditioner in BiCG algorithm [20-24].



## CHAPTER 3

### RADAR CROSS SECTION (RCS)

Radar cross section (RCS) is defined as the area intercepting the amount of the power that, when scattered isotropically, produces at the receiver a density that is equal to the density scattered by the actual target [3]. RCS of a target is a function of the polarization of the incident wave, the angle of incidence, the angle of observation, the geometry of the target, the electrical properties of the target, and the frequency of operation. The units are taken per squared wavelength in decibels ( $10 \log \frac{RCS}{\lambda^2}$  [dB]) in calculations.

#### 3.1. Radar Cross Section Computation of Flat Plate

A radar detects or tracks a target, and sometimes can identify it, only because there is an echo signal. It is critical in the design and operation of radars to be able to quantify or otherwise describe the echo in terms of target's characteristics such as size, shape, and orientation. For that purpose a target is ascribed an effective area called the radar cross section.

An object exposed to an electromagnetic wave disperses incident energy in all directions. This spatial distribution of energy is called a scattering. The energy scattered back to the source of the wave constitutes the radar echo of the object. The intensity of the echo is described by the RCS of the object. The formal definition of radar cross section is [62]

$$\sigma = \lim_{R \rightarrow \infty} 4\pi R^2 \frac{|\mathbf{E}^s|^2}{|\mathbf{E}^{in}|^2} \quad (3.1)$$

where  $E_o$  is the electric field strength of the incident wave impinging on the target and  $E_s$  is the electric-field strength of the scattered wave at the radar. The derivation of the

expression assumes that a target extracts power from an incident wave and then radiates that power uniformly in all directions. RCS is therefore a comparison of scattered power density at the receiver with the incident power density at the target. When the electric field strengths in (3.1) are replaced with the magnetic field strengths, it is necessary to calculate the power scattered in some other direction then back to the transmitter. If the distance  $R$  is measured from the target to the receiver, backscattering is defined.

A larger RCS indicates that an object is more easily detected. An object reflects a limited amount of radar energy. RCS of a radar target is an effective area that intercepts the transmitted radar power and then scatters that power isotropically back to the radar receiver. The RCS of a target is the area required to intercept the transmitted power density at the target such that if the total intercepted power were re-radiated isotropically, the power density actually observed at the receiver is produced. This is explained by the monostatic (the transmitter and receiver are at the same location) scattering. When the location of the transmitter and receiver are different, then bistatic scattering is observed. RCS of a target is a very important parameter which gives its scattering properties.

RCS is calculated from the far field components of the electric field which are obtained from the transverse component of the magnetic vector potential

$$\mathbf{E}^s = -j\omega\mathbf{A}_T \quad (3.2)$$

In Figure 3.1, the scattered field is shown for a flat plate with  $L_x \times L_y$  dimension which is illuminated with a plane wave with the azimuth and elevation incident angles  $\varphi_{in}$  and  $\theta_{in}$  respectively.  $E_{\theta}^{in}$  (the incident electric field is perpendicular to the plane of incidence),  $E_{\varphi}^{in}$  (the incident electric field is parallel to the plane of incidence) are the incident electric field components. The  $x$  and  $y$  components of the incident electric fields  $E_x^{in}$  and  $E_y^{in}$  are obtained from  $E_{\theta}^{in}$

$$E_{\theta}^{in} = E_0 e^{jk(x \sin \theta_{in} \cos \varphi_{in} + y \sin \theta_{in} \sin \varphi_{in})} \quad (3.3)$$

$$E_x^{in} = E_0 \hat{\theta} \cdot \hat{x} = E_0 e^{jk(x \sin \theta_{in} \cos \varphi_{in} + y \sin \theta_{in} \sin \varphi_{in})} \cos \theta_{in} \cos \varphi_{in} \quad (3.4)$$

$$E_y^{in} = E_\theta \hat{\theta} \cdot \hat{y} = E_0 e^{jk(x \sin \theta_m \cos \varphi_m + y \sin \theta_m \sin \varphi_m)} \cos \theta_m \sin \varphi_m. \quad (3.5)$$

The incident electric field components,  $E_x^{in}$  and  $E_y^{in}$  are obtained from  $E_\varphi^{in}$

$$E_\varphi^{in} = E_0 e^{jk(x \sin \theta_m \cos \varphi_m + y \sin \theta_m \sin \varphi_m)} \quad (3.6)$$

$$E_x^{in} = E_\varphi \hat{\varphi} \cdot \hat{x} = E_0 e^{jk(x \sin \theta_m \cos \varphi_m + y \sin \theta_m \sin \varphi_m)} (-\sin \varphi_m) \quad (3.7)$$

$$E_y^{in} = E_\varphi \hat{\varphi} \cdot \hat{y} = E_0 e^{jk(x \sin \theta_m \cos \varphi_m + y \sin \theta_m \sin \varphi_m)} (\cos \varphi_m). \quad (3.8)$$

Time dependency,  $e^{j\omega t}$  is used in the above equations. The scattered electric fields is obtained by the vector sum of the vertical and horizontal components of the electric field at the elevation and azimuth scattering angles  $\theta_s$  and  $\varphi_s$  respectively.

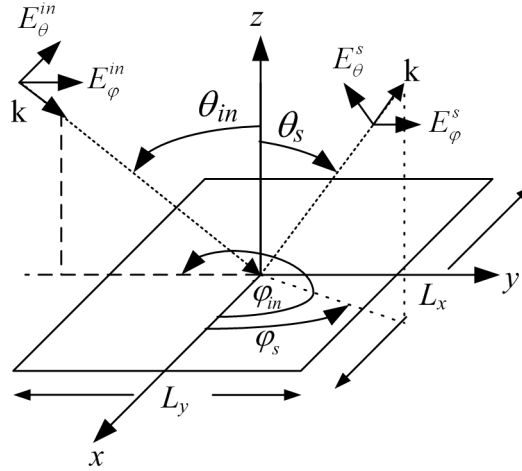


Figure 3.1. Field representation of the flat plate.

In the far zone, the scattered electric field can be obtained as follows

$$\mathbf{E}^s = \hat{\theta} E_\theta^s + \hat{\varphi} E_\varphi^s \quad (3.9)$$

where the vertical polarization case is calculated as

$$\begin{aligned}
E_{\theta}^s &= -j\omega A_{\theta} \quad A_{\theta} = (A_x \hat{x} \cdot \hat{\theta} + A_y \hat{y} \cdot \hat{\theta} + A_z \hat{z} \cdot \hat{\theta}) \\
E_{\theta}^s &= -j\omega (A_x \cos \theta_s \cos \varphi_s + A_y \cos \theta_s \sin \varphi_s - A_z \sin \theta_s), \quad (3.10)
\end{aligned}$$

and the horizontal polarization case is calculated as

$$\begin{aligned}
E_{\varphi}^s &= -j\omega A_{\varphi} \quad A_{\varphi} = (A_x \hat{x} \cdot \hat{\varphi} + A_y \hat{y} \cdot \hat{\varphi} + A_z \hat{z} \cdot \hat{\varphi}) \\
E_{\varphi}^s &= -j\omega (-A_x \sin \varphi_s + A_y \cos \varphi_s) \quad , \quad (3.11)
\end{aligned}$$

The  $x$  and  $y$  directed currents on the plate constitute only  $x$  and  $y$  directed magnetic vector potential, so  $A_z = 0$ . The magnetic vector potential is given as in [1-4]

$$\mathbf{A} = \frac{\mu}{4\pi} \iiint_V \mathbf{J}(\mathbf{r}') \frac{e^{-jk|\mathbf{r}-\mathbf{r}'|}}{|\mathbf{r}-\mathbf{r}'|} dv. \quad (3.12)$$

Far field radiation zone is represented in Figure 3.2. The distance between observation and source points is approximated in terms of the Figure 3.2 given below.

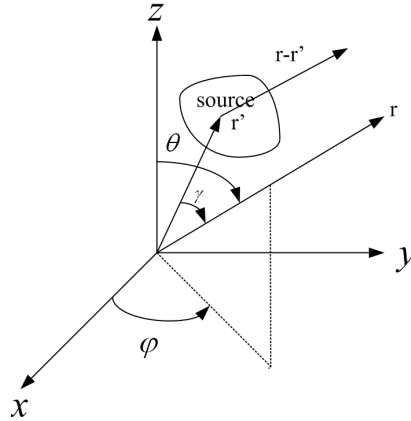


Figure 3.2. Far field radiation field for a geometry.

The approximated value of the  $|\mathbf{r}-\mathbf{r}'|$  can be obtained by using Taylor expansion method such that (at far field)

$$|\mathbf{r}-\mathbf{r}'| = \sqrt{(\mathbf{r}-\mathbf{r}') \cdot (\mathbf{r}-\mathbf{r}')} = \sqrt{r^2 - 2\mathbf{r} \cdot \mathbf{r}' + r'^2} \cong r - \vec{r}' \cdot \hat{r}, \quad r \gg r' \quad (3.13)$$

where  $2\mathbf{r}\cdot\mathbf{r}' = 2rr' \cos \rho$  and  $r - \mathbf{r}'\cdot\mathbf{r} = r - r' \cos \gamma$ .

On the surface of the plate there is  $x$  and  $y$  directed currents, so the resulting magnetic vector potential can be given as

$$\vec{A} = \frac{\mu}{4\pi} \frac{\exp(-jkr)}{r} \iint_S (J_x \hat{x} + J_y \hat{y}) \exp(jkr' \cos \gamma) ds' \quad (3.14)$$

and

$$\begin{aligned} \mathbf{r}'\cdot\mathbf{r} &= r' \cos \gamma = (x' \hat{x} + y' \hat{y}) \cdot (\hat{x} \sin \theta \cos \varphi + \hat{y} \sin \theta \sin \varphi + \hat{z} \cos \theta) \\ &= x' \sin \theta \cos \varphi + y' \sin \theta \sin \varphi \end{aligned} \quad (3.15)$$

The unknown current densities  $J_x$  and  $J_y$  can be expanded by known basis functions given in the equation (2.3) as explained in the previous chapter. The unknown current densities defined for flat plate geometries are given

$$J_x(x, y) \cong \sum_{s=1}^N a_s B_{x(s)}(x, y) \quad (3.16)$$

$$J_y(x, y) \cong \sum_{s=1}^K b_s B_{y(s)}(x, y) \quad (3.17)$$

Then, the  $x$  and  $y$  components of the magnetic vector potentials are calculated as

$$A_x = \frac{\mu}{4\pi} \frac{e^{-jkr}}{r} \sum_{s=1}^N a_s \int_{p(o)a-a}^{p(o)a+a} \int_{q(o)b-b}^{q(o)b} B_{x(s)} e^{jk(x' \sin \theta_m \cos \varphi_m + y' \sin \theta_m \sin \varphi_m)} dx' dy' \quad (3.18)$$

$$A_y = \frac{\mu}{4\pi} \frac{e^{-jkr}}{r} \sum_{s=1}^K b_s \int_{\bar{q}(o)b-b}^{\bar{q}(o)b+b} \int_{\bar{p}(o)a-a}^{\bar{p}(o)a} B_{y(s)} e^{jk(x' \sin \theta_m \cos \varphi_m + y' \sin \theta_m \sin \varphi_m)} dx' dy' \quad (3.19)$$

The scattered electric fields are derived and given as

$$E_{\theta}^s = \frac{-j\omega\mu}{4\pi} \frac{\exp(-jkr)}{r} \left( \sum_s a_s I_1 \right) \cos \theta_s \cos \varphi_s - \frac{j\omega\mu}{4\pi} \frac{\exp(-jkr)}{r} \left( \sum_s b_s I_2 \right) \cos \theta_s \sin \varphi_s \quad (3.20)$$

$$E_{\varphi}^s = \frac{j\omega\mu}{4\pi} \frac{\exp(-jkr)}{r} \left( \sum_s a_s I_1 \right) \sin \varphi_s - \frac{j\omega\mu}{4\pi} \frac{\exp(-jkr)}{r} \left( \sum_s b_s I_2 \right) \cos \varphi_s \quad (3.21)$$

where  $I_1$  and  $I_2$  are given as

$$I_1 = \int_{p(o)a-a}^{p(o)a+a} \int_{q(o)b-b}^{q(o)b} B_{x(s)} \exp( jkx' \sin \theta_{in} \cos \varphi_{in} + jky' \sin \theta_{in} \sin \varphi_{in} ) dx' dy' \quad (3.22)$$

$$I_2 = \int_{\bar{q}(o)b-b}^{\bar{q}(o)b+b} \int_{\bar{p}(o)a-a}^{\bar{p}(o)a} B_{y(s)} \exp( jkx' \sin \theta_{in} \cos \varphi_{in} + jky' \sin \theta_{in} \sin \varphi_{in} ) dx' dy' \quad (3.23)$$

and the radar cross section parameters for co-polarized vertical-vertical (VV), horizontal-horizontal (HH) and cross-polarized vertical-horizontal (VH), horizontal-vertical (HV) cases are obtained as follows

$$\text{RCS VV} = \lim_{R \rightarrow \infty} 4\pi R^2 \frac{|\mathbf{E}_{\theta}^s|^2}{|\mathbf{E}_{\theta}^{in}|^2} \quad (3.24)$$

$$\text{RCS VH} = \lim_{R \rightarrow \infty} 4\pi R^2 \frac{|\mathbf{E}_{\theta}^s|^2}{|\mathbf{E}_{\varphi}^{in}|^2} \quad (3.25)$$

$$\text{RCS HH} = \lim_{R \rightarrow \infty} 4\pi R^2 \frac{|\mathbf{E}_{\varphi}^s|^2}{|\mathbf{E}_{\varphi}^{in}|^2} \quad (3.26)$$

$$\text{RCS HV} = \lim_{R \rightarrow \infty} 4\pi R^2 \frac{|\mathbf{E}_{\varphi}^s|^2}{|\mathbf{E}_{\theta}^{in}|^2} \quad (3.27)$$

where  $R$  is the distance between object and target.

In the next chapter, rooftop basis functions are used in MoM formulation. The scattering results for arbitrary plate geometries are obtained with the rooftop based MoM formulation.

## CHAPTER 4

# METHOD OF MOMENTS BY ROOFTOP BASIS FUNCTIONS

Rooftop basis functions are used in MoM with Galerkin procedure in order to solve electromagnetic scattering problem. They are defined with subsectional pulse and triangular function. These functions are widely used for obtaining surface currents on planar scatterers and for expanding the surface current density on flat conducting plates. The coefficients of the rooftop functions represent the vector component normal to an edge and the expansion provides normal continuity.

### 4.1. Rooftop Basis Functions

Rooftop basis functions are constituted with the multiplication of standard triangle and pulse functions, which are given in [3]. Their three dimensional pictures are given in Figure 4.1.

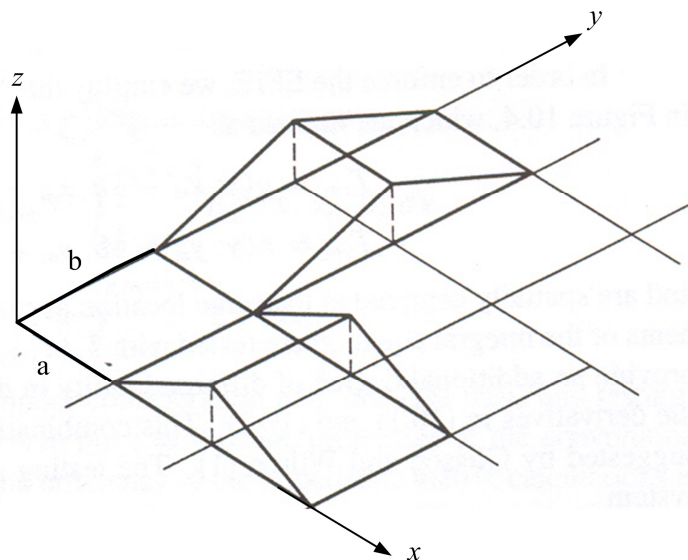


Figure 4.1. Rooftop basis functions.



The location of the rooftop basis functions within the rectangular-cell mesh is given in Figure 4.2. All cells in the model have the dimension  $a \times b$ , the rooftop functions are given

$$B_{x(s)}(x', y') = \text{tr}(x'; p(s)a - a, p(s)a, p(s)a + a) \text{pulse}(y'; q(s)b - b, q(s)b), \quad (4.1)$$

$$B_{y(s)}(x', y') = \text{tr}(y'; \bar{q}(s)b - b, \bar{q}(s)b, \bar{q}(s)b + b) \text{pulse}(x'; \bar{p}(s)a - a, \bar{p}(s)a). \quad (4.2)$$

The center points of the cells  $m_1$  and  $m_2$  are which correspond to  $B_x$  and  $B_y$  respectively given in the Figure 4.2.

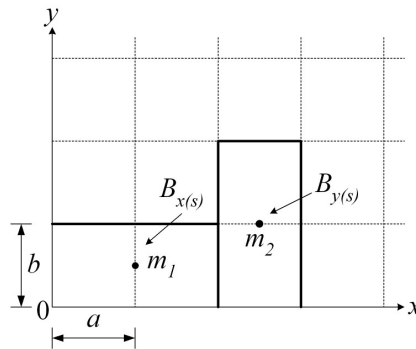


Figure 4.2. Location of the rooftop basis functions within the rectangular cell mesh

$$m_1 \left( p(s)a, q(s)b - \frac{b}{2} \right), m_2 \left( \bar{p}(s)a - \frac{a}{2}, \bar{q}(s)b \right).$$

Table 4.1. Location of the basis functions.

Symbols	Definitions
$s$	Indice belong to source points (integer).
$p(s)a$ (meter)	Location of the sinc function in $x$ direction for $B_x$
$q(s)b$ (meter)	Location of the pulse function in $y$ direction for $B_x$
$\bar{p}(s)a$ (meter)	Location of the pulse function in $y$ direction for $B_y$
$\bar{q}(s)b$ (meter)	Location of the sinc function in $x$ direction for $B_y$

The unknown current density is obtained by expanding rooftop functions with the basis functions given in (4.1) and (4.2) such as

$$J_x(x', y') \cong \sum_{s=1}^N a_s B_{x(s)}(x', y') \quad (4.3)$$

$$J_y(x', y') \cong \sum_{s=1}^K b_s B_{y(s)}(x', y'). \quad (4.4)$$

No basis functions are used at the edges along the structure boundary, since the currents at the boundary must vanish in the direction perpendicular to the edge.

The scattered field,  $E^s$  is given in frequency domain and obtained by the convolution terms as

$$\mathbf{E}^s = -j\omega\mathbf{A} - \nabla\Phi \quad (4.5)$$

where

$$\mathbf{A} = \mu \mathbf{J} * G \text{ and } \Phi = \frac{1}{\epsilon} \rho * G. \quad (4.6)$$

The convolution between current density and Green's function is defined as

$$\mathbf{J} * G = \int_{-\infty}^{\infty} \int_{-\infty}^{\infty} \mathbf{J}(x', y') G(x-x', y-y') dx' dy'. \quad (4.7)$$

Table 4.2. Definitions of the functions and vectors.

Symbols	Definitions
$\mathbf{A}$	Magnetic vector potential
$\Phi$	Scalar electric potential
$\mathbf{J}$ (A/m)	Surface current density
$\rho$ (C/m <sup>3</sup> )	Volume charge density
$G$	Green function
$\mu$ (H/m)	permeability
$\epsilon$ (F/m)	permittivity

The IE should satisfy the boundary condition on perfectly electric conductor (PEC) plate as follows

$$\left(\mathbf{E}^{in} + \mathbf{E}^s\right)_{tan} = 0 \quad (4.8)$$

and it can be obtained by using continuity equation

$$\nabla \cdot \mathbf{J} + j\omega\rho = 0. \quad (4.9)$$

By using equations (4.5)-(4.9) the integral equations including convolution terms are obtained as

$$-j\omega\mu[J_x * G] + \frac{1}{j\omega\epsilon} \frac{\partial}{\partial x} \left[ \frac{\partial J_x}{\partial x'} * G \right] + \frac{1}{j\omega\epsilon} \frac{\partial}{\partial x} \left[ \frac{\partial J_y}{\partial y'} * G \right] = -E_x^{in} \quad \text{on } S \text{ (surface)} \quad (4.10)$$

$$-j\omega\mu[J_y * G] + \frac{1}{j\omega\epsilon} \frac{\partial}{\partial y} \left[ \frac{\partial J_y}{\partial y'} * G \right] + \frac{1}{j\omega\epsilon} \frac{\partial}{\partial y} \left[ \frac{\partial J_x}{\partial x'} * G \right] = -E_y^{in} \quad \text{on } S \text{ (surface)}. \quad (4.11)$$

where

$$G(|\vec{r} - \vec{r}'|) = \frac{e^{-jkR}}{4\pi R}, \quad R = \sqrt{(x-x')^2 + (y-y')^2}. \quad (4.12)$$

and  $R = |\vec{r} - \vec{r}'|$  is the distance between observation and source points.

The  $x$  and  $y$  components of the integral equation are tested with  $T_x$  and  $T_y$  respectively, which are the same functions as the basis functions. This is required by the procedure used in this chapter because of the Galerkin procedure. The testing functions are given as

$$T_{x(o)}(x, y) = \text{tr} \left( x; p(o)a-a, p(o)a, p(o)a+a \right) \text{pulse} \left( y; q(o)b-b, q(o)b \right) \quad (4.13)$$

$$T_{y(o)}(x, y) = \text{tr} \left( y; \bar{q}(o)b-b, \bar{q}(o)b, \bar{q}(o)b+b \right) \text{pulse} \left( x; \bar{p}(o)a-a, \bar{p}(o)a \right) \quad (4.14)$$

where  $o$  as seen in (4.13)-(4.14) are observation points.

The testing process produces  $(N+K) \times (N+K)$  system such that

$$\begin{bmatrix} A_{NN} & B_{NK} \\ C_{KN} & D_{KK} \end{bmatrix} \begin{bmatrix} a_s \\ b_s \end{bmatrix} = \begin{bmatrix} E_N \\ F_K \end{bmatrix} \quad (4.15)$$

where

$$A_{NN} = -j\omega\mu \left\langle B_{x(s)}(x', y') * G, T_{x(o)} \right\rangle + \frac{1}{j\omega\epsilon} \left\langle \frac{\partial}{\partial x} \left( \frac{\partial B_{x(s)}(x', y')}{\partial x'} * G \right), T_{x(o)} \right\rangle \quad \begin{array}{l} o = 1, 2, \dots N. \\ s = 1, 2, \dots N. \end{array} \quad (4.16)$$

$$B_{NK} = \frac{1}{j\omega\epsilon} \left\langle \frac{\partial}{\partial x} \left( \frac{\partial B_{y(s)}(x', y')}{\partial y'} * G \right), T_{x(o)} \right\rangle \quad \begin{array}{l} o = 1, 2, \dots N. \\ s = 1, 2, \dots K. \end{array} \quad (4.17)$$

$$C_{KN} = \frac{1}{j\omega\epsilon} \left\langle \frac{\partial}{\partial y} \left( \frac{\partial B_{x(s)}(x', y')}{\partial x'} * G \right), T_{y(o)} \right\rangle \quad \begin{array}{l} o = 1, 2, \dots K. \\ s = 1, 2, \dots N. \end{array} \quad (4.18)$$

$$D_{KK} = -j\omega\mu \left\langle B_{y(s)}(x', y') * G, T_{y(o)} \right\rangle + \frac{1}{j\omega\epsilon} \left\langle \frac{\partial}{\partial y} \left( \frac{\partial B_{y(s)}(x', y')}{\partial y'} * G \right), T_{y(o)} \right\rangle \quad \begin{array}{l} o = 1, 2, \dots K. \\ s = 1, 2, \dots K. \end{array} \quad (4.19)$$

$o$  and  $s$  seen in (4.16)-(4.19) are the observation and source points respectively. Differentiation and convolution operators commute in order to obtain functions after convolutions and the above MoM matrix elements become

$$A_{NN} = -j\omega\mu \left\langle G, T_{x(o)}(x, y) * B_{x(s)}(-x, -y) \right\rangle + \frac{1}{j\omega\epsilon} \left\langle \left( G, \frac{\partial^2}{\partial x^2} (T_{x(o)}(x, y) * B_{x(s)}(-x, -y)) \right) \right\rangle, \quad \begin{array}{l} o = 1, 2, \dots N. \\ s = 1, 2, \dots N. \end{array} \quad (4.20)$$

$$B_{NK} = \frac{1}{j\omega\epsilon} \left\langle \left( G, \frac{\partial^2}{\partial x \partial y} (T_{x(o)}(x, y) * B_{y(s)}(-x, -y)) \right) \right\rangle, \quad \begin{array}{l} o = 1, 2, \dots N. \\ s = 1, 2, \dots K. \end{array} \quad (4.21)$$

$$C_{KN} = \frac{1}{j\omega\epsilon} \left\langle \left( G, \frac{\partial^2}{\partial y \partial x} (T_{y(o)}(x, y) * B_{x(s)}(-x', -y')) \right) \right\rangle, \quad \begin{array}{l} o = 1, 2, \dots K. \\ s = 1, 2, \dots N. \end{array} \quad (4.22)$$

$$D_{KK} = -j\omega\mu \left\langle G, T_{y(o)}(x, y) * B_{y(s)}(-x, -y) \right\rangle + \frac{1}{j\omega\epsilon} \left\langle \left( G, \frac{\partial^2}{\partial y^2} (T_{y(o)}(x, y) * B_{y(s)}(-x, -y)) \right) \right\rangle. \quad \begin{array}{l} o = 1, 2, \dots K. \\ s = 1, 2, \dots K. \end{array} \quad (4.23)$$

As an example, in (4.10), the first term of the integral equation is obtained

$$\int_{-\infty}^{\infty} \int_{-\infty}^{\infty} G(x, y) \left[ T_{x(o)}(x, y) * B_{x(s)}(-x, -y) \right] dx dy. \quad (4.24)$$

The basis functions include symmetric functions and the convolution terms can be given as follows

$$T_{x(o)}(x, y) * B_{x(s)}(-x, -y) = q_1(\bar{x}; -2a, 2a) tr(\bar{y}; -b, b) \quad (4.25)$$

$$T_{x(o)}(x, y) * B_{y(s)}(-x, -y) = q_2\left(\bar{x}; -\frac{3a}{2}, \frac{3a}{2}\right) q_2\left(\bar{y}; -\frac{3b}{2}, \frac{3b}{2}\right) \quad (4.26)$$

$$T_{y(o)}(x, y) * B_{y(s)}(-x, -y) = q_1(\bar{y}; -2a, 2a) tr(\bar{x}; -b, b) \quad (4.27)$$

$$T_{y(o)}(x, y) * B_{x(s)}(-x, -y) = q_2\left(\bar{y}; -\frac{3a}{2}, \frac{3a}{2}\right) q_2\left(\bar{x}; -\frac{3b}{2}, \frac{3b}{2}\right) \quad (4.28)$$

where  $\bar{x} = x - (p(o) - p(s))a$  and  $\bar{y} = y - (q(o) - q(s))b$ , for  $B_x$  and  $T_x$ ,

$\bar{x} = x - (\bar{p}(o) - \bar{p}(s))a$  and  $\bar{y} = y - (\bar{q}(o) - \bar{q}(s))b$ , for  $B_y$  and  $T_y$ ,

$\bar{x} = x - (p(o) - \bar{p}(s))a - \frac{a}{2}$  and  $\bar{y} = y - (q(o) - \bar{q}(s))b - \frac{b}{2}$ , for  $B_y$  and  $T_x$ ,

$\bar{x} = x - (\bar{p}(o) - p(s))a - \frac{a}{2}$  and  $\bar{y} = y - (\bar{q}(o) - q(s))b - \frac{b}{2}$ , for  $B_x$  and  $T_y$ .

The above functions  $q_1$ ,  $q_2$  and  $tr$  are piecewise continuous and are given as

$$q_1(x; -2a, 2a) = \begin{cases} 0, & x \leq -2a \\ \frac{x^3 + 6ax^2 + 12a^2x + 8a^3}{6a^2}, & -2a < x \leq -a \\ \frac{-3x^3 - 6x^2a + 4a^3}{6a^2}, & -a < x \leq 0 \\ \frac{3x^3 - 6x^2a + 4a^3}{6a^2}, & 0 < x \leq a \\ \frac{-x^3 + 6ax^2 - 12a^2x + 8a^3}{6a^2}, & a < x \leq 2a \\ 0, & x > 2a \end{cases}, \quad (4.29)$$

$$q_2\left(x; -\frac{3a}{2}, \frac{3a}{2}\right) = \begin{cases} 0, & x \leq -\frac{3a}{2} \\ \frac{9}{8}a + \frac{3xa}{2a} + \frac{x^2a}{2a^2}, & -\frac{3a}{2} < x \leq -\frac{a}{2} \\ \frac{3}{4}a - \frac{x^2a}{a^2}, & -\frac{a}{2} < x \leq \frac{a}{2} \\ \frac{9}{8}a - \frac{3xa}{2a} + \frac{x^2a}{2a^2}, & \frac{a}{2} < x \leq \frac{3a}{2} \\ 0, & x > \frac{3a}{2} \end{cases}, \quad (4.30)$$

$$tr(x; -a, a) = \begin{cases} 0, & x \leq -a \\ a+x, & -a < x \leq 0 \\ a-x, & 0 < x \leq a \\ 0, & x > a \end{cases}. \quad (4.31)$$

The functions (4.29)-(4.31) obtained from the convolution terms are differentiated partially in the IE. Then, these terms are integrated with the Green's function. The first term of the IE away from the singularity region is

$$\int_{-b+v}^{b+v} \int_{-2a+u}^{2a+u} G(x, y) q_1(x-u) tr(y-v) dx dy \quad (4.32)$$

where  $u = a(p(o) - p(s))$ ,  $v = b(q(o) - q(s))$ . When the source and the observation regions are overlapped, there is singularity in the integrand which has  $1/R$  form. For  $R = 0$ , the singular part of the integrand is extracted and the singular part is evaluated analytically as given in [3]. The remaining part is evaluated numerically. The resulting integral is

$$\int_{-b+v}^{b+v} \int_{-2a+u}^{2a+u} \left[ G(x, y) q_1(x-u) \operatorname{tr}(y-v) - \frac{q_1(-u) \operatorname{tr}(-v)}{4\pi R} \right] dx dy + q_1(-u) \operatorname{tr}(-v) \int_{-b+v}^{b+v} \int_{-2a+u}^{2a+u} \frac{dx dy}{4\pi \sqrt{x^2 + y^2}}. \quad (4.33)$$

The singular part of the integral is evaluated by applying coordinate transformation in [3] with the following steps

$$\begin{aligned} \int_{-b+v}^{b+v} \int_{-2a+u}^{2a+u} \frac{dx dy}{\sqrt{x^2 + y^2}} &= (x_1 + \alpha) \ln \left( \frac{y_1 + \beta + R_{22}}{y_1 - \beta + R_{21}} \right) + (x_1 - \alpha) \ln \left( \frac{y_1 - \beta + R_{11}}{y_1 + \beta + R_{12}} \right) \\ &+ (y_1 + \beta) \ln \left( \frac{x_1 + \alpha + R_{22}}{x_1 - \alpha + R_{21}} \right) + (y_1 - \beta) \ln \left( \frac{x_1 - \alpha + R_{11}}{x_1 + \alpha + R_{12}} \right) \end{aligned} \quad (4.34)$$

where

$$R_{22} = \sqrt{(x_1 + \alpha)^2 + (y_1 + \beta)^2} \quad (4.35)$$

$$R_{21} = \sqrt{(x_1 + \alpha)^2 + (y_1 - \beta)^2} \quad (4.36)$$

$$R_{11} = \sqrt{(x_1 - \alpha)^2 + (y_1 - \beta)^2} \quad (4.37)$$

$$R_{12} = \sqrt{(x_1 - \alpha)^2 + (y_1 + \beta)^2} \quad (4.38)$$

and

$$\begin{aligned} x_1 &= -(x_b + x_a)/2 \\ y_1 &= -(y_b + y_a)/2 \\ \alpha &= (x_b - x_a)/2 \\ \beta &= (y_b - y_a)/2 \end{aligned} \quad (4.39)$$

such that  $x_a = -2a + u$ ,  $x_b = 2a + u$ ,  $y_a = -b + v$  and  $y_b = b + v$ .

The second term of the IE away from the singularity region is given as

$$- \int_{-b+v}^{b+v} \int_{-2a+u}^{2a+u} G(x, y) n(x-u) tr(y-v) dx dy \quad (4.40)$$

where  $n = \frac{\partial^2}{\partial x^2} q_1(x-u, y-v)$ . In a similar way with the previous section, the integral equation for the singularity region is obtained as

$$- \int_{-b+v}^{b+v} \int_{-2a+u}^{2a+u} \left[ G(x, y) n(x-u) tr(y-v) - \frac{n(-u) tr(-v)}{4\pi R} \right] dx dy - n(-u) tr(-v) \int_{-b+v}^{b+v} \int_{-2a+u}^{2a+u} \frac{dx dy}{4\pi \sqrt{x^2 + y^2}} \quad (4.41)$$

The third term of IE in (4.10) can be obtained in a very similar way with the previous terms. The integral given below should be solved numerically away from the singular region

$$- \int_{-\frac{3b}{2}+v}^{\frac{3b}{2}+v} \int_{-\frac{3a}{2}+u}^{\frac{3a}{2}+u} G(x, y) m(x-u) m(y-v) dx dy \quad (4.42)$$

where  $m(x-u) = \frac{\partial}{\partial x} q_2(x-u)$  and  $m(y-v) = \frac{\partial}{\partial y} q_2(y-v)$ . This integral is modified for the singularity region that includes  $R = 0$ . It can be rewritten as

$$- \int_{-\frac{3}{2}b+v}^{\frac{3}{2}b+v} \int_{-\frac{3}{2}a+u}^{\frac{3}{2}a+u} \left[ G(x, y) m(x-u) m(y-v) - \frac{m(-u) m(-v)}{4\pi R} \right] dx dy - m(-u) m(-v) \int_{-\frac{3}{2}b+v}^{\frac{3}{2}b+v} \int_{-\frac{3}{2}a+u}^{\frac{3}{2}a+u} \frac{dx dy}{4\pi \sqrt{x^2 + y^2}} \quad (4.43)$$

Other terms of the equation (4.11) can be determined in a similar way. After all matrix elements are obtained the system will be solved by using the excitation vector. Once the system is solved, the coefficient column vector is obtained. The current density is determined by using the coefficient vector.



## CHAPTER 5

# METHOD OF MOMENTS BY SINC-SINC BASIS FUNCTIONS

In this chapter, the MoM formulation is derived with sinc type basis functions. The main contribution is to obtain accurate scattering results with sinc-sinc based compact formulation. Reducing CPU time with sinc based formulation is another purpose when compared with the well known rooftop. If the sinc basis functions are placed at  $x$  and  $y$  directions on the plate geometry, then they are called sinc-sinc type basis functions. Sinc-sinc type basis functions are used in MoM with Galerkin procedure in order to solve scattering from flat arbitrary plate that is illuminated with a plane wave. The analytical properties of the sinc function are used in the formulation, so the number of integrals to be evaluated numerically is decreased efficiently and MoM matrix elements are obtained in less CPU time. The scattered field is formulated in terms of convolutions. Since MoM is applied with Galerkin procedure, sinc convolutions are obtained in the formulations. By using mathematical properties in Appendix B, the integral equations are solved practically.

### 5.1. Sinc Function

The normalized sinc function [33],  $\text{sinc}(x) = \frac{\sin(\pi x)}{\pi x}$  and its analytical properties are given in the Appendix B and they are used in the applications of the MoM formulations.

Sinc function is chosen as basis function in the MoM formulation. In order to understand the use of the sinc function its location is given for one direction in Figure 5.1. The location of the basis function and subintervals are given for a strip  $L_x = 6$  between  $(-3,3)$  in Figure 5.1(a). The sinc function basis for the  $x$  direction is given as

$$B_{x(s)}(x) = \text{sinc}(2W_x x - p(s)) \quad (5.1)$$

and it can be seen in Figure 5.1(b) for  $p(s)=1$ . The magnitude of the sinc function tails rapidly go to zero while the interval goes to infinity. The linear combination of the basis functions for  $N=5$  is given in the Figure 5.1(c). The approximate function given in Figure 5.1(c) can be obtained by the linear combination of these complete set of orthogonal functions with some coefficients such that

$$J_x(x) \cong \sum_{s=1}^N a_s B_{x(s)}(x). \quad (5.2)$$

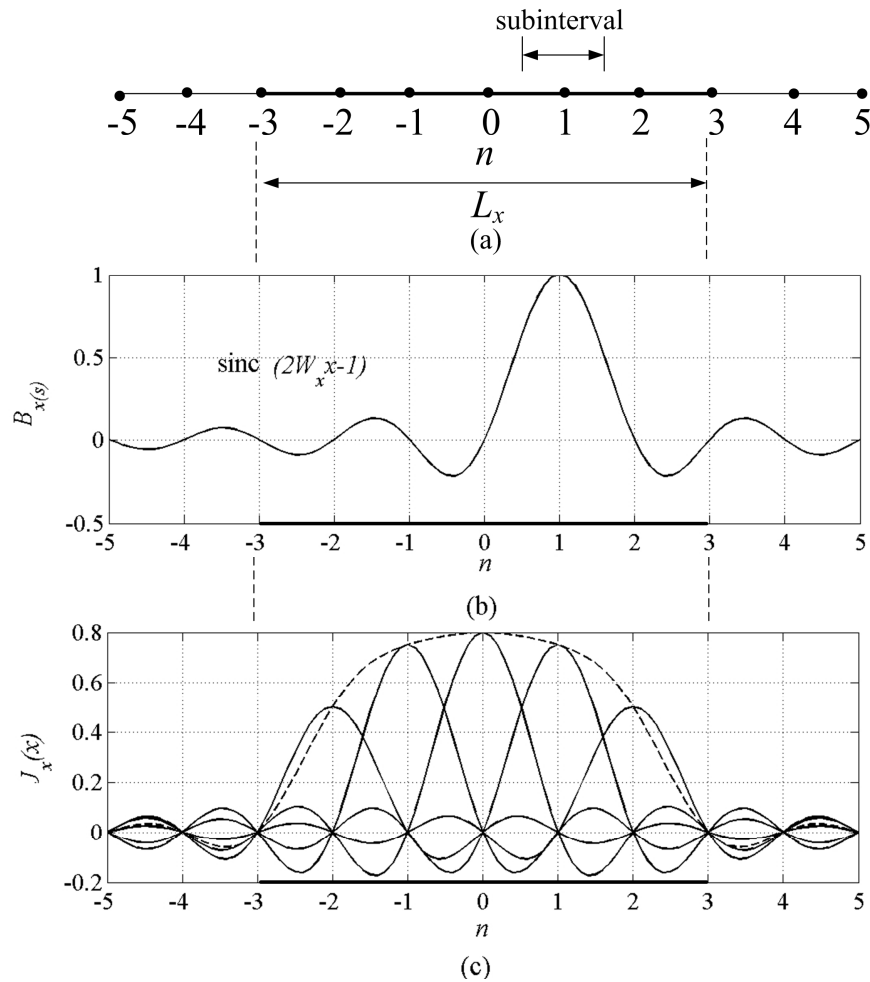


Figure 5.1. Subsectional sinc basis for  $W_x = 500$ ,  $N = 5$ . (a) points and subintervals  $n$ , (b)  $\text{sinc}(2W_x x - n)$  for  $n = 1$ , (c) approximated function.

## 5.2. Sinc-Sinc Basis Functions

The scattered field is obtained by the convolution terms as follows

$$\mathbf{E}^s = -j\omega\mathbf{A} - \nabla\Phi \quad (5.3)$$

where

$$\mathbf{A} = \mu \mathbf{J} * G \quad \text{and} \quad \Phi = \frac{1}{\epsilon} \rho * G. \quad (5.4)$$

The unknown current densities can be obtained by expanding with the known basis such as

$$J_x(x, y) = \sum_{s=1}^N a_s B_{x(s)}(x, y) \quad (5.5)$$

$$J_y(x, y) = \sum_{s=1}^K b_s B_{y(s)}(x, y) \quad (5.6)$$

Two sinc functions in  $x$  and  $y$  perpendicular directions are multiplied as follows

$$B_{x(s)}(x, y) = \text{sinc}(2W_x x - p(s)) \text{sinc}(2W_y y - q(s)) \quad s = 1, 2, \dots, N. \quad (5.7)$$

$$B_{y(s)}(x, y) = \text{sinc}(2W_y y - \bar{q}(s)) \text{sinc}(2W_x x - \bar{p}(s)) \quad s = 1, 2, \dots, K. \quad (5.8)$$

where  $W_x$  and  $W_y$  are the bandwidths of the sinc functions. Three dimensional plot of the sinc function for  $W = 500$ ,  $t_x = t_y = \frac{1}{2W}$  and  $p(s) = q(s) = 60$  is given in Figure 5.2. It is shown in terms of location of the basis functions at  $x$  and  $y$  directions.

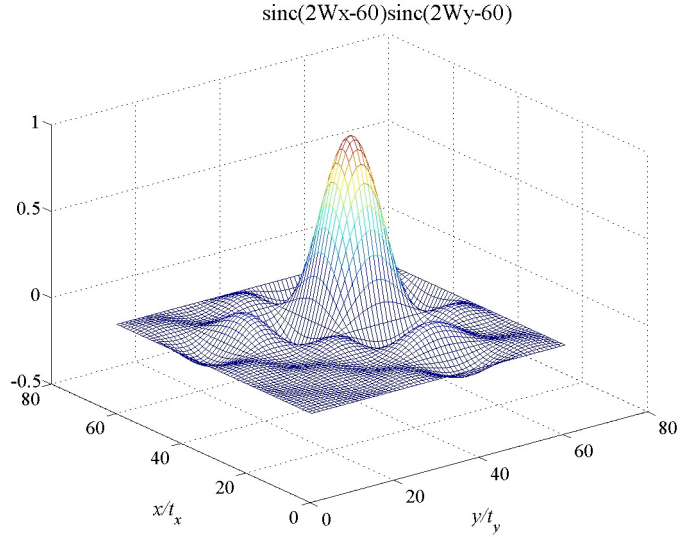


Figure 5.2. 3D plot of the sinc-sinc basis functions.

The flat plate illuminated with a plane wave is solved in this study by using the sinc type basis functions in conventional MoM with Galerkin and non-Galerkin procedures. The locations of the basis functions in  $x$  and  $y$  directions are given in Figure 5.3 such as  $m_1(p(s)t_x, q(s)t_y)$ ,  $m_2(\bar{p}(s)t_x, \bar{q}(s)t_y)$  respectively.

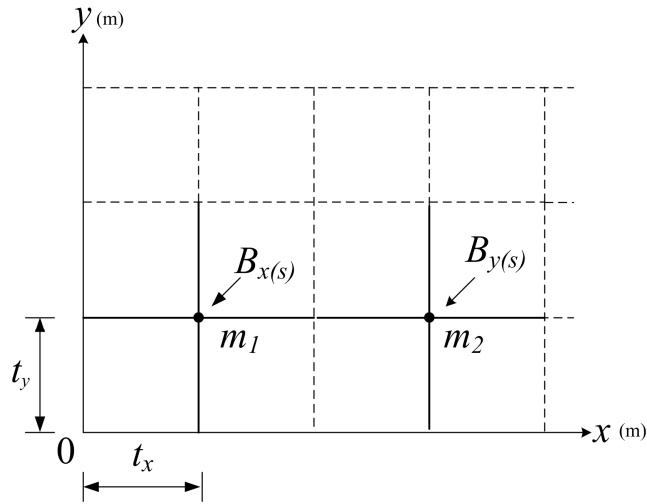


Figure 5.3. Location of the sinc-sinc basis functions within the rectangular cell mesh  $m_1(p(s)t_x, q(s)t_y)$ ,  $m_2(\bar{p}(s)t_x, \bar{q}(s)t_y)$ .

The IE can be obtained by using the well-known boundary conditions on perfectly electric conductor (PEC) as follows

$$\left( \mathbf{E}^{in} + \mathbf{E}^s \right)_{tan} = 0. \quad (5.9)$$

By using the continuity equation

$$\nabla \cdot \mathbf{J} + j\omega\rho = 0 \quad (5.10)$$

the resulting integral equations can be obtained in terms of convolution terms which are given below

$$-j\omega\mu[J_x * G] + \frac{1}{j\omega\varepsilon} \frac{\partial}{\partial x} \left[ \frac{\partial J_x}{\partial x'} * G \right] + \frac{1}{j\omega\varepsilon} \frac{\partial}{\partial x} \left[ \frac{\partial J_y}{\partial y'} * G \right] = -E_x^{in} \quad \text{on } S \quad (5.11)$$

$$-j\omega\mu[J_y * G] + \frac{1}{j\omega\varepsilon} \frac{\partial}{\partial y} \left[ \frac{\partial J_y}{\partial y'} * G \right] + \frac{1}{j\omega\varepsilon} \frac{\partial}{\partial y} \left[ \frac{\partial J_x}{\partial x'} * G \right] = -E_y^{in} \quad \text{on } S \quad (5.12)$$

where

$$G(|\mathbf{r} - \mathbf{r}'|) = \frac{e^{-jkR}}{4\pi R}, \quad R = \sqrt{(x-x')^2 + (y-y')^2}. \quad (5.13)$$

The convolutions in equations (5.11) and (5.12) are termed as  $H_x$  and  $H_y$  functions given as

$$H_x(x, y, p(s), q(s)) = \int_{-\infty}^{\infty} \int_{-\infty}^{\infty} B_{x(s)}(x', y') G(x-x', y-y') dx' dy' \quad (5.14)$$

$$H_y(x, y, \bar{p}(s), \bar{q}(s)) = \int_{-\infty}^{\infty} \int_{-\infty}^{\infty} B_{y(s)}(x', y') G(x-x', y-y') dx' dy' \quad (5.15)$$

where  $(x, y)$  and  $(x', y')$  are the points for observation and source respectively. The IE can be obtained after expanding the current densities into the sinc functions series as follows:

$$c_1 \sum_{s=1}^N a_s H_x(x, y, p(s), q(s)) + c_2 \sum_{s=1}^N a_s \frac{\partial^2}{\partial x^2} H_x(x, y, p(s), q(s)) + c_2 \sum_{s=1}^K b_s \frac{\partial^2}{\partial x \partial y} H_y(x, y, \bar{p}(s), \bar{q}(s)) = -E_x^{in} \quad (5.16)$$

$$c_1 \sum_{s=1}^K b_s H_y(x, y, \bar{p}(s), \bar{q}(s)) + c_2 \sum_{s=1}^K b_s \frac{\partial^2}{\partial y^2} H_y(x, y, \bar{p}(s), \bar{q}(s)) + c_2 \sum_{s=1}^N a_s \frac{\partial^2}{\partial y \partial x} H_x(x, y, p(s), q(s)) = -E_y^{in} \quad (5.17)$$

where  $c_1 = -j\omega\mu$  and  $c_2 = \frac{1}{j\omega\epsilon}$ .

The sinc functions have quasi-localized property given in [14] and this property increases when bandwidth  $W$  increases. While the bandwidth of the sinc function increases, the tails become less important in terms of amplitude. Therefore the derivatives that appear in the original IE can be evaluated by finite difference manner just considering the peak values of the sinc basis. Furthermore, in order to use mathematical properties of the sinc function (given in the Appendix) in the formulation of the problem,  $H_x(x, y, p(s), q(s))$  given in (5.14) can be expanded in a double sinc series with the coefficients  $hx_{d,r}^{f,n}$ , given in the following equation

$$H_x(x, y, p(s), q(s)) = \sum_{o=1}^N hx_{d,r}^{f,n} \text{sinc}(2W_x x - p(o)) \text{sinc}(2W_y y - q(o)). \quad (5.18)$$

where  $d = p(o)$ ,  $r = q(o)$  and  $f = p(s)$ ,  $n = q(s)$ . Since the sinc functions constitute a complete orthogonal set of functions the coefficients  $hx_{d,r}^{f,n}$  ( $hy_{d,r}^{f,n}$ ) is obtained easily. This is one of the main crucial points of the formulation. By this way, i. e. using the equations (5.14) and (5.18), the coefficients  $hx_{d,r}^{f,n}$  ( $hy_{d,r}^{f,n}$ ) is determined. Both sides of the equation above are multiplied and integrated with the sinc functions. The resulting coefficients are given as follows

$$hx_{d,r}^{f,n} = \frac{1}{t_x t_y} \int_{-\infty}^{\infty} \int_{-\infty}^{\infty} \text{sinc}(2W_x x - p(o)) \text{sinc}(2W_y y - q(o)) dx dy, \\ \times \int_{-\infty}^{\infty} \int_{-\infty}^{\infty} \text{sinc}(2W_x x' - p(s)) \text{sinc}(2W_y y' - q(s)) G(x - x', y - y') dx' dy' \quad (5.19)$$

so the integrals are obtained by using  $x - x' = u$  and  $y - y' = v$  coordinate transformations. Then, one can use the properties of the sinc functions given in the Appendix. The resulting coefficients are given below

$$hx_{d,r}^{f,n} \equiv \frac{1}{t_x t_y} \int_{-\infty}^{\infty} \int_{-\infty}^{\infty} G(u,v) \text{sinc}(2W_x u - p(o) + p(s)) \text{sinc}(2W_y v - q(o) + q(s)) dudv. \quad (5.20)$$

When the difference between the locations of observation and source points  $|p(o) - p(s)| \geq 2$  and  $|q(o) - q(s)| \geq 2$ , i.e. far region, the above equation is approximated by

$$hx_{d,r}^{f,n} \equiv G(|p(o) - p(s)| t_x, |q(o) - q(s)| t_y) \quad (5.21)$$

as given in Appendix B. Otherwise, the equation (5.20) should be evaluated numerically.

The approximate solution of the coefficients generally can be written in a piecewise manner as given below

$$hx_{d,r}^{f,n} \equiv \begin{cases} \int_{-\infty}^{\infty} \int_{-\infty}^{\infty} G(u,v) \text{sinc}(2W_x u - p(o) + p(s)) \text{sinc}(2W_y v - q(o) + q(s)) dudv, & |L| < 2, |M| < 2 \\ G(|L| t_x, |M| t_y), & \text{otherwise} \end{cases} \quad (5.22)$$

where  $L = p(o) - p(s)$ ,  $M = q(o) - q(s)$  and  $t_x = t_y = 1/(2W)$ .

The coefficients  $hy_{d,r}^{\bar{f},\bar{n}}$  which constitute  $H_y(x, y, \bar{p}(s), \bar{q}(s))$  can be obtained by the similar procedure given above such that

$$H_y(x, y, \bar{p}(s), \bar{q}(s)) = \sum_{o=1}^K hy_{d,r}^{\bar{f},\bar{n}} \text{sinc}(2W_y y - \bar{q}(o)) \text{sinc}(2W_x x - \bar{p}(o)) \quad (5.23)$$

However, these coefficients  $hx_{d,r}^{f,n}$  and  $hy_{d,r}^{\bar{f},\bar{n}}$  depend on the difference between source and observation point coordinates, so these coefficients are equal. The  $hy_{d,r}^{\bar{f},\bar{n}}$  coefficients are given as

$$hy_{d,\bar{r}}^{\bar{f},\bar{n}} \cong \begin{cases} \int_{-\infty}^{\infty} \int_{-\infty}^{\infty} G(u,v) \text{sinc}(2W_x u - \bar{p}(o) + \bar{p}(s)) \text{sinc}(2W_y v - \bar{q}(o) + \bar{q}(s)) dudv, & |L| < 2, |M| < 2 \\ G(|L|t_x, |M|t_y), & \text{otherwise} \end{cases} \quad (5.24)$$

where  $L = \bar{p}(o) - \bar{p}(s)$ ,  $M = \bar{q}(o) - \bar{q}(s)$  and  $t_x = t_y = 1/(2W)$ .

In Figure 5.4 the pseudocode for obtaining the coefficients  $hx_{d,r}^{f,n}$ ,  $hy_{d,\bar{r}}^{\bar{f},\bar{n}}$  are given. The code is determined in terms of the equations (5.18), (5.22) and (5.24).

```

For  $s=1, \dots, N$ .
Set  $(p(s), q(s))$ , the coordinates of the source points for the  $J_x$ .
Set  $(\bar{p}(s), \bar{q}(s))$ , the coordinates of the source points for the  $J_y$ .
For  $o=1, \dots, K$ .
Set  $(p(o), q(o)), (\bar{p}(o), \bar{q}(o))$  the coordinates of the observation points.
Define  $u = p(o) - p(s)$ ,  $v = q(o) - q(s)$ 
 $N1$ : discretization number
For  $u=0, 1, \dots, 2 \times N1$ , Do
For  $v=0, 1, \dots, 2 \times N1$ , Do
If  $(u < 2, v < 2)$  then
Numerically compute  $hx_{d,r}^{f,n}, hy_{d,\bar{r}}^{\bar{f},\bar{n}}$  for  $|L| < 2, |M| < 2$ 
Else
Use the approximated function
End if
End do
End do

```

Figure 5.4. Pseudocode of determining the coefficients  $hx_{d,r}^{f,n}$ ,  $hy_{d,\bar{r}}^{\bar{f},\bar{n}}$ .

Since the number of the location points are not the same,  $H_x$  and  $H_y$  functions are different. However the coefficients  $hx_{d,r}^{f,n}$  and  $hy_{d,\bar{r}}^{\bar{f},\bar{n}}$ , which can be computed similarly, depend on the difference between source and observation points. The series expansion in equation (5.14) with coefficient produces the first term of the integral equation. In the other terms, the partial derivatives couples like  $\frac{\partial^2}{\partial x^2}$  and  $\frac{\partial^2}{\partial x \partial y}$ ,  $\frac{\partial^2}{\partial y^2}$  and  $\frac{\partial^2}{\partial y \partial x}$ , will be handled by finite difference approach on the series expansion given in equation



(5.14) and (5.15) respectively. Then, the both sides of these equations will be tested by using same type functions as used in expansion. As in the procedure given above the two coupled integral equations have the following terms,

$$c_1 t_x t_y \sum_{s=1}^N a_s h x_{d,r}^{f,n} + \frac{t_y}{t_x} c_2 \sum_{s=1}^N a_s \left[ h x_{d+1,r}^{f,n} - 2h x_{d,r}^{f,n} + h x_{d-1,r}^{f,n} \right] + c_2 \sum_{s=1}^K b_s \left[ \frac{h y_{d+1,r+1}^{\bar{f},\bar{n}} - h y_{d-1,r+1}^{\bar{f},\bar{n}} - h y_{d+1,r-1}^{\bar{f},\bar{n}} + h y_{d-1,r-1}^{\bar{f},\bar{n}}}{4} \right]$$

$$= -t_x t_y E_x^{in}(dt_x, rt_y)$$

(5.24)

$$c_1 t_x t_y \sum_{s=1}^K b_s h y_{\bar{d},\bar{r}}^{\bar{f},\bar{n}} + \frac{t_x}{t_y} c_2 \sum_{s=1}^K b_s \left[ h y_{\bar{d},\bar{r}+1}^{\bar{f},\bar{n}} - 2h y_{\bar{d},\bar{r}}^{\bar{f},\bar{n}} + h y_{\bar{d},\bar{r}-1}^{\bar{f},\bar{n}} \right] + c_2 \sum_{s=1}^N a_s \left[ \frac{h x_{d+1,\bar{r}+1}^{f,n} - h x_{d-1,\bar{r}+1}^{f,n} - h x_{d+1,\bar{r}-1}^{f,n} + h x_{d-1,\bar{r}-1}^{f,n}}{4} \right]$$

$$= -t_x t_y E_y^{in}(\bar{d}t_x, \bar{r}t_y)$$

(5.25)

where  $c_1 = -j\omega\mu$ ,  $c_2 = \frac{1}{j\omega\epsilon}$ ,  $f$  belongs to  $(p(s), q(s))$  pairs,  $\bar{f}$  belongs to  $(\bar{p}(s), \bar{q}(s))$

pairs,

$d = p(o)$  and  $r = q(o)$   $o = 1, 2, \dots, N$ ,  $\bar{d} = \bar{p}(o)$  and  $\bar{r} = \bar{q}(o)$   $o = 1, 2, \dots, K$ . The

representations  $(dt_x, rt_y)$  and  $(\bar{d}t_x, \bar{r}t_y)$  are  $x$  and  $y$  coordinates of the observation

points.

The pseudocodes of obtaining MoM matrix elements are given in Figure (5.5) and (5.6). The detailed explanation of the symbols are given in the equations (5.24) and (5.25). In Figure 5.5,  $A_{NN}$  is obtained by the coefficients obtained through co term calculations in terms of  $o$  and  $s$ , observation and source points respectively. On the other hand,  $B_{NK}$  is obtained by applying numerical differentiation to the coefficients which are obtained through cross term calculations. In Figure (5.6), the MoM matrix elements are obtained in a similar manner with the previous pseudocode given in Figure (5.5).  $D_{KK}$  is obtained by the coefficients obtained through co term calculations in terms of  $\bar{o}$  and  $\bar{s}$ , observation and source points for  $T_y$  and  $B_y$  respectively. On the other hand,  $C_{KN}$  is obtained by applying numerical differentiation to the coefficients

which are obtained through cross term calculations in terms of  $\bar{o}$  and  $s$  for  $T_y$  and  $B_x$ . The horizontal and vertical components of the incident electric fields are calculated for each directions  $x$  and  $y$ . Then, the linear matrix system is solved by using LU decomposition subroutines dgefam and dgeslm given in Figure 5.7 to find the unknown current density coefficients. In the first subroutine dgefam the overall matrix  $T$  is separated into  $L$  and  $U$  factors. Then the factorized matrix is solved with excitation vector  $E_v^{inc}$ . In Figure 5.8, the pseudocode of the current density coefficients for the horizontal polarization case is given. The overall matrix is same but the right hand side of the linear matrix system is calculated for horizontal polarization in this case. Furthermore, linear matrix system is solved with TFQMR as an alternative way in order to reduce the overall CPU when compared to SuperNEC.

```

For  $o = 1, 2, \dots N$  Do
Obtain  $d = p(o), r = q(o)$ 
For  $s = 1, 2, \dots K$  Do
Obtain  $f = p(s), n = q(s)$ 


$$A_{NN}(o, s) = c_1 t_x t_y h x_{d,r}^{f,n} + c_2 \frac{t_y}{t_x} \left[ h x_{d+1,r}^{f,n} - 2 h x_{d,r}^{f,n} + h x_{d-1,r}^{f,n} \right]$$


End do
For  $\bar{s} = 1, 2, \dots K$  Do
Obtain  $\bar{f} = \bar{p}(s), \bar{n} = \bar{q}(s)$ 


$$B_{NK}(o, \bar{s}) = c_2 \left[ \frac{h y_{d+1,r+1}^{\bar{f},\bar{n}} - h y_{d-1,r+1}^{\bar{f},\bar{n}} - h y_{d+1,r-1}^{\bar{f},\bar{n}} + h y_{d-1,r-1}^{\bar{f},\bar{n}}}{4} \right]$$


End do
Obtain the right hand side excitation  $F = -t_x t_y E_{x_v}^{in}(dt_x, rt_y)$  and  $G = -t_x t_y E_{x_h}^{in}(dt_x, rt_y)$ 
End do

```

Figure 5.5. Obtaining the MoM matrix elements for the IE (5.24).

```

For  $\bar{o} = 1, 2, \dots K$  Do
Obtain  $\bar{d} = \bar{p}(\bar{o}), \bar{r} = \bar{q}(\bar{o})$ 
For  $s = 1, 2, \dots N$  Do
Obtain  $f = p(s), n = q(s)$ 

$$C_{KN}(\bar{o}, s) = c_2 \left[ \frac{hx_{\bar{d}+1, \bar{r}+1}^{f, n} - hx_{\bar{d}-1, \bar{r}+1}^{f, n} - hx_{\bar{d}+1, \bar{r}-1}^{f, n} + hx_{\bar{d}-1, \bar{r}-1}^{f, n}}{4} \right]$$

End do
For  $\bar{s} = 1, 2, \dots K$  Do
Obtain  $\bar{f} = \bar{p}(s), \bar{n} = \bar{q}(s)$ 

$$D_{KK}(\bar{o}, \bar{s}) = c_2 \frac{t_x}{t_y} \left[ hy_{\bar{d}+1, \bar{r}}^{\bar{f}, \bar{n}} - 2hy_{\bar{d}, \bar{r}}^{\bar{f}, \bar{n}} + hx_{\bar{d}-1, \bar{r}}^{\bar{f}, \bar{n}} \right] + c_1 t_x t_y hy_{\bar{d}, \bar{r}}^{\bar{f}, \bar{n}}$$

End do
Obtain  $-t_x t_y E_{y_v}^{in}(\bar{d}t_x, \bar{r}t_y)$  and  $-t_x t_y E_{y_h}^{in}(\bar{d}t_x, \bar{r}t_y)$ 
End do

```

Figure 5.6. Obtaining the MoM matrix elements for the IE (5.25).

```

Obtain  $T = \begin{bmatrix} A_{NN} & B_{NK} \\ C_{KN} & D_{KK} \end{bmatrix}$ 

$$E_v^{inc} = -t_x t_y \begin{bmatrix} E_{x_v}^{in} \\ E_{y_v}^{in} \end{bmatrix} = F$$

 $SINIR = (N) + (K)$ 
Solve  $dgefam(T, SINIR, IPVT, INFO)$ 
Solve  $dgeslm(T, SINIR, IPVT, E_v^{in})$ 

```

Figure 5.7. Pseudocode of obtaining current coefficients for vertical polarization .

```

Obtain  $T = \begin{bmatrix} A_{NN} & B_{NK} \\ C_{KN} & D_{KK} \end{bmatrix}$ 

$$E_h^{inc} = -t_x t_y \begin{bmatrix} E_{x_h}^{in} \\ E_{y_h}^{in} \end{bmatrix} = G$$

 $SINIR = (N) + (K)$ 
Solve  $dgefam(T, SINIR, IPVT, INFO)$ 
Solve  $dgeslm(T, SINIR, IPVT, E_h^{in})$ 

```

Figure 5.8. Pseudocode of obtaining current coefficients for horizontal polarization .

As seen in pseudocodes given in (5.5) and (5.6), numerical differentiation is applied to coefficients by using both the forward and central difference methods in this study. The finite difference derivative errors can be reduced by decreasing mesh size at

a reasonable level. The analytical properties of the sinc functions are used in the sinc-sinc formulation. As a result, the number of integrals is decreased two times while using sinc functions as basis functions. By the way, accurate scattering results are obtained when compared with the known software SuperNEC. Only double integrals are evaluated in the near field regions and no integration is evaluated in the other region. The matrix elements and coefficients are obtained with less computational effort. By improving the MoM formulation in order to obtain more accurate results, different type of basis functions are used. Therefore, in the next section, in order to reduce the overflow problem the pulse type basis function is chosen parallel to the edge direction. By this way, better simulation results are obtained. The overflow problem at the edges is explained in the next chapter in details.

## CHAPTER 6

# METHOD OF MOMENTS BY SINC-PULSE BASIS FUNCTIONS

To improve the accuracy of the numerical results, different types of basis functions might be used. Therefore, in this section, in order to reduce the overflow problem, the pulse type basis function is chosen parallel to the edge direction. The main difference between the previous section and this one is that the pulse basis is chosen perpendicular to the edge direction. Sinc basis is chosen again in the parallel direction. Hence, the analytical properties of the sinc functions can be used only at one direction in the formulation.

### 6.1. Overflow Problem

There is continuity at the parallel direction with respect to the direction of the current density. *Problem is*

- There exists singular behavior at the edge in the perpendicular direction with respect to the direction of the current density.

Sinc functions overflow at the parallel direction of the edge of the flat arbitrary plate. In order to avoid overflowing of the sinc functions at the edge, pulse basis is used on the parallel direction of the edge instead of the sinc function. The overflow problem at the edge is given in Figure 6.1.

### 6.2. Sinc-Pulse Basis Functions

The approximate current density of the illuminated plate can be expanded with the basis functions below

$$B_{x(s)} = \text{sinc}(2W_x x - p(s)) \text{pulse}(y, q(s)t_y - t_y, q(s)t_y), \quad s = 1, 2, \dots, N. \quad (6.1)$$

$$B_{y(s)} = \text{sinc}(2W_y y - \bar{q}(s)) \text{pulse}(x, \bar{p}(s)t_x - t_x, \bar{p}(s)t_x), \quad s = 1, 2, \dots, K. \quad (6.2)$$

where  $N$  and  $K$  are the sampling points for  $x$  and  $y$  directed currents. Three dimensional plot of the sinc function for  $W = 500$ ,  $t_x = \frac{1}{2W}$  and  $p(s) = 60$  is given in Figure 6.2. It is shown in terms of the location of the basis function at  $x$  direction.

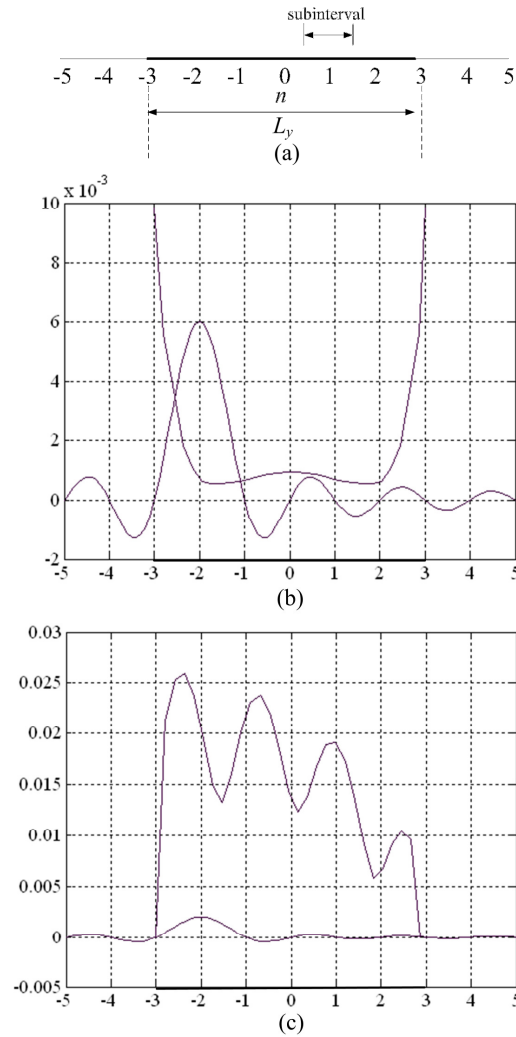


Figure 6.1. Overflow of the sinc function on the interval  $x \in (-3, 3)$ . (a) subintervals, (b) ycut overflow for  $\text{sinc}(x+2)$ , (c) xcut overflow.

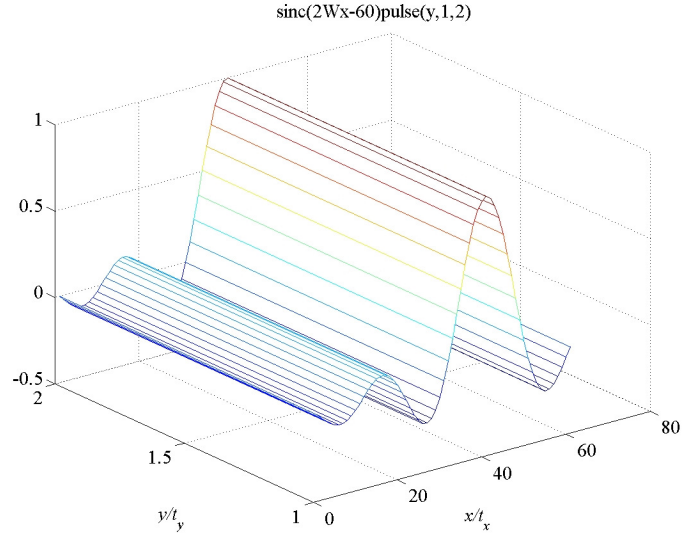


Figure 6.2. 3D plot of the sinc-pulse basis functions  $(\text{sinc}(2W_x x - 60)\text{pulse}(y, 1, 2))$ .

The locations of the basis functions at  $x$  and  $y$  directions are given in Figure 6.3 such as  $m_1(p(s)t_x, q(s)t_y - t_y/2)$  and  $m_2(\bar{p}(s)t_x - t_x/2, \bar{q}(s)t_y)$ . Each cell boundaries for the basis functions  $B_{x(s)}$  and  $B_{y(s)}$  are given in Figure 6.3.

The unknown current densities in  $x$  and  $y$  directions can be expanded in terms of these mentioned basis functions such as

$$J_x(x, y) \cong \sum_{s=1}^N a_s B_{x(s)}(x, y) \quad (6.3)$$

$$J_y(x, y) \cong \sum_{s=1}^K b_s B_{y(s)}(x, y) \quad (6.4)$$

The derivation of the sinc-sinc based MoM formulation is given in the previous section. The main difference between the previous section and this one is to choose pulse basis parallel to the edge direction. As in the equations (5.11) and (5.12) in the previous section, the IE is going to be solved in the same way. They can be given again in the equation below

$$-j\omega\mu[J_x * G] + \frac{1}{j\omega\epsilon} \frac{\partial}{\partial x} \left[ \frac{\partial J_x}{\partial x'} * G \right] + \frac{1}{j\omega\epsilon} \frac{\partial}{\partial x} \left[ \frac{\partial J_y}{\partial y'} * G \right] = -E_x^{in} \quad \text{on } S \quad (6.5)$$

$$-j\omega\mu[J_y * G] + \frac{1}{j\omega\epsilon} \frac{\partial}{\partial y} \left[ \frac{\partial J_y}{\partial y'} * G \right] + \frac{1}{j\omega\epsilon} \frac{\partial}{\partial y} \left[ \frac{\partial J_x}{\partial x'} * G \right] = -E_y^{in} \quad \text{on } S \quad (6.6)$$

The differentiations over the sources are applied to the Green's function by using integration by parts. After they are applied to the observation parameter, they are taken out of the convolution integrals. The integrals above can be given as follows

$$-j\omega\mu \underbrace{[J_x * G]}_1 + \frac{1}{j\omega\epsilon} \underbrace{\frac{\partial^2}{\partial x^2} [J_x * G]}_2 + \frac{1}{j\omega\epsilon} \underbrace{\frac{\partial^2}{\partial x \partial y} [J_y * G]}_3 = -E_x^{in} \quad \text{on } S \quad (6.7)$$

$$-j\omega\mu \underbrace{[J_y * G]}_4 + \frac{1}{j\omega\epsilon} \underbrace{\frac{\partial^2}{\partial y^2} [J_y * G]}_5 + \frac{1}{j\omega\epsilon} \underbrace{\frac{\partial^2}{\partial y \partial x} [J_x * G]}_6 = -E_y^{in} \quad \text{on } S \quad (6.8)$$

Each IE is constituted by three convolution terms. There are six terms totally. The two terms of each IE given above are obtained, since the second terms of the IE's are second order derivatives of the first terms. Thus, the first and third convolution terms of the IE's are derived in this section.

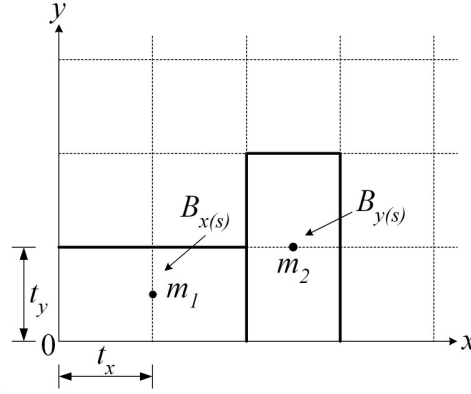


Figure 6.3. Location of the sinc-pulse basis functions within the rectangular cell mesh  $m_1(p(s)t_x, q(s)t_y - t_y/2)$  and  $m_2(\bar{p}(s)t_x - t_x/2, \bar{q}(s)t_y)$ .

### 6.2.1. Sinc-Pulse Formulation with Galerkin Procedure

Testing functions which are applied are same with the basis functions in this procedure. These functions are given as



$$T_{x(o)} = \text{sinc}(2W_x x - p(o)) \text{pulse}(y, q(o)t_y - t_y, q(o)t_y), \quad o = 1, 2, \dots, N. \quad (6.9)$$

$$T_{y(o)} = \text{sinc}(2W_y y - \bar{q}(o)) \text{pulse}(x, \bar{p}(o)t_x - t_x, \bar{p}(o)t_x), \quad o = 1, 2, \dots, K. \quad (6.10)$$

If the integral equation, which is constituted by basis function oriented along  $x$  axis, is tested with weighting function oriented along  $x$  axis, then the obtained term is called co-term.

The convolutions in equations (6.7) and (6.8) are termed as  $\tilde{H}_x$  and  $\tilde{H}_y$  functions given as

$$\tilde{H}_x(x, y, p(s), q(s)) = \int_{-\infty}^{\infty} \int_{-\infty}^{\infty} B_{x(s)}(x', y') G(x - x', y - y') dx' dy' \quad (6.11)$$

$$\tilde{H}_y(x, y, \bar{p}(s), \bar{q}(s)) = \int_{-\infty}^{\infty} \int_{-\infty}^{\infty} B_{y(s)}(x', y') G(x - x', y - y') dx' dy' \quad (6.12)$$

where  $(x, y)$  and  $(x', y')$  are the points for observation and source respectively. The IE can be obtained after expanding the current densities into the sinc functions series as follows:

$$c_1 \sum_{s=1}^N a_s \tilde{H}_x(x, y, p(s), q(s)) + c_2 \sum_{s=1}^N a_s \frac{\partial^2}{\partial x^2} \tilde{H}_x(x, y, p(s), q(s)) + c_2 \sum_{s=1}^K b_s \frac{\partial^2}{\partial x \partial y} \tilde{H}_y(x, y, \bar{p}(s), \bar{q}(s)) = -E_x^{in} \quad (6.13)$$

$$c_1 \sum_{s=1}^K b_s \tilde{H}_y(x, y, \bar{p}(s), \bar{q}(s)) + c_2 \sum_{s=1}^K b_s \frac{\partial^2}{\partial y^2} \tilde{H}_y(x, y, \bar{p}(s), \bar{q}(s)) + c_2 \sum_{s=1}^N a_s \frac{\partial^2}{\partial y \partial x} \tilde{H}_x(x, y, p(s), q(s)) = -E_y^{in} \quad (6.14)$$

where  $c_1 = -j\omega\mu$  and  $c_2 = \frac{1}{j\omega\epsilon}$ .

In order to avoid overflowing at the edge, pulse basis is used on the parallel direction of the edge instead of the sinc function.  $\tilde{H}_x$  function is expanded to sinc and pulse functions and it is given as

$$\tilde{H}_x(x, y, p(s), q(s)) = \sum_{o=1}^N \tilde{h}_{d,r}^{f,n} \text{sinc}(2W_x x - p(o)) \text{pulse}(y, q(o)t_y - t_y, q(o)t_y). \quad (6.15)$$

where  $d = p(o)$  and  $r = q(o)$ ,  $f = p(s)$ ,  $n = q(s)$ .

Since the sinc and pulse functions constitute an orthogonal set of functions the coefficients  $\tilde{h}_{d,r}^{f,n}$  is obtained easily. This is one of the main crucial points of the formulation. By this way, i. e. using the equations (6.11) and (6.15), the coefficient  $\tilde{h}_{d,r}^{f,n}$  is determined. Both sides of the equation above are multiplied and integrated with the sinc and pulse functions. The resulting coefficients are given as follows

$$\begin{aligned} t_x t_y \tilde{h}_{d,r}^{f,n} &\equiv \int_{q(o)t_y - t_y}^{q(o)t_y} \int_{-\infty}^{\infty} \text{sinc}(2W_x x - p(o)) \text{pulse}(y, q(o)t_y - t_y, q(o)t_y) \\ &\times \int_{q(s)t_y - t_y}^{q(s)t_y} \int_{-\infty}^{\infty} \text{sinc}(2W_x x' - p(s)) \text{pulse}(y', q(s)t_y - t_y, q(s)t_y) G(x - x', y - y') dx' dy' dx dy \end{aligned} \quad (6.16)$$

If the integrals of the same functions with the same variables are calculated, it is obtained that

$$\begin{aligned} t_x t_y \tilde{h}_{d,r}^{f,n} &\equiv \int_{q(o)t_y - t_y}^{q(o)t_y} \text{pulse}(y, q(o)t_y - t_y, q(o)t_y) \int_{q(s)t_y - t_y}^{q(s)t_y} \text{pulse}(y', q(s)t_y - t_y, q(s)t_y) \\ &\times \int_{-\infty}^{\infty} \text{sinc}(2W_x x' - p(s)) \int_{-\infty}^{\infty} \text{sinc}(2W_x x - p(o)) G(x - x', y - y') dx' dx dy dy' \end{aligned} \quad (6.17)$$

Let assume that  $x - x' = u$  and  $y - y' = v$ . Sinc-sinc convolution gives again a sinc function as given in Appendix B. Pulse-pulse convolution gives a triangular function. Using these properties, (6.17) becomes

$$t_x t_y \tilde{h}x_{d,r}^{f,n} = t_y \int_{(q(o)-q(s))t_y-t_y}^{(q(o)-q(s))t_y+t_y} R(v-(q(o)-q(s))t_y) t_x \int_{-\infty}^{\infty} \text{sinc}(2W_x u - p(o) + p(s)) G(u, v) dudv \quad (6.18)$$

where

$$R(v-v_o) = \begin{cases} 0, & v < v_o - t_y \\ \frac{-v_o + v}{t_y} + I, & v_o - t_y \leq v < v_o \\ \frac{v_o - v}{t_y} + I, & v_o \leq v < v_o + t_y \\ 0, & v > v_o + t_y \end{cases}, \quad (6.19)$$

and  $v_o = (q(o) - q(s))t_y$ . By using the analytical properties given in Appendix B, the first term of the IE in (6.7) becomes,

$$\tilde{h}x_{d,r}^{f,n} = \int_{(q(o)-q(s))t_y-t_y}^{(q(o)-q(s))t_y+t_y} R(v-(q(o)-q(s))t_y) \int_{-\infty}^{\infty} \text{sinc}(2W_x u - p(o) + p(s)) G(u, v) dudv \quad (6.20)$$

and this equation is solved numerically away from the singularity region. If  $(p(s) \neq p(o))$  and  $(q(s) \neq q(o))$ , the above equation is approximated to the integral

$$\tilde{h}x_{d,r}^{f,n} = t_x \int_{(q(o)-q(s))t_y-t_y}^{(q(o)-q(s))t_y+t_y} R(v-(q(o)-q(s))t_y) G(|p(s) - p(o)|_{t_x}, v) dv. \quad (6.21)$$

The singularity condition occurs for  $p(s) = p(o)$  and  $q(s) = q(o)$  and this singularity should be extracted from the integrand and it is integrated analytically by hand. The calculations are done on the computer. The coefficients is calculated with

$$\tilde{h}x_{d,r}^{f,n} = \int_{(q(o)-q(s))t_y-t_y}^{(q(o)-q(s))t_y+t_y} \int_{-\infty}^{\infty} \left[ R(v) \text{sinc}(2W_x u) G(u, v) - \frac{I}{4\pi R} \right] dudv + \int_{(q(o)-q(s))t_y-t_y}^{(q(o)-q(s))t_y+t_y} \int_{-\infty}^{\infty} \frac{I}{4\pi R} dudv. \quad (6.22)$$

The approximate solution of the coefficients generally can be written in a piecewise manner as given below

$$\tilde{h}_{d,r}^{f,n} = \begin{cases} \int_{(q(o)-q(s))t_y-t_y}^{(q(o)-q(s))t_y+t_y} R(v-(q(o)-q(s))t_y) \int_{-\infty}^{\infty} \text{sinc}(2W_x u - p(o) + p(s)) G(u,v) dudv, & \begin{matrix} |p(o)-p(s)| < 1 \\ |q(o)-q(s)| < 1 \end{matrix} \\ t_x \int_{(q(o)-q(s))t_y-t_y}^{(q(o)-q(s))t_y+t_y} R(v-(q(o)-q(s))t_y) G(|p(s)-p(o)|t_x, v) dv, & \text{otherwise} \end{cases} \quad (6.23)$$

The coefficients  $\tilde{h}_{d,r}^s$  which constitute  $\tilde{H}_y(x, y, \bar{p}(k), \bar{q}(k))$  can be obtained by the similar procedure given above such that

$$\tilde{H}_y(x, y, \bar{p}(s), \bar{q}(s)) = \sum_{o=1}^K \tilde{h}_{d,\bar{r}}^{\bar{f},\bar{n}} \text{sinc}(2W_y y - \bar{q}(o)) \text{pulse}(x, \bar{p}(o)t_x - t_x, \bar{p}(o)t_x) \quad (6.24)$$

where  $\bar{d} = \bar{p}(o)$  and  $\bar{r} = \bar{q}(o)$ ,  $\bar{f} = \bar{p}(s)$  and  $\bar{n} = \bar{q}(s)$ .

Testing function is oriented in the same direction (y direction) with basis function. From the equations (6.12) and (6.24), it is obtained that

$$\begin{aligned} t_x t_y \tilde{h}_{d,\bar{r}}^{\bar{f},\bar{n}} &\equiv \int_{\bar{p}(o)t_x-t_x}^{\bar{p}(o)t_x} \int_{-\infty}^{\infty} \text{sinc}(2W_y y - \bar{q}(o)) \text{pulse}(x, \bar{p}(o)t_x - t_x, \bar{p}(o)t_x) \\ &\times \int_{\bar{p}(s)t_x-t_x}^{\bar{p}(s)t_x} \int_{-\infty}^{\infty} \text{sinc}(2W_y y' - \bar{q}(s)) \text{pulse}(x', \bar{p}(s)t_x - t_x, \bar{p}(s)t_x) G(x-x', y-y') dx' dy' dx dy \end{aligned} \quad (6.25)$$

If the integrals of the same functions with the same variables are calculated, it is given as

$$\begin{aligned}
t_x t_y \tilde{h}_{\bar{d}, \bar{r}}^{\bar{f}, \bar{n}} &\equiv \int_{\bar{p}(o)t_x - t_x}^{\bar{p}(o)t_x} \text{pulse}(x, \bar{p}(o)t_x - t_x, \bar{p}(o)t_x) \int_{\bar{p}(s)t_y - t_y}^{\bar{p}(s)t_y} \text{pulse}(x', \bar{p}(s)t_x - t_x, \bar{p}(s)t_x) \\
&\times \int_{-\infty}^{\infty} \text{sinc}(2W_y y' - \bar{q}(s)) \int_{-\infty}^{\infty} \text{sinc}(2W_y y - \bar{q}(o)) G(x - x', y - y') dy' dy dx dx'
\end{aligned} \quad (6.26)$$

Let assume that  $x - x' = u$  and  $y - y' = v$ . Sinc-sinc convolution gives again a sinc function as given in Appendix B. Pulse-pulse convolution gives a triangular function. Using these results, (6.26) becomes

$$t_x t_y \tilde{h}_{\bar{d}, \bar{r}}^{\bar{f}, \bar{n}} = t_x \int_{(\bar{p}(o) - \bar{p}(s))t_x - t_x}^{(\bar{p}(o) - \bar{p}(s))t_x + t_x} R(u - (\bar{p}(o) - \bar{p}(s))t_x) t_y \int_{-\infty}^{\infty} \text{sinc}(2W_y v - \bar{q}(o) + \bar{q}(s)) G(u, v) dudv \quad (6.27)$$

By using the analytical properties given in Appendix B, the first term of the IE in (6.8) becomes

$$\tilde{h}_{\bar{d}, \bar{r}}^{\bar{f}, \bar{n}} = \int_{(\bar{p}(o) - \bar{p}(s))t_x - t_x}^{(\bar{p}(o) - \bar{p}(s))t_x + t_x} R(u - (\bar{p}(o) - \bar{p}(s))t_x) \int_{-\infty}^{\infty} \text{sinc}(2W_y v - \bar{q}(o) + \bar{q}(s)) G(u, v) dudv \quad (6.28)$$

and this equation is solved numerically everywhere but in the singularity region. If  $(\bar{p}(s) \neq \bar{p}(o))$  and  $(\bar{q}(s) \neq \bar{q}(o))$  the above equation is approximated to the integral

$$\tilde{h}_{\bar{d}, \bar{r}}^{\bar{f}, \bar{n}} = t_y \int_{(\bar{p}(o) - \bar{p}(s))t_x - t_x}^{(\bar{p}(o) - \bar{p}(s))t_x + t_x} R(u - (\bar{p}(o) - \bar{p}(s))t_x) G(u, |\bar{q}(s) - \bar{q}(o)|t_y) du \quad (6.29)$$

The singularity condition occurs for  $\bar{p}(s) = \bar{p}(o)$  and  $\bar{q}(s) = \bar{q}(o)$  and this singularity should be extracted from the integrand and it is integrated analytically. The coefficients can be calculated with

$$\tilde{h}_{\bar{d}, \bar{r}}^{\bar{f}, \bar{n}} = \int_{(\bar{p}(o) - \bar{p}(s))t_x - t_x}^{(\bar{p}(o) - \bar{p}(s))t_x + t_x} \int_{-\infty}^{\infty} \left[ R(u) \text{sinc}(2W_y v) G(u, v) - \frac{1}{4\pi R} \right] dudv + \int_{(\bar{p}(o) - \bar{p}(s))t_x - t_x}^{(\bar{p}(o) - \bar{p}(s))t_x + t_x} \int_{-\infty}^{\infty} \frac{1}{4\pi R} dudv \quad (6.30)$$

The approximate solution of the coefficients generally can be written in a piecewise manner as given below

$$\tilde{h}_{d,\bar{r}}^{f,\bar{n}} = \begin{cases} \int_{(\bar{p}(o)-\bar{p}(s))t_x-t_x}^{(\bar{p}(o)-\bar{p}(s))t_x+t_x} R(u-(\bar{p}(o)-\bar{p}(s))t_x) \int_{-\infty}^{\infty} \text{sinc}(2W_y v - \bar{q}(o) + \bar{q}(s)) G(u,v) dv du, & \begin{cases} |\bar{p}(o)-\bar{p}(s)| < 1 \\ |\bar{q}(o)-\bar{q}(s)| < 1 \end{cases} \\ t_y \int_{(\bar{p}(o)-\bar{p}(s))t_x-t_x}^{(\bar{p}(o)-\bar{p}(s))t_x+t_x} R(u-(\bar{p}(o)-\bar{p}(s))t_x) G(u, |\bar{q}(s)-\bar{q}(o)| t_y) du, & \text{otherwise} \end{cases} \quad (6.31)$$

$$a) \text{ First term: } -j\omega\mu \sum_{s=1}^N a_s \langle \tilde{H}_{x(s)}, T_x \rangle$$

The first term of the integral equation (IE) given in equation (6.7) is an example of a co-term and obtained with the convolution of the basis function and the Green's function as given in the equation (6.11).  $\tilde{H}_x$  is expanded to sinc and pulse functions given in (6.15). After expanding the whole IE is tested with the weighting function  $T_x$ . The testing procedure is represented with the inner product which means double integration between terms  $\tilde{H}_x$  and  $T_x$ . The first term of the IE given in (6.7) is obtained as follows

$$\begin{aligned} -j\omega\mu \sum_{s=1}^N a_s \langle \tilde{H}_{x(s)}, T_x \rangle &= -j\omega\mu \sum_{s=1}^N a_s \int_{-\infty}^{\infty} \int_{-\infty}^{\infty} T_x(x,y) \tilde{H}_{x(s)}(x,y,p(s),q(s)) dx dy \\ &= -j\omega\mu t_y \sum_{s=1}^N a_s \tilde{h}_{d,r}^{f,n} \end{aligned} \quad (6.32)$$

Since the sinc functions and pulse functions are orthogonal functions, series sum of  $\tilde{H}_x$  drops after testing. The pseudocode for determining the coefficients  $\tilde{h}_{d,r}^{f,n}$  is given in the Figure 6.4. Discretization numbers for x and y directions are given  $N1$  and  $K1$  respectively, which are equal to 30 for  $2\lambda$  plate geometry (the discretization number is 15 for each wavelength).

```

Set  $\left( p(s), q(s) - \frac{I}{2} \right), \left( \bar{p}(s) - \frac{I}{2}, \bar{q}(s) \right)$  the coordinates of the source points for x
and y directed currents respectively.
Set  $\left( p(o), q(o) - \frac{I}{2} \right), \left( \bar{p}(o) - \frac{I}{2}, \bar{q}(o) \right)$  the coordinates of the observation points.
 $u = p(o) - p(s)$ 
 $v = q(o) - q(s)$ 
N1 = discretization number
K1 = discretization number
For  $u = 0, 1, \dots, N1$ , Do
For  $v = -K1, \dots, 1, \dots, K1$ , Do
If  $(u == 0, v == 0)$  then
Evaluate the singularity condition analytically.
Solve the overall  $\tilde{h}_{d,r}^{f,n}$  numerically (eq 6.22).
Else
Solve the integral with Taylor series expansion analytically (eq 6.21).
End If
End do
End do

```

Figure 6.4. Pseudocode of determining the coefficients  $\tilde{h}_{d,r}^{f,n}$ .

$$b) \text{ Second term: } \frac{1}{j\omega\epsilon} \sum_{s=1}^N a_s \left\langle \frac{\partial^2}{\partial x^2} \tilde{H}_x(x, y, p(s), q(s)), T_x \right\rangle$$

The second term of the IE (6.7) is obtained by numerical differentiating over coefficients after testing procedure. The term is given as

$$\frac{1}{j\omega\epsilon} \sum_{s=1}^N a_s \int_{-\infty}^{\infty} \int_{-\infty}^{\infty} T_x(x, y) \frac{\partial^2}{\partial x^2} \tilde{H}_x(x, y, p(s), q(s)) dx dy = \frac{1}{j\omega\epsilon} \sum_{s=1}^N a_s t_x t_y \left( \frac{\tilde{h}_{d+1,r}^{f,n} - 2\tilde{h}_{d,r}^{f,n} + \tilde{h}_{d-1,r}^{f,n}}{t_x^2} \right) \quad (6.33)$$

$$c) \text{ Third term: } \frac{1}{j\omega\epsilon} \sum_{s=1}^K b_s \left\langle \frac{\partial^2}{\partial x \partial y} \tilde{H}_y(x, y, \bar{p}(s), \bar{q}(s)), T_x \right\rangle$$

The third term of the IE (6.7) is an example of a cross-term. It is constituted by applying  $T_x$  testing functions to the near field integral constituted by  $B_y$  basis functions. The term is given as

$$\begin{aligned}
\frac{I}{j\omega\epsilon} \sum_{s=1}^K b_s \int_{-\infty}^{\infty} \int_{-\infty}^{\infty} T_x(x, y) \frac{\partial^2}{\partial x \partial y} \tilde{H}_y(x, y) dx dy &= \frac{I}{j\omega\epsilon} \sum_{s=1}^K b_s \frac{\partial^2}{\partial x \partial y} \sum_{o=1}^K \tilde{h}_{y_{d,r}}^{\bar{f}, \bar{n}} \int_{-\infty}^{\infty} \int_{-\infty}^{\infty} \text{sinc}(2W_x x - p(o)) \text{pulse}(x, \bar{p}(s), t_x) dx \\
&\quad \int_{-\infty}^{\infty} \int_{-\infty}^{\infty} \text{sinc}(2W_y y - \bar{q}(o)) \text{pulse}(y, q(o), t_y) dy \\
&= \frac{I}{j\omega\epsilon} \sum_{s=1}^K b_s \sum_{o=1}^K \frac{\tilde{h}_{y_{d+1,r+1}}^{\bar{f}, \bar{n}} - \tilde{h}_{y_{d-1,r+1}}^{\bar{f}, \bar{n}} - \tilde{h}_{y_{d+1,r-1}}^{\bar{f}, \bar{n}} + \tilde{h}_{y_{d-1,r-1}}^{\bar{f}, \bar{n}}}{4t_x t_y} \\
&\quad \int_{-\infty}^{\infty} \int_{-\infty}^{\infty} \text{sinc}(2W_x x - p(o)) \text{pulse}(x, \bar{p}(s), t_x) \int_{-\infty}^{\infty} \int_{-\infty}^{\infty} \text{sinc}(2W_y y - \bar{q}(o)) \text{pulse}(y, q(o), t_y) dy dx
\end{aligned} \tag{6.34}$$

The series sum of  $\tilde{H}_y$  given in (6.24) is not dropped after testing because of the sinc and pulse integrals.

The integrals in  $x$  and  $y$  directions should be calculated for each point on the surface and multiplied in order to construct matrix coefficients. When the matrix filling time is compared, it will take 150 times much time than the previous chapter explained sinc-sinc based results in obtaining the coefficients.

```

Set  $\left( p(s), q(s) - \frac{I}{2} \right), \left( \bar{p}(s) - \frac{I}{2}, \bar{q}(s) \right)$  the coordinates of the source points.
Set  $\left( p(o), q(o) - \frac{I}{2} \right), \left( \bar{p}(o) - \frac{I}{2}, \bar{q}(o) \right)$  the coordinates of the observation points.
For  $s = 1, \dots, N$ , Do
  pu=1;
  For  $o = 1, \dots, K$ , Do
    Call simpsonbir1(sincx,  $(\bar{p}(s) - I)t_x, (\bar{p}(s))t_x, \bar{p}(s)$ , integral1)
     $I_1(\text{pu}, s) = \text{integral1}$ 
    Call simpsonbir1(sincx,  $(q(o) - I)t_y, (q(o))t_y, q(o)$ , integral2)
     $I_2(\text{pu}, o) = \text{integral2}$ 
  pu=pu+1
  End do
  NM(s)=pu-1
End do

```

Figure 6.5. Pseudocode of obtaining only the integrals for the third term.



$$d) \text{ Fourth term: } -j\omega\mu \sum_{s=1}^K b_s \langle \tilde{H}_{y(s)}, T_y \rangle$$

The fourth term of the integral equation (IE) given in equation (6.8) is an example of a co-term and obtained with the convolution of the basis function and the Green's function as given in the equation (6.12).  $\tilde{H}_y$  is expanded to sinc and pulse functions given in (6.24). After expanding the whole IE is tested with the weighting function  $T_y$ . The testing procedure is represented with the inner product which means double integration between terms  $\tilde{H}_y$  and  $T_y$ . The fourth term in the IE given in (6.8) is obtained as follows

$$-j\omega\mu \sum_{s=1}^K b_s \int_{-\infty}^{\infty} \int_{-\infty}^{\infty} T_y(x, y) \tilde{H}_y(x, y, \bar{p}(s), \bar{q}(s)) dx dy = -j\omega\mu t_x t_y \sum_{s=1}^K b_s \tilde{h}_{y_{\bar{d}, \bar{r}}}^{\bar{f}, \bar{n}}. \quad (6.35)$$

Since the sinc functions and pulse functions are orthogonal functions, series sum of  $\tilde{H}_y$  drops after testing. The pseudocode for determining the coefficients  $\tilde{h}_{y_{\bar{d}, \bar{r}}}^{\bar{f}, \bar{n}}$  is given in the Figure 6.5. Gaussian quadrature is used by taking the one dimensional integral in the approximated case.

```

Set  $\left( p(s), q(s) - \frac{1}{2} \right), \left( \bar{p}(s) - \frac{1}{2}, \bar{q}(s) \right)$  the coordinates of the source points.
Set  $\left( p(o), q(o) - \frac{1}{2} \right), \left( \bar{p}(o) - \frac{1}{2}, \bar{q}(o) \right)$  the coordinates of the observation points.
 $u = \bar{p}(o) - \bar{p}(s)$ 
 $v = \bar{q}(o) - \bar{q}(s)$ 
For  $u = -N1, \dots, 1, \dots, N1$ , Do
For  $v = 0, 1, \dots, K1$ , Do
If  $(u == 0, v == 0)$  then
Evaluate the singularity condition analytically.
Solve  $\tilde{h}_{y_{\bar{d}, \bar{r}}}^{\bar{f}, \bar{n}}$  numerically.
Else
Solve the integral with Taylor series expansion.
End do
End do

```

Figure 6.6. Pseudocode of determining the coefficients  $\tilde{h}_{y_{\bar{d}, \bar{r}}}^{\bar{f}, \bar{n}}$ .

$$e) \text{Fifth term: } \frac{1}{j\omega\epsilon} \sum_{s=1}^K b_s \left\langle \frac{\partial^2}{\partial y^2} \tilde{H}_y(x, y, \bar{p}(s), \bar{q}(s)), T_y \right\rangle$$

The fifth term in the IE (6.8) is obtained by numerical differentiating over coefficients  $\tilde{h}_{y_{d,\bar{r}}}^s$  after testing procedure. The term is given as

$$\frac{1}{j\omega\epsilon} \sum_{s=1}^K b_s \int_{-\infty}^{\infty} \int_{-\infty}^{\infty} T_y(x, y) \frac{\partial^2}{\partial y^2} \tilde{H}_y(x, y, \bar{p}(s), \bar{q}(s)) dx dy = \frac{1}{j\omega\epsilon} \sum_{s=1}^K b_s t_x t_y \left( \frac{\tilde{h}_{y_{d,\bar{r}-1}}^{\bar{f},\bar{n}} - 2\tilde{h}_{y_{d,\bar{r}}}^{\bar{f},\bar{n}} + \tilde{h}_{y_{d,\bar{r}+1}}^{\bar{f},\bar{n}}}{t_y^2} \right). \quad (6.36)$$

$$e) \text{ Sixth term: } \frac{1}{j\omega\epsilon} \sum_{s=1}^N a_s \left\langle \frac{\partial^2}{\partial y \partial x} \tilde{H}_x(x, y, p(s), q(s)), T_y \right\rangle$$

The third term of the IE in Equation (6.8) is constituted by testing the integral constituted by  $B_x$  oriented along  $x$  axis with  $T_y$  oriented along  $y$  axis. This cross term is given as

$$\begin{aligned} \frac{1}{j\omega\epsilon} \sum_{s=1}^N a_s \int_{-\infty}^{\infty} \int_{-\infty}^{\infty} T_y(x, y) \frac{\partial^2}{\partial y \partial x} \tilde{H}_x(x, y) dx dy &= \frac{1}{j\omega\epsilon} \sum_{s=1}^N a_s \frac{\partial^2}{\partial y \partial x} \sum_{o=1}^K \tilde{h}_{x_{d,\bar{r}}}^{f,n} \int_{-\infty}^{\infty} \int_{-\infty}^{\infty} \text{sinc}(2W_y y - \bar{q}(o)) \text{pulse}(y, q(s), t_y) dy \\ &\quad \int_{-\infty}^{\infty} \int_{-\infty}^{\infty} \text{sinc}(2W_x x - p(s)) \text{pulse}(x, \bar{p}(o), t_x) dx \\ &= \frac{1}{j\omega\epsilon} \sum_{s=1}^N a_s \sum_{o=1}^K \frac{\tilde{h}_{x_{d+1,\bar{r}+1}}^{f,n} - \tilde{h}_{x_{d+1,\bar{r}-1}}^{f,n} - \tilde{h}_{x_{d-1,\bar{r}+1}}^{f,n} + \tilde{h}_{x_{d-1,\bar{r}-1}}^{f,n}}{4t_x t_y} \\ &\quad \int_{-\infty}^{\infty} \int_{-\infty}^{\infty} \text{sinc}(2W_y y - \bar{q}(o)) \text{pulse}(y, q(s), t_y) \int_{-\infty}^{\infty} \int_{-\infty}^{\infty} \text{sinc}(2W_x x - p(s)) \text{pulse}(x, \bar{p}(o), t_x) dx dy \end{aligned} \quad (6.37)$$

The series sum of  $\tilde{H}_x$  given in (6.37) is not dropped after testing because of the sinc and pulse integrals.

The integrals in  $x$  and  $y$  directions should be calculated for each point on the surface and multiplied in order to construct matrix coefficients. When the matrix filling time is compared, the time for solving the coefficients of the above cross terms takes 150 times much time than the previous chapter explained sinc-sinc based formulation.

The main contribution of this thesis is to obtain scattering results with a high accuracy in less CPU time. Another procedure that never disturbs the accuracy should be tried while calculating the coefficients in less CPU time than the Galerkin procedure mentioned. Therefore, the analytical properties of the sinc functions can be used again in the formulation as mentioned in the previous chapter. Equations (6.38) and (6.39) are given the integral equations which include coefficients for x ( $\tilde{h}_x$ ) and y ( $\tilde{h}_y$ ) directed current densities respectively.

$$\begin{aligned}
& -j\omega\mu t_x t_y \sum_{s=1}^N a_s \tilde{h}_{d,r}^{f,n} + \frac{1}{j\omega\epsilon} \sum_{s=1}^N a_s t_x t_y \left( \frac{\tilde{h}_{d+1,r}^{f,n} - 2\tilde{h}_{d,r}^{f,n} + \tilde{h}_{d-1,r}^{f,n}}{t_x^2} \right) \\
& + \frac{1}{j\omega\epsilon} \sum_{s=1}^K b_s \sum_{o=1}^K \frac{\tilde{h}_{d+1,r+1}^{f,\bar{n}} - \tilde{h}_{d-1,r+1}^{f,\bar{n}} - \tilde{h}_{d+1,r-1}^{f,\bar{n}} + \tilde{h}_{d-1,r-1}^{f,\bar{n}}}{4t_x t_y} \\
& \quad \underbrace{\int_{-\infty}^{\infty} \int_{-\infty}^{\infty} \text{sinc}(2W_x x - p(o)) \text{pulse}(x, \bar{p}(s), t_x)}_{I_1} \underbrace{\int_{-\infty}^{\infty} \int_{-\infty}^{\infty} \text{sinc}(2W_y y - \bar{q}(o)) \text{pulse}(y, q(o), t_y)}_{I_2} dy dx
\end{aligned} \tag{6.38}$$

$$\begin{aligned}
& -j\omega\mu t_x t_y \sum_{s=1}^K b_s \tilde{h}_{d,\bar{r}}^{f,\bar{n}} + \frac{1}{j\omega\epsilon} \sum_{s=1}^K b_s t_x t_y \left( \frac{\tilde{h}_{d,\bar{r}-1}^{f,\bar{n}} - 2\tilde{h}_{d,\bar{r}}^{f,\bar{n}} + \tilde{h}_{d,\bar{r}+1}^{f,\bar{n}}}{t_y^2} \right) \\
& + \frac{1}{j\omega\epsilon} \sum_{s=1}^N a_s \sum_{o=1}^K \frac{\tilde{h}_{d+1,\bar{r}+1}^{f,n} - \tilde{h}_{d+1,\bar{r}-1}^{f,n} - \tilde{h}_{d-1,\bar{r}+1}^{f,n} + \tilde{h}_{d-1,\bar{r}-1}^{f,n}}{4t_x t_y} \\
& \quad \int_{-\infty}^{\infty} \int_{-\infty}^{\infty} \text{sinc}(2W_y y - \bar{q}(o)) \text{pulse}(y, q(s), t_y) \int_{-\infty}^{\infty} \int_{-\infty}^{\infty} \text{sinc}(2W_x x - p(s)) \text{pulse}(x, \bar{p}(o), t_x) dx dy
\end{aligned} \tag{6.39}$$

```

For  $o = 1, 2, \dots N$  Do
Obtain  $d, r$ 
 $d = p(o)$ 
 $r = q(o)$ 
For  $s = 1, 2, \dots N$  Do
Obtain  $p(s), q(s)$ 

$$A_{NN}(o, s) = -j\omega\mu t_x t_y \tilde{h}x_{d,r}^{f,n} + \frac{1}{j\omega\epsilon} \frac{t_y}{t_x} \left[ \tilde{h}x_{d+1,r}^{f,n} - 2\tilde{h}x_{d,r}^{f,n} + \tilde{h}x_{d-1,r}^{f,n} \right]$$

End do
For  $\bar{s} = 1, 2, \dots K$  Do
Obtain  $\bar{p}(s), \bar{q}(s)$ 
Sum=0
For  $\bar{o} = 1, 2, \dots NM(o)$  Do
AT1= $I_1(\bar{o}, o)$ ;
AT2= $I_2(\bar{o}, o)$ ;
 $\tilde{d} = \bar{p}(\bar{o})$ 
 $\tilde{r} = \bar{q}(\bar{o})$ 

$$B_{NK}(\bar{o}, \bar{s}) = \frac{1}{j\omega\epsilon} \left[ \frac{hy_{\tilde{d}+1, \tilde{r}+1}^{\tilde{f}, \tilde{n}} - hy_{\tilde{d}-1, \tilde{r}+1}^{\tilde{f}, \tilde{n}} - hy_{\tilde{d}+1, \tilde{r}-1}^{\tilde{f}, \tilde{n}} + hy_{\tilde{d}-1, \tilde{r}-1}^{\tilde{f}, \tilde{n}}}{4t_x t_y} \right] AT1 \times AT2$$

SUM=SUM+ $B_{NK}$ 
End do
End do
Obtain  $-t_x t_y E_{x_v}^{in}(dt_x, rt_y)$  and  $-t_x t_y E_{x_h}^{in}(dt_x, rt_y)$ 
End do

```

Figure 6.7. Obtaining the MoM matrix elements for the Galerkin MoM obtained in (6.38).

```

For  $\bar{o} = 1, 2, \dots K$  Do
Obtain  $\bar{d}, \bar{r}$ 
 $\bar{d} = \bar{p}(o)$ 
 $\bar{r} = \bar{q}(o)$ 
For  $\bar{s} = 1, 2, \dots K$  Do
Obtain  $\bar{p}(s), \bar{q}(s)$ 


$$D_{KK}(\bar{o}, \bar{s}) = -j\omega\mu t_x t_y \tilde{h}y_{\bar{d}, \bar{r}}^{\bar{f}, \bar{n}} + \frac{I}{j\omega\epsilon} \frac{t_y}{t_x} \left[ \tilde{h}y_{\bar{d}+1, \bar{r}}^{\bar{f}, \bar{n}} - 2\tilde{h}y_{\bar{d}, \bar{r}}^{\bar{f}, \bar{n}} + \tilde{h}y_{\bar{d}-1, \bar{r}}^{\bar{f}, \bar{n}} \right]$$


End do
For  $s = 1, 2, \dots N$  Do
Obtain  $p(s), q(s)$ 
Sum=0
For  $\bar{o} = 1, 2, \dots NM(o)$  Do
AT1= $I_1(\bar{o}, o)$ ;
AT2= $I_2(\bar{o}, o)$ ;
 $\tilde{d} = p(\bar{o})$ 
 $\tilde{r} = q(\bar{o})$ 


$$C_{KN}(\bar{o}, s) = \frac{I}{j\omega\epsilon} \left[ \frac{hx_{\bar{d}+1, \tilde{r}+1}^{f, n} - hx_{\bar{d}-1, \tilde{r}+1}^{f, n} - hx_{\bar{d}+1, \tilde{r}-1}^{f, n} + hx_{\bar{d}-1, \tilde{r}-1}^{f, n}}{4t_x t_y} \right] AT2 \times AT1$$


SUM=SUM+ $C_{KN}$ 
End do
End do
Obtain  $-t_x t_y E_{y_v}^{in}(\bar{d}t_x, \bar{r}t_y)$  and  $-t_x t_y E_{y_h}^{in}(\bar{d}t_x, \bar{r}t_y)$ 
End do

```

Figure 6.8. Obtaining the MoM matrix elements for the Galerkin MoM obtained in (6.39).

## 6.2.2. Sinc-Pulse Formulation with Non Galerkin Procedure

Testing functions which are applied are different from the basis functions in this procedure. These functions are impulsive sinc functions at  $x$  axis and  $y$  axis whose bandwidths are given as  $\tilde{W}_x$  and  $\tilde{W}_y$ . They are given as

$$T_{x(o)} = \text{sinc}\left(2\tilde{W}_x x - p(o)\right) \text{sinc}\left(2\tilde{W}_y y - \left(q(o) - \frac{I}{2}\right)\right), \quad (6.40)$$

$$T_{y(o)} = \text{sinc}\left(2\tilde{W}_y y - \bar{q}(o)\right) \text{sinc}\left(2\tilde{W}_x x - \left(\bar{p}(o) - \frac{1}{2}\right)\right), \quad (6.41)$$

The integral equations, which we apply the MoM, are the same with the ones detailed in (6.7) and (6.8) of the Galerkin case. The first, second, fourth and fifth terms of the IEs (6.7) and (6.8) are the examples for the co-terms. The third and sixth terms are the cross-terms.

$$a) \text{ First term: } -j\omega\mu \sum_{s=1}^N a_s \langle H_{xx}, T_x \rangle$$

The first term of the integral equation (IE) given in (6.7) is obtained with the convolution of the basis function and the Green's function such as

$$B_{M(s)}(x', y') * G(x-x', y-y') = \underbrace{\int_{-\infty}^{\infty} \int_{-\infty}^{\infty} \text{sinc}(2W_x x' - p(s)) \text{pulse}(y', q(s)t_y, -t_y, q(s)t_y) G(x-x', y-y') dx' dy'}_{H_{xx}(x, y, p(s), q(s))} \quad (6.42)$$

where  $(x, y)$  and  $(x', y')$  are the observation and source points.  $H_{xx}$  represents testing with  $T_x$  of the near field integral that is constituted by the basis  $B_x$ . It can be expanded in a double series with the coefficients  $h_{xx_{d,r}^{f,n}}$  multiplied with the complete orthogonal sinc functions set, such as

$$H_{xx}(x, y, p(s), q(s)) = \sum_{o=1}^N h_{xx_{d,r}^{f,n}} \underbrace{\text{sinc}(2\tilde{W}_x x - p(o)) \text{sinc}\left(2\tilde{W}_y y - \left(q(o) - \frac{1}{2}\right)\right)}_{T_x}. \quad (6.43)$$

The location of the sinc functions in  $x$  and  $y$  directions are at  $p(o)t_x$  and  $q(o)t_y - t_y/2$  respectively. Testing function is oriented in the same axis with the basis function. Using the integral (6.42) it is obtained that

$$hxx_{d,r}^{f,n} \equiv \int_{-\infty}^{\infty} \int_{-\infty}^{\infty} \text{sinc}(2W_x x' - p(s)) \text{pulse}(y', q(s)t_y - t_y, q(s)t_y) G(p(o)t_x - x', q(o)t_y - t_y / 2 - y') dx' dy' \quad (6.44)$$

and this equation is solved numerically everywhere but in the singularity region. While  $|p(s) - p(o)| \geq 3$  or  $|q(s) - q(o)| \geq 3$ , the above equation can be approximated to the equation below

$$hxx_{d,r}^{f,n} = t_x \int_{Mt_y - t_y / 2}^{Mt_y + t_y / 2} \frac{e^{-jkR}}{4\pi R} dv \quad (6.45)$$

where  $M = q(o) - q(s)$  and  $R = \sqrt{(t_x(p(o) - p(s)))^2 + v^2}$ . The integrand in equation (6.45) has no singularity in the mentioned region and the exponent can be expanded to the Taylor series. Then, the first five terms can be computed analytically. By this way, the integral can be taken very fast and accurately [57].

While  $|p(s) - p(o)| < 3$  and  $|q(s) - q(o)| < 3$  i.e. near field region closer to singularity, then the double integral in equation (6.44) will be written by extracting the singularity given as follows

$$hxx_{d,r}^{f,n} = \frac{1}{4\pi} \int_{q(s)t_y - t_y}^{q(s)t_y} \int_{-\infty}^{\infty} \left[ \frac{\text{sinc}(2W_x x' - p(s)) e^{-jkR} - \text{sinc}(p(o) - p(s))}{R} \right] dx' dy' \quad (6.46)$$

$$+ \frac{1}{4\pi} \text{sinc}(p(o) - p(s)) \int_{q(s)t_y - t_y}^{q(s)t_y} \int_{-\infty}^{\infty} \frac{1}{R} dx' dy'$$

where  $R = \sqrt{(p(o)t_x - x')^2 + (q(o)t_y - t_y / 2 - y')^2}$ . The equation (6.46) is written for  $p(s) \neq p(o)$  case. Under the condition that  $p(s) = p(o)$ , i.e.  $\text{sinc}(p(o) - p(s)) = 1$ , in this case the equation becomes

$$hxx_{d,r}^{f,n} = \frac{1}{4\pi} \int_{q(s)t_y - t_y}^{q(s)t_y} \int_{-\infty}^{\infty} \frac{\text{sinc}(2W_x x' - p(s)) e^{-jkR} - 1}{R} dx' dy' + \frac{1}{4\pi} \int_{q(s)t_y - t_y}^{q(s)t_y} \int_{-\infty}^{\infty} \frac{1}{R} dx' dy'. \quad (6.47)$$

The singularities in the equations (6.46) and (6.47) can be handled by the analytical solution explained in the study [2]. Additionally, the detailed calculation of the singularity is given in equation (4.34). After testing the IE (6.7) with  $T_x$ , the first term is obtained as

$$\begin{aligned} -j\omega\mu \sum_{s=1}^N a_s \langle H_{xx}, T_x \rangle &= -j\omega\mu \sum_{s=1}^N a_s \int_{-\infty}^{\infty} \int_{-\infty}^{\infty} T_x(x, y) H_{xx}(x, y, p(s), q(s)) dx dy \\ &= -j\omega\mu \tilde{t}_x \tilde{t}_y \sum_{s=1}^N a_s hxx_{d,r}^{f,n} \end{aligned} \quad (6.48)$$

where  $\tilde{t}_x = \frac{I}{2\tilde{W}_x}$ ,  $\tilde{t}_y = \frac{I}{2\tilde{W}_y}$ . The series sum of  $H_{xx}$  drops because sinc functions are orthogonal functions.

The pseudocode for solving the coefficients  $hxx_{d,r}^{f,n}$  is given in Figure 6.9.

```

Set  $\left(p(s), q(s) - \frac{I}{2}\right), \left(\bar{p}(s) - \frac{I}{2}, \bar{q}(s)\right)$  the coordinates of the source points for x and
y directed current densities respectively.
Set  $\left(p(o), q(o) - \frac{I}{2}\right), \left(\bar{p}(o) - \frac{I}{2}, \bar{q}(o)\right)$  the coordinates of the observation points.
 $u = p(o) - p(s)$ 
 $v = q(o) - q(s)$ 
N1 discretization number
K1 discretization number
For  $u = -N1, \dots, 1, \dots, N1$ , Do
For  $v = -K1, \dots, 1, \dots, K1$ , Do
If  $(\text{abs}(u) < 3 \text{ and } \text{abs}(v) < 3)$  then
Solve double integral including singularity condition.
Else
Solve by using Taylor series expansion
End if
End do
End do

```

Figure 6.9. Pseudocode of determining the coefficients  $hxx_{d,r}^{f,n}$ .

**b) Second term:** 
$$\frac{1}{j\omega\epsilon} \sum_{s=1}^N a_s \left\langle \frac{\partial^2}{\partial x^2} H_{xx(s)}(x, y, p(s), q(s)), T_x \right\rangle$$



The second terms of the IE (6.7) can be obtained by differentiating over the coefficients  $hxx_{d,r}^{f,n}$  by using central difference methods. Then, the integral equation is tested with the weighting function  $T_x$ ,

$$\frac{1}{j\omega\epsilon} \sum_{s=1}^N a_s \int_{-\infty}^{\infty} \int_{-\infty}^{\infty} T_x(x, y) \frac{\partial^2}{\partial x^2} H_{xx(s)}(x, y, p(s), q(s)) dx dy = \frac{1}{j\omega\epsilon} \tilde{t}_x \tilde{t}_y \sum_{s=1}^N a_s \left( \frac{hxx_{d+1,r}^{f,n} - 2hxx_{d,r}^{f,n} + hxx_{d-1,r}^{f,n}}{t_x^2} \right) \quad (6.49)$$

$$c) \text{ Third term: } \frac{1}{j\omega\epsilon} \sum_{s=1}^K b_s \left\langle \frac{\partial^2}{\partial x \partial y} H_{xy(s)}(x, y, \bar{p}(s), \bar{q}(s)), T_x \right\rangle$$

The third terms of IE's (6.7) is called cross term and they can be obtained by  $B_y$  (basis oriented in y axis),  $T_x$  (testing oriented in x axis). The third term of the IE in (6.7) can be given as follows

$$\frac{\partial}{\partial x} \frac{\partial}{\partial y} \int_{-\infty}^{\infty} \int_{-\infty}^{\infty} B_{y(s)}(x', y') G(x-x', y-y') dx' dy'. \quad (6.50)$$

The convolution between basis and Green function can be represented by

$$H_{xy}(x, y, \bar{p}(s), \bar{q}(s)) = \int_{-\infty}^{\infty} \int_{-\infty}^{\infty} B_{y(s)}(x', y') G(x-x', y-y') dx' dy' \quad (6.51)$$

where  $H_{xy}$  represents testing the near field radiation of the basis function  $B_y$  with  $T_x$  function. It can be expanded by using orthogonal set of sinc functions

$$H_{xy}(x, y, \bar{p}(s), \bar{q}(s)) = \sum_{o=1}^N hxy_{d,r}^{f,n} \underbrace{\text{sinc}\left(2\tilde{W}_x x - p(o)\right) \text{sinc}\left(2\tilde{W}_y y - \left(q(o) - \frac{1}{2}\right)\right)}_{T_x} \quad (6.52)$$

and the location of the sinc functions in x and y directions are at  $p(o)t_x$  and  $q(o)t_y - t_y/2$  respectively. The coefficients can be obtained by (6.51) and (6.52) and given as follows

$$hxy_{d,r}^{f,n} \equiv \int_{-\infty}^{\infty} \int_{-\infty}^{\infty} \text{sinc}(2\tilde{W}_y y' - \bar{q}(s)) \text{pulse}(x', \bar{p}(s)\tilde{t}_x - \tilde{t}_x, \bar{p}(s)\tilde{t}_x) G(p(o)\tilde{t}_x - x', q(o)\tilde{t}_y - \tilde{t}_y/2 - y') dx' dy'. \quad (6.53)$$

The above integral is approximated to a single integral for the case  $|\bar{p}(s) - p(o)| \geq 3$  and  $|\bar{q}(s) - q(o)| \geq 3$  by using the properties given in the Appendix B. The upper and lower limits are determined in terms of the location of the pulse function such as

$$hxy_{d,r}^{f,n} = t_y \int_{x_s - \tilde{t}_x/2}^{x_s + \tilde{t}_x/2} \frac{e^{-jkR}}{4\pi R} dx' \quad (6.54)$$

where  $R = \sqrt{(p(o)\tilde{t}_x - x')^2 + (q(o)\tilde{t}_y - \tilde{t}_y/2 - \bar{q}(s)\tilde{t}_y)^2}$  and  $x_s = \bar{p}(s)\tilde{t}_x - \tilde{t}_x/2$ . Let change the variables to  $u = p(o)\tilde{t}_x - x'$ . Then the above equation becomes

$$hxy_{d,r}^{f,n} = t_y \int_{(p(o) - \bar{p}(s))\tilde{t}_x}^{(p(o) - \bar{p}(s))\tilde{t}_x + \tilde{t}_x} \frac{e^{-jkR}}{4\pi R} dx' \quad (6.55)$$

where  $R = \sqrt{u^2 + ((q(o) - \bar{q}(s))\tilde{t}_y - \tilde{t}_y/2)^2}$ . The integral in equation (6.55) is computed by using Taylor series expansion procedure [57]. For the near field region,  $|\bar{p}(s) - p(o)| < 3$  and  $|\bar{q}(s) - q(o)| < 3$ , the singularity should be extracted from the integrand and evaluated analytically the same as given for co-terms. After testing the third term becomes

$$\begin{aligned} & \frac{1}{j\omega\epsilon} \sum_{s=1}^K b_s \left\langle \frac{\partial^2}{\partial x \partial y} H_{xy}(x, y, \bar{p}(s), \bar{q}(s)), T_x \right\rangle = \\ & \frac{1}{j\omega\epsilon} \sum_{s=1}^K b_s \int_{-\infty}^{\infty} \int_{-\infty}^{\infty} T_x(x, y) \frac{\partial^2}{\partial x \partial y} H_{xy}(x, y, \bar{p}(s), \bar{q}(s)) dx dy = \\ & \frac{1}{j\omega\epsilon} \tilde{t}_x \tilde{t}_y \sum_{s=1}^K b_s \left( \frac{hxy_{d+1,r+1}^{f,n} - hxy_{d-1,r+1}^{f,n} - hxy_{d+1,r-1}^{f,n} + hxy_{d-1,r-1}^{f,n}}{4t_x t_y} \right) \end{aligned} \quad (6.56)$$

Because sinc functions are orthogonal functions the series sum of  $H_{xy}$  drops and numerical differentiation is applied to the coefficients  $hxy_{d,r}^{f,n}$ .

$$d) \text{ Fourth term: } -j\omega\mu \sum_{s=1}^K b_s \langle H_{yy}, T_y \rangle$$

The same procedure is valid for  $H_{yy}(x, y, \bar{p}(s), \bar{q}(s))$  that can be expanded with  $hyy_{d,\bar{r}}^s$  coefficients similarly. The coefficients belong to the co-terms of the equation (6.8). The first term of this integral equation (IE) given in (6.8) is obtained with the convolution of the basis function and the Green's function such as

$$B_{y(s)}(x', y') * G(x-x', y-y') = \underbrace{\int_{-\infty}^{\infty} \int_{-\infty}^{\infty} \text{sinc}(2W_y y' - \bar{q}(s)) \text{pulse}(x', \bar{p}(s)t_x - t_x, \bar{p}(s)t_x) G(x-x', y-y') dx' dy'}_{H_{yy}(x, y, \bar{p}(s), \bar{q}(s))} \quad (6.57)$$

where  $H_{yy}$  represents the near field radiation of the basis function  $B_y$  testing with  $T_y$ . It can be expanded in a double series with the coefficients  $hyy_{d,\bar{r}}^{f,n}$  multiplied with the complete orthogonal impulsive sinc functions set, such as

$$H_{yy}(x, y, \bar{p}(s), \bar{q}(s)) = \sum_{o=1}^K hyy_{d,\bar{r}}^{\bar{f},\bar{n}} \underbrace{\text{sinc}(2\tilde{W}_y y - \bar{q}(o)) \text{sinc}\left(2\tilde{W}_x x - \left(\bar{p}(o) - \frac{1}{2}\right)\right)}_{T_y}. \quad (6.58)$$

The integral equation constituted by  $B_y$  basis is tested with  $T_y$ . The coefficients,  $hyy_o^s$  is obtained by using (6.57) and (6.58) such that

$$hyy_{d,\bar{r}}^{\bar{f},\bar{n}} \equiv \int_{-\infty}^{\infty} \int_{-\infty}^{\infty} \text{sinc}(2\tilde{W}_y y' - \bar{q}(s)) \text{pulse}(x', \bar{p}(s)\tilde{t}_x - t_x, \bar{p}(s)\tilde{t}_x) G(\bar{p}(o)\tilde{t}_x - \tilde{t}_x/2 - x', \bar{q}(o)\tilde{t}_y - y') dx' dy' \quad (6.59)$$

While  $|\bar{p}(s) - \bar{p}(o)| \geq 3$  or  $|\bar{q}(s) - \bar{q}(o)| \geq 3$ , the equation above can be approximated to the equation below

$$h_{yy}^{\bar{f}, \bar{n}} = t_y \int_{\tilde{L}_x - \tilde{t}_x / 2}^{\tilde{L}_x + \tilde{t}_x / 2} \frac{e^{-jkR}}{4\pi R} du \quad (6.60)$$

where  $L = \bar{p}(o) - \bar{p}(s)$  and  $R = \sqrt{(\tilde{t}_y (\bar{q}(o) - \bar{q}(s)))^2 + u^2}$ . The integral equation (6.60) can be evaluated by Taylor series expansion [56].

While  $|\bar{q}(s) - \bar{q}(o)| < 3$  and  $|\bar{p}(s) - \bar{p}(o)| < 3$  i.e. near field region closer to singularity, then the double integral in equation (6.59) will be written by extracting the singularity as in the following equation

$$h_{yy}^{\bar{f}, \bar{n}} = \frac{1}{4\pi} \int_{\bar{p}(s)\tilde{t}_x - \tilde{t}_x}^{\bar{p}(s)\tilde{t}_x} \int_{-\infty}^{\infty} \left[ \frac{\text{sinc}(2W_y y' - \bar{q}(s)) e^{-jkR} - \text{sinc}(\bar{q}(o) - \bar{q}(s))}{R} \right] dx' dy' + \frac{1}{4\pi} \text{sinc}(\bar{q}(o) - \bar{q}(s)) \int_{\bar{p}(s)\tilde{t}_x - \tilde{t}_x}^{\bar{p}(s)\tilde{t}_x} \int_{-\infty}^{\infty} \frac{1}{R} dx' dy' \quad (6.61)$$

where  $R = \sqrt{(\bar{q}(o)\tilde{t}_y - y')^2 + (\bar{p}(o)\tilde{t}_x - \tilde{t}_x / 2 - x')^2}$ . The equation (6.61) is written for  $\bar{q}(s) \neq \bar{q}(o)$  case. Under the condition that  $\bar{q}(s) = \bar{q}(o)$ , i.e.  $\text{sinc}(\bar{q}(o) - \bar{q}(s)) = 1$ , in this case the equation becomes

$$h_{yy}^{\bar{f}, \bar{n}} = \frac{1}{4\pi} \int_{\bar{p}(s)\tilde{t}_x - \tilde{t}_x}^{\bar{p}(s)\tilde{t}_x} \int_{-\infty}^{\infty} \frac{\text{sinc}(2W_y y' - \bar{q}(s)) e^{-jkR} - 1}{R} dx' dy' + \frac{1}{4\pi} \int_{\bar{p}(s)\tilde{t}_x - \tilde{t}_x}^{\bar{p}(s)\tilde{t}_x} \int_{-\infty}^{\infty} \frac{1}{R} dx' dy'. \quad (6.62)$$

The singularities in the equations (6.61) and (6.62) can be handled by the analytical solution explained in the study [2]. Additionally, the detailed calculation of the singularity is given in equation (4.34).

Fourth term is obtained after testing procedure in an equality given below

$$-j\omega\mu \sum_{s=1}^K b_s \int_{-\infty}^{\infty} \int_{-\infty}^{\infty} T_y(x, y) H_{yy}(x, y, \bar{p}(s), \bar{q}(s)) dx dy = -j\omega\mu \tilde{t}_x \tilde{t}_y \sum_{s=1}^K b_s h_{yy}^{\bar{f}, \bar{n}}. \quad (6.63)$$

$$e) \text{ Fifth term: } \frac{1}{j\omega\epsilon} \sum_{s=1}^K b_s \left\langle \frac{\partial^2}{\partial y^2} H_{yy}(x, y, \bar{p}(s), \bar{q}(s)), T_y \right\rangle$$

The second terms of the IE (6.8), i.e. fifth term can be obtained by differentiating over these coefficients by using central difference methods. Then, the terms of integral equation are tested with  $T_y$ . The series sum of  $H_{yy}$  drops after the testing procedure such as

$$\frac{1}{j\omega\epsilon} \sum_{s=1}^K b_s \int_{-\infty}^{\infty} \int_{-\infty}^{\infty} T_y(x, y) \frac{\partial^2}{\partial y^2} H_{yy}(x, y, \bar{p}(s), \bar{q}(s)) dx dy = \frac{1}{j\omega\epsilon} \tilde{t}_x \tilde{t}_y \sum_{s=1}^K b_s \left( \frac{hyy_{d,\bar{r}-1}^{\tilde{f},\bar{n}} - 2hyy_{d,\bar{r}}^{\tilde{f},\bar{n}} + hyy_{d,\bar{r}+1}^{\tilde{f},\bar{n}}}{t_y^2} \right) \quad (6.64)$$

$$f) \text{ Sixth term: } \frac{1}{j\omega\epsilon} \sum_{s=1}^N a_s \left\langle \frac{\partial^2}{\partial y \partial x} H_{yx}(x, y, p(s), q(s)), T_y \right\rangle$$

The same procedure is valid for the third term of the IE (6.8). It can be obtained by  $B_x$  (basis oriented in  $x$  axis),  $T_y$  (testing oriented in  $y$  axis) pairs respectively. The third term of the IE in (6.8) can be given as follows

$$\frac{\partial}{\partial y} \frac{\partial}{\partial x} \int_{-\infty}^{\infty} \int_{-\infty}^{\infty} B_{x(s)}(x', y') G(x-x', y-y') dx' dy' \quad (6.65)$$

The convolution between basis and Green function can be represented by

$$H_{yx}(x, y, p(s), q(s)) = \int_{-\infty}^{\infty} \int_{-\infty}^{\infty} B_{x(s)}(x', y') G(x-x', y-y') dx' dy' \quad (6.66)$$

where  $H_{yx}$  is related with the near field radiation of the basis function  $B_x$  testing with  $T_y$ . It can be expanded by using orthogonal set of impulsive sinc functions

$$H_{yx}(x, y, p(s), q(s)) = \sum_{o=1}^K h_{yx_{d,\bar{r}}^{f,n}} \text{sinc}(2\tilde{W}_y y - \bar{q}(o)) \text{sinc}\left(2\tilde{W}_x x - \left(\bar{p}(o) - \frac{1}{2}\right)\right) \quad (6.67)$$

and the location of the sinc functions in  $x$  and  $y$  directions are at  $\bar{q}(o)t_y$  and  $\bar{p}(o)t_x - t_x/2$  respectively. The coefficients can be obtained by (6.66) and (6.67) and given as follows

$$hyx_{d,\bar{r}}^{f,n} \equiv \int_{-\infty}^{\infty} \int_{-\infty}^{\infty} \text{sinc}(2\tilde{W}_x x' - p(s)) \text{pulse}(y', q(s)\tilde{t}_y - \tilde{t}_y, q(s)\tilde{t}_y) G(\bar{p}(o)\tilde{t}_x - \tilde{t}_x/2 - x', \bar{q}(o)\tilde{t}_y - y') dx' dy'. \quad (6.68)$$

The above integral is approximated to a single integral for the case  $|p(s) - \bar{p}(o)| \geq 3$  and  $|q(s) - \bar{q}(o)| \geq 3$  by using the properties given in the Appendix B. The upper and lower limits are determined in terms of the location of the pulse function such as

$$hyx_{d,\bar{r}}^{f,n} = t_x \int_{y_s - \tilde{t}_y/2}^{y_s + \tilde{t}_y/2} \frac{e^{-jkR}}{4\pi R} dy' \quad (6.69)$$

where  $R = \sqrt{(\bar{p}(o)\tilde{t}_x - p(s)\tilde{t}_x - \tilde{t}_x/2)^2 + (\bar{q}(o)\tilde{t}_y - y')^2}$  and  $y_s = q(s)\tilde{t}_y - \tilde{t}_y/2$ . Let change the variables to  $v = \bar{q}(o)t_y - y'$ . Then the equation above becomes

$$hyx_{d,\bar{r}}^{f,n} = t_x \int_{(\bar{q}(o)-q(s))\tilde{t}_y}^{(\bar{q}(o)-q(s))\tilde{t}_y + \tilde{t}_y} \frac{e^{-jkR}}{4\pi R} dv \quad (6.70)$$

where  $R = \sqrt{v^2 + ((\bar{p}(o) - p(s))\tilde{t}_x - \tilde{t}_x/2)^2}$ . For the near field region,  $|p(s) - \bar{p}(o)| < 3$  and  $|q(s) - \bar{q}(o)| < 3$ , the singularity should be extracted from the integrand and evaluated analytically following the same procedure as in co-terms. Numerical differentiation is applied to the coefficients and the term is tested with  $T_y$ .

$$\begin{aligned} & \frac{1}{j\omega\epsilon} \sum_{s=1}^N a_s \frac{\partial^2}{\partial y \partial x} \int_{-\infty}^{\infty} \int_{-\infty}^{\infty} T_y(x, y) H_{yx}(x, y, p(s), q(s)) dx dy = \\ & \frac{1}{j\omega\epsilon} \tilde{t}_x \tilde{t}_y \sum_{s=1}^N a_s \left( \frac{hyx_{d+1,\bar{r}+1}^{f,n} - hyx_{d+1,\bar{r}-1}^{f,n} - hyx_{d-1,\bar{r}+1}^{f,n} + hyx_{d-1,\bar{r}-1}^{f,n}}{4t_x t_y} \right) \end{aligned} \quad (6.71)$$

The resulting equation with these coefficients are given as follows

$$\begin{aligned}
c_1 \tilde{t}_x \tilde{t}_y \sum_{s=1}^N a_s h_{xx}^{f,n} + \frac{c_2 \tilde{t}_x \tilde{t}_y}{t_x^2} \sum_{s=1}^N a_s \left[ h_{xx}^{f,n} - 2h_{xx}^{f,n} + h_{xx}^{f,n} \right] + c_2 \tilde{t}_x \tilde{t}_y \sum_{s=1}^K b_s \left[ \frac{h_{xy}^{\bar{f},\bar{n}} - h_{xy}^{\bar{f},\bar{n}} - h_{xy}^{\bar{f},\bar{n}} + h_{xy}^{\bar{f},\bar{n}}}{4t_x t_y} \right] \\
\cong -\tilde{t}_x \tilde{t}_y E_x^{in} (dt_x, rt_y - t_y / 2)
\end{aligned} \tag{6.72}$$

$$\begin{aligned}
c_1 \tilde{t}_x \tilde{t}_y \sum_{s=1}^K b_s h_{yy}^{\bar{f},\bar{n}} + \frac{c_2 \tilde{t}_x \tilde{t}_y}{t_y^2} \sum_{s=1}^K b_s \left[ h_{yy}^{\bar{f},\bar{n}} - 2h_{yy}^{\bar{f},\bar{n}} + h_{yy}^{\bar{f},\bar{n}} \right] + c_2 \tilde{t}_x \tilde{t}_y \sum_{s=1}^N a_s \left[ \frac{h_{yx}^{f,n} - h_{yx}^{f,n} - h_{yx}^{f,n} + h_{yx}^{f,n}}{4t_x t_y} \right] \\
\cong -\tilde{t}_x \tilde{t}_y E_y^{in} (\bar{d}t_x - t_x / 2, \bar{r}t_y)
\end{aligned} \tag{6.73}$$

where  $c_1 = -j\omega\mu$ ,  $c_2 = \frac{1}{j\omega\epsilon}$ ,  $\tilde{t}_x = \frac{l}{2\bar{W}_x}$ ,  $\tilde{t}_y = \frac{l}{2\bar{W}_y}$ ,  $f$  belongs to  $(p(s), q(s))$  pairs,  $\bar{f}$  belongs to  $(\bar{p}(s), \bar{q}(s))$  pairs,  $\bar{d} = \bar{p}(o)$  and  $\bar{r} = \bar{q}(o)$   $o = 1, 2, \dots, K$ ,  $d = p(o)$  and  $r = q(o)$  and  $o = 1, 2, \dots, N$ . The representations  $(dt_x, rt_y)$  and  $(\bar{d}t_x, \bar{r}t_y)$  are  $x$  and  $y$  coordinates of the observation points. Obtaining of the MoM matrix elements are shown in Figure 6.10.

Numerical differentiation is applied to coefficients by using forward and central difference methods given in Appendix A. These finite difference derivative errors can be reduced by decreasing mesh size at a reasonable level. Also, the overflow problem is tried to be reduced by this selection of the basis functions as sinc-pulse. The main difference from the previous section is choosing pulse basis parallel to the edge of the plate. Analytical properties of the sinc function given in Appendix B are used in the integral calculations. Since the sinc function approximation is used in the integral solutions, an error occurs in the coefficient matrix elements. The relative error coming from main matrix elements will be discussed in the next section. Some numerical results of the proposed formulations such as bistatic scattering from flat arbitrary plate at different observation angles are obtained and compared with the well known rooftop and SuperNEC in the next section.

For  $o = 1, 2, \dots NI$  Do

Obtain  $d, r$

For  $s = 1, 2, \dots NI$  Do

Obtain  $p(s), q(s)$

$$A_{NN}(o, s) = c_1 \tilde{t}_x \tilde{t}_y hxx_{d,r}^{f,n} + c_2 \frac{\tilde{t}_x \tilde{t}_y}{t_x^2} \left[ hxx_{d+1,r}^{f,n} - 2hxx_{d,r}^{f,n} + hxx_{d-1,r}^{f,n} \right]$$

End do

For  $\bar{s} = 1, 2, \dots KI$  Do

Obtain  $\bar{p}(s), \bar{q}(s)$

$$B_{NK}(o, \bar{s}) = c_2 \tilde{t}_x \tilde{t}_y \left[ \frac{hxy_{d+1,r+1}^{\bar{f},\bar{n}} - hxy_{d-1,r+1}^{\bar{f},\bar{n}} - hxy_{d+1,r-1}^{\bar{f},\bar{n}} + hxy_{d-1,r-1}^{\bar{f},\bar{n}}}{4t_x t_y} \right]$$

End do

Obtain  $-\tilde{t}_x \tilde{t}_y E_{x_v}^{in}(dt_x, rt_y)$  and  $-\tilde{t}_x \tilde{t}_y E_{x_h}^{in}(dt_x, rt_y)$

End do

For  $\bar{o} = 1, 2, \dots KI$  Do

Obtain  $\bar{d}, \bar{r}$

For  $\bar{s} = 1, 2, \dots KI$  Do

Obtain  $\bar{p}(s), \bar{q}(s)$

$$D_{KK}(\bar{o}, \bar{s}) = c_1 \tilde{t}_x \tilde{t}_y hyy_{\bar{d},\bar{r}}^{\bar{f},\bar{n}} + c_2 \frac{\tilde{t}_x \tilde{t}_y}{t_x^2} \left[ hyy_{\bar{d}+1,\bar{r}}^{\bar{f},\bar{n}} - 2hyy_{\bar{d},\bar{r}}^{\bar{f},\bar{n}} + hyy_{\bar{d}-1,\bar{r}}^{\bar{f},\bar{n}} \right]$$

End do

For  $s = 1, 2, \dots NI$  Do

Obtain  $p(s), q(s)$

$$C_{KN}(\bar{o}, s) = c_2 \tilde{t}_x \tilde{t}_y \left[ \frac{hyx_{\bar{d}+1,\bar{r}+1}^{f,n} - hyx_{\bar{d}-1,\bar{r}+1}^{f,n} - hyx_{\bar{d}+1,\bar{r}-1}^{f,n} + hyx_{\bar{d}-1,\bar{r}-1}^{f,n}}{4t_x t_y} \right]$$

End do

Obtain  $-\tilde{t}_x \tilde{t}_y E_{y_v}^{in}(\bar{d}t_x, \bar{r}t_y)$  and  $-\tilde{t}_x \tilde{t}_y E_{y_h}^{in}(\bar{d}t_x, \bar{r}t_y)$

End do

Figure 6.10. Obtaining the MoM matrix elements for the IE's (6.72) and (6.73).



## CHAPTER 7

### NUMERICAL RESULTS

The current densities and bistatic scattering results are given for arbitrary flat geometries which are illuminated with a uniform electromagnetic plane wave coming from  $(\theta^i, \varphi^i)$  direction which is shown in Figure 7.1. The numerical results of the proposed sinc-sinc and sinc-pulse based MoM formulations are given for different incident and observation directions. The bandwidth of the sinc function,  $W$ , is taken 500 and the halfwidth of the subintervals,  $t_x$ , is taken  $1/(2W)$  in the simulations. Simulations are carried out on a personal computer, which has Intel (R) CPU 1.8 GHz processor with 2.49 GB RAM on the windows operating system. After simulations it has been observed that at least 15 discretizations for each wavelength are enough in the numerical modeling to get accurate and convergent results. The Fortran90 computer codes are developed for sinc-sinc and sinc-pulse based formulations. The pseudocodes of the programs are given in chapter 5 and chapter 6. The main subroutines which are used in codes are given in Appendix C. The simulation results obtained from the sinc based formulations are in good agreement with those obtained from SuperNEC and ordinary rooftop. The bistatic scattering are presented here for co-polarized and cross-polarized cases.

#### 7.1. Square Flat Plate

The geometry of the square flat plate illuminated with a plane wave with the incident elevation angle  $\theta_i$  and azimuth angles  $\varphi_m$  are shown in Figure 7.1. Galerkin sinc-sinc and Galerkin rooftop based MoM simulation results are compared with those of the non-Galerkin pulse-sinc based results. The x directed current densities of rooftop, sinc-sinc and sinc-pulse based formulations are given in Figure 7.2 for  $1\lambda \times 1\lambda$  square plate at the vertical polarization with the angles  $\theta_i = 45^\circ$ ,  $\varphi_m = 0^\circ$  respectively.

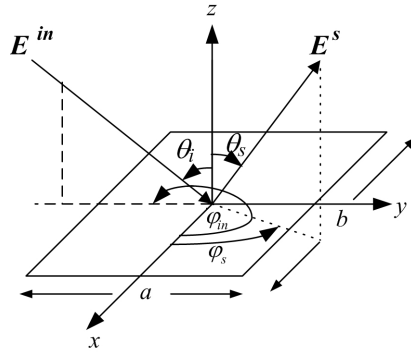
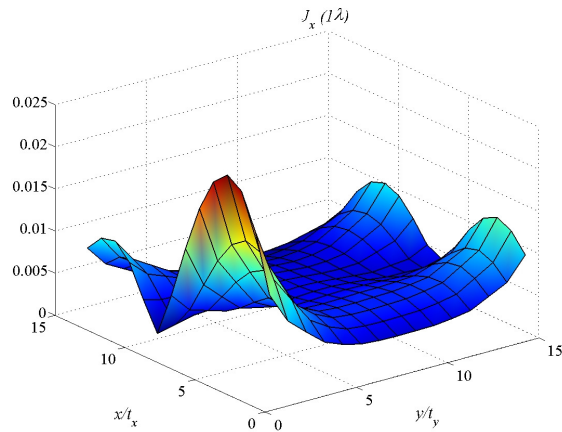
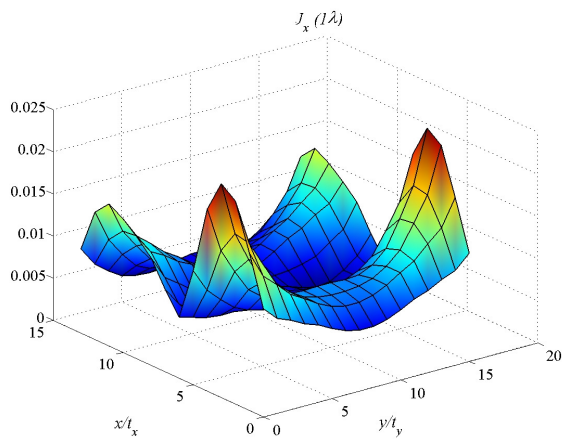


Figure 7.1. Flat plate illuminated with a plane wave.

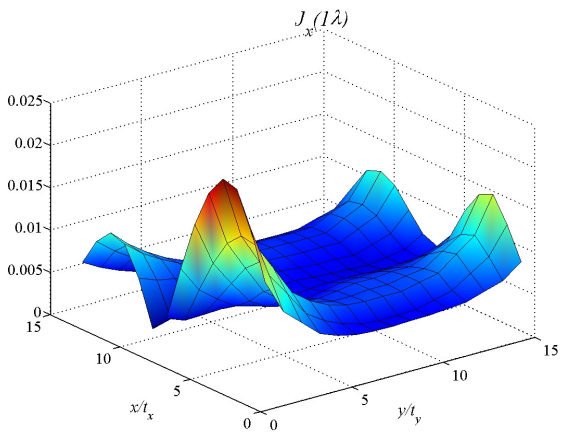
One can observe from the Figure 7.2 that the results obtained from sinc based formulations are similar with those of rooftop basis. The relative error between the solutions of the current densities obtained from sinc pulse based and rooftop is 1%, while the relative error between sinc-sinc and rooftop results remains at 10% even in the high discretization levels. The current densities are compared for ycut ( $x=0$ ) and xcut situations in Figure 7.3. The x directed current density results of those of the sinc-pulse are more similar to those of the rooftop than the sinc-sinc based results. The x directed current densities of  $2\lambda \times 2\lambda$  flat square plates for the vertical polarization are given in Figure 7.4. The ycut ( $x=0$ ) and xcut ( $y=0$ ) situations of the x directed current density for  $2\lambda \times 2\lambda$  flat plate is given in Figure 7.5. The maximum discretization number is 30, and  $n_x = 1, 2, \dots, 30$  and  $n_y = 1, 2, \dots, 30$ . Sinc-pulse and sinc-sinc based results are similar to rooftop based results. Vertically polarized y directed current densities of sinc-sinc, sinc-pulse and rooftop based formulations are given in Figure 7.6. Sinc-pulse based current densities are similar to rooftop based simulation results. When the ycut ( $x=0$ ) and xcut ( $y=0$ ) situations of the y directed current density for  $2\lambda \times 2\lambda$  flat plate is compared in Figure 7.7, it is seen that they are generally following the same plot each other.



(a) rooftop



(b) sinc-sinc

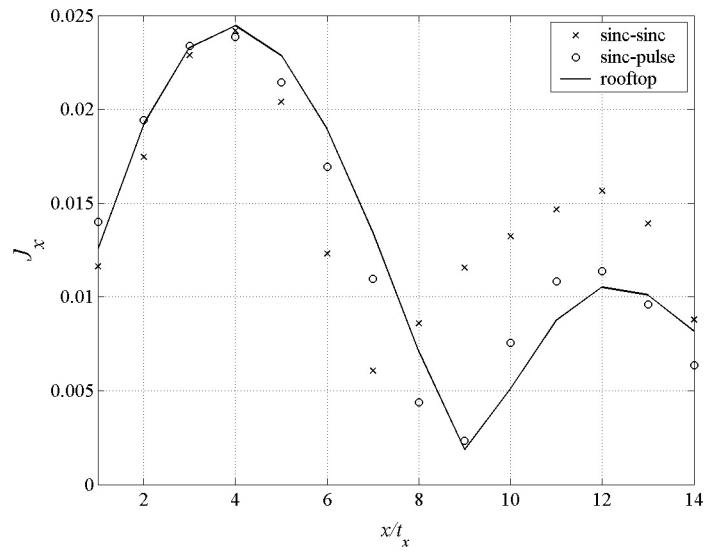


(b) pulse-sinc

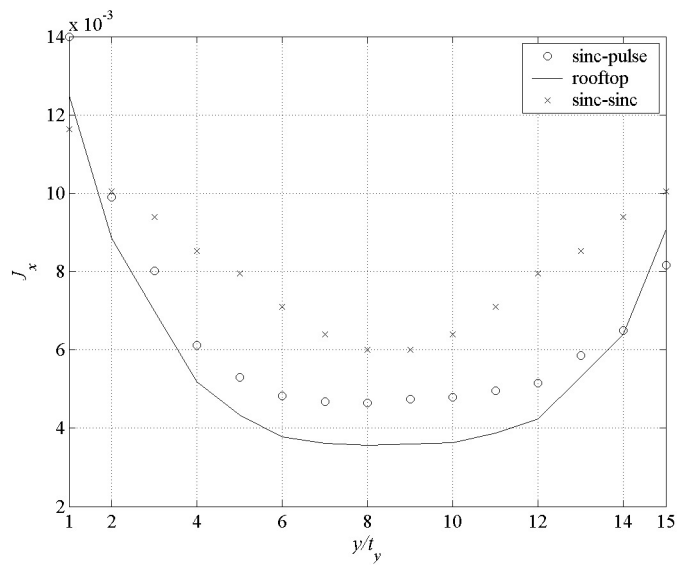
Figure 7.2. x directed current densities at the vertical polarization for  $1\lambda \times 1\lambda$  square flat plate with  $\theta_i = 45^\circ$ ,  $\varphi_m = 0^\circ$ ,  $t_x = t_y = \frac{1}{2W}$  and  $W = 500$ .

The vertically polarized x directed current densities for  $4\lambda \times 4\lambda$ ,  $5\lambda \times 5\lambda$ ,  $6\lambda \times 6\lambda$  square flat plates are given in Figure 7.8 for the rooftop based simulation

results. The ripples at x and y directions are increasing while the dimension of the geometry increases.

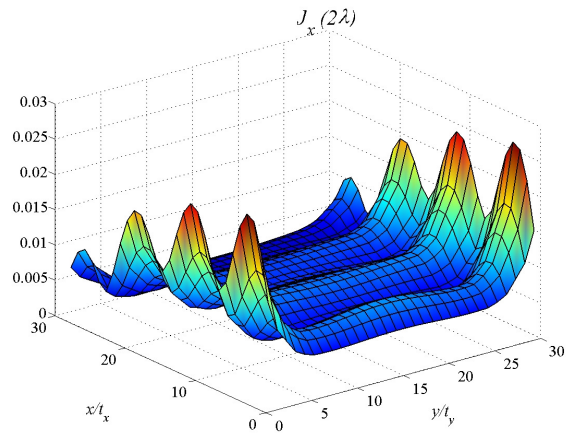


(a)

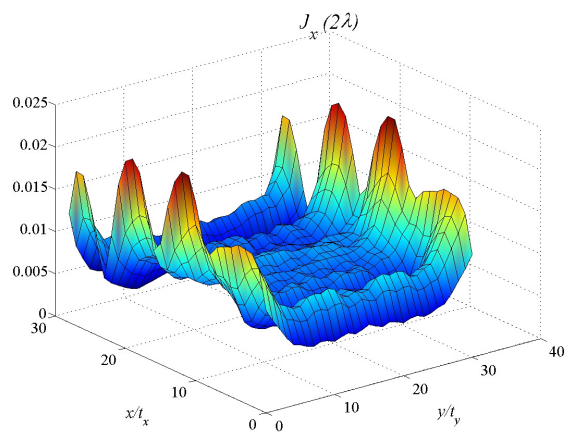


(b)

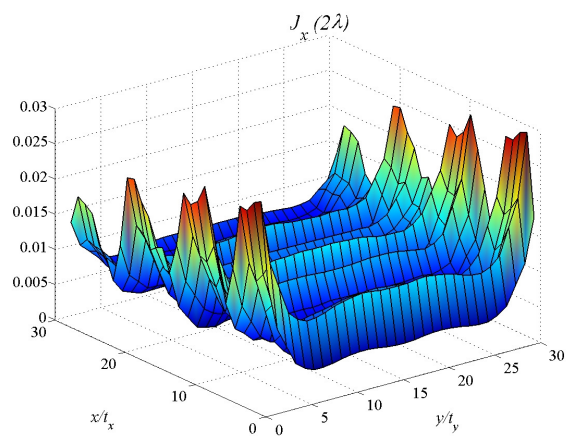
Figure 7.3. Comparison of the current densities at  $\theta_i = 45^\circ$ ,  $\varphi_{in} = 0^\circ$ . (a) ycut, (b) xcut.



(a) rooftop

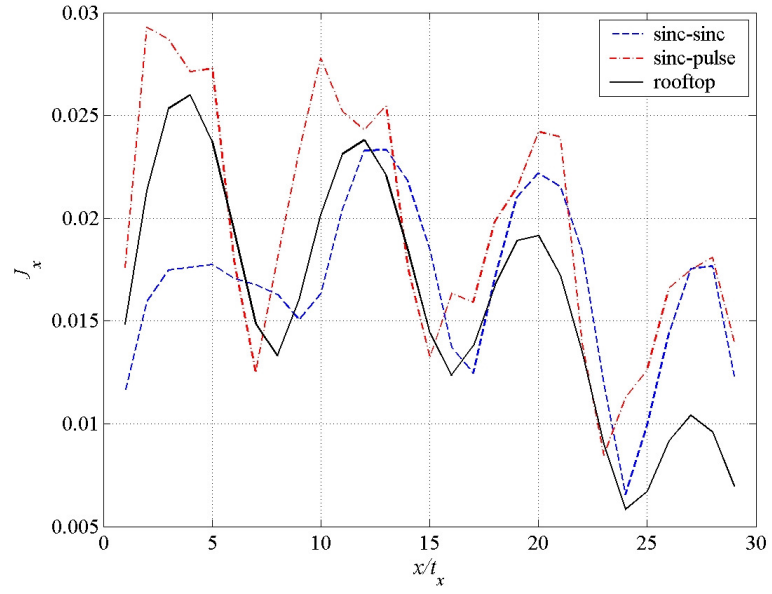


(b) sinc-sinc

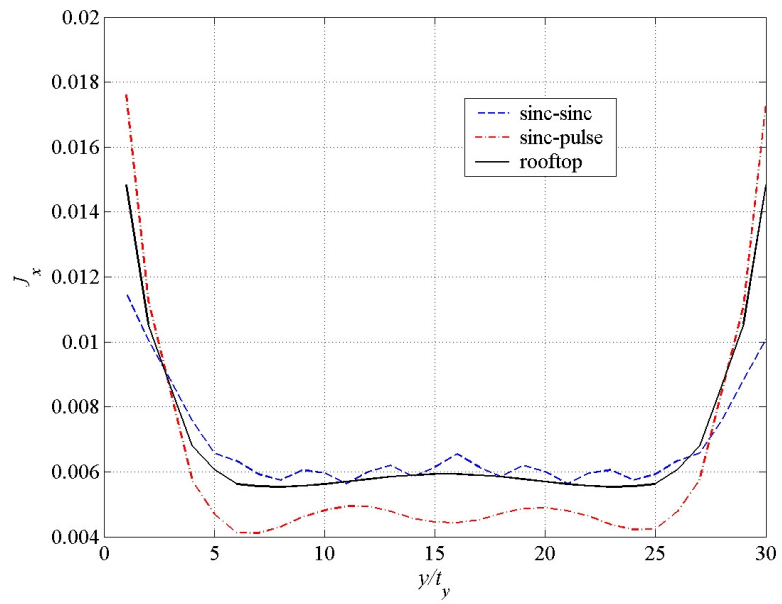


(c) sinc-pulse

Figure 7.4. x directed current densities at the vertical polarization for  $2\lambda \times 2\lambda$  square flat plate with  $\theta_i = 45^\circ$ ,  $\varphi_{in} = 0^\circ$ .

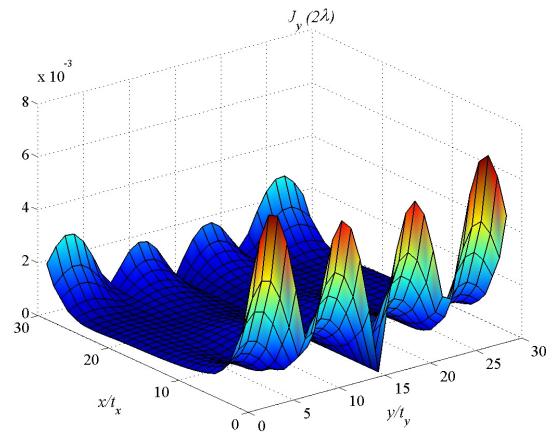


(a)

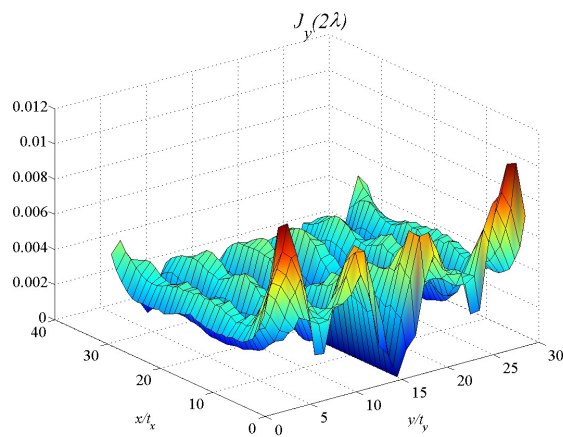


(b)

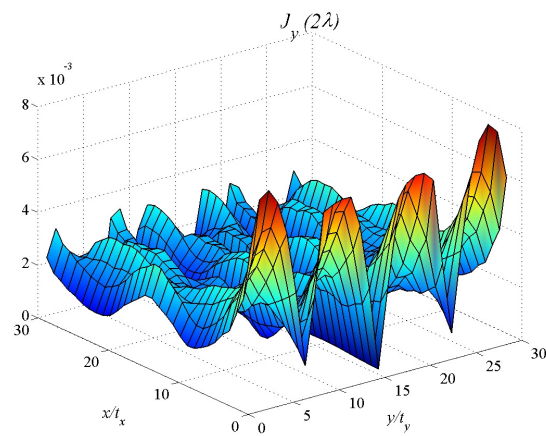
Figure 7.5. Compare of the vertically polarized x directed current densities at  $\theta_i = 45^\circ$ ,  $\varphi_m = 0^\circ$  for  $2\lambda \times 2\lambda$  square flat plates. (a) ycut, (b) xcut.



(a)

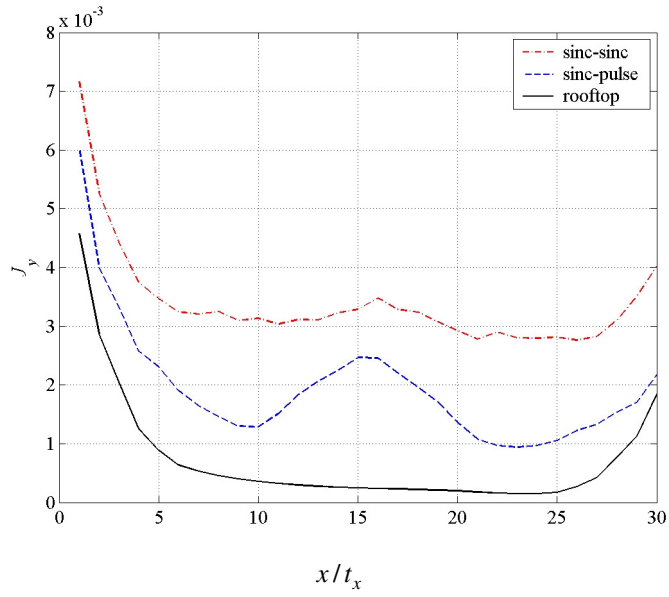


(b)

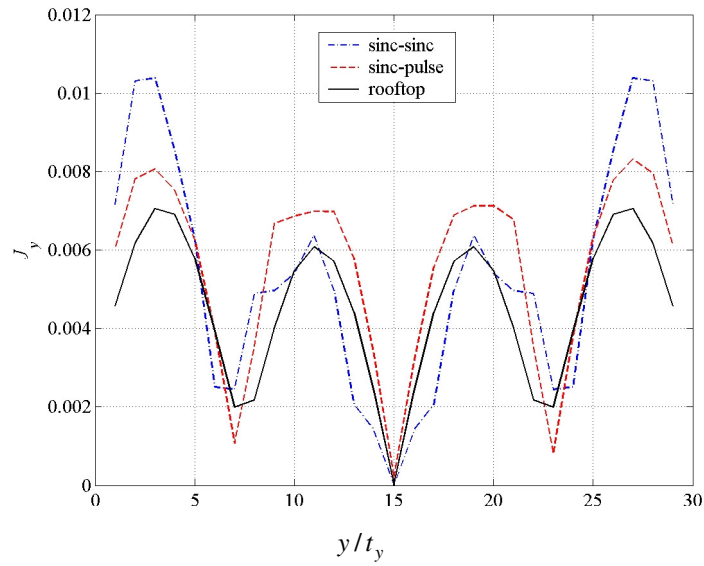


(c)

Figure 7.6. Vertically polarized  $y$  directed current densities at  $\theta_i = 45^\circ$ ,  $\varphi_m = 0^\circ$  for  $2\lambda \times 2\lambda$  square flat plates. (a) rooftop, (b) sinc-sinc, (c) sinc-pulse.



(a)



(b)

Figure 7.7. Comparison of the vertically polarized  $y$  directed current densities at  $\theta_i = 45^\circ$ ,  $\varphi_m = 0^\circ$  for  $2\lambda \times 2\lambda$  square flat plates. (a)  $y$ cut, (b)  $x$ cut.



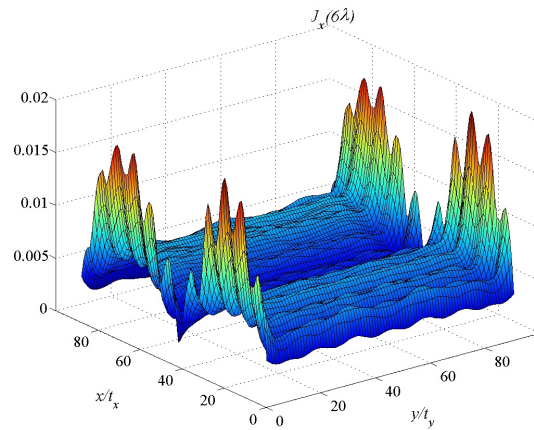
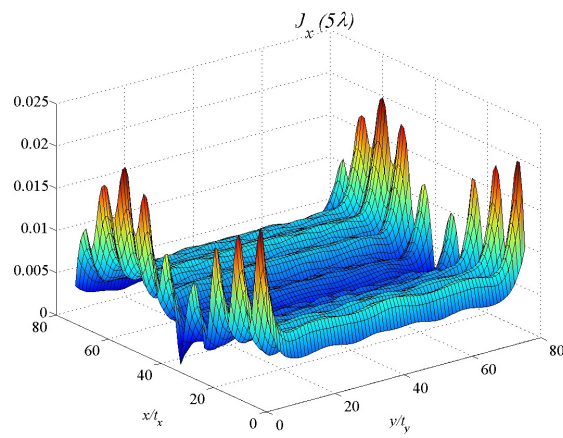
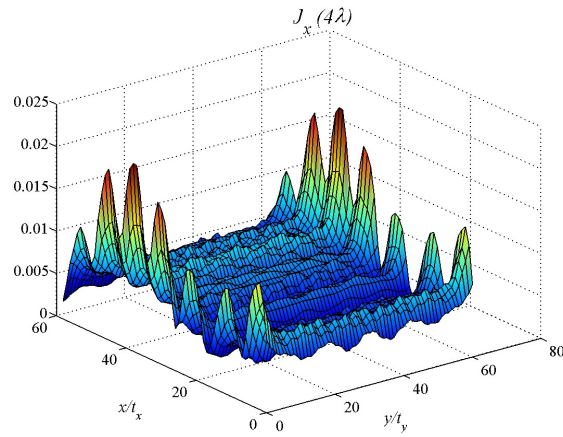


Figure 7.8. The vertically polarized  $x$  directed current densities of square flat plates at  $\theta_i = 45^\circ$ ,  $\varphi_{in} = 0^\circ$ :  $4\lambda \times 4\lambda$ ,  $5\lambda \times 5\lambda$ ,  $6\lambda \times 6\lambda$ .

The numerical results for bistatic RCS values are given in Figure 7.9 and Figure 7.10 for the  $4\lambda \times 4\lambda$  square flat plate shown in Figure 7.1. The results are in good agreement with those of the rooftop and SuperNEC ones. The results are nearly same

for all observation elevation angles. In the Figure 7.1, the plate is illuminated with incident angles,  $\varphi_{in} = 60^\circ$  and  $\theta_i = 45^\circ$  and bistatic scattering is observed at an angle  $\varphi_s = 60^\circ$  for cross- (vertical-horizontal, horizontal-vertical) and co-polarized (vertical-vertical, horizontal-horizontal) cases in terms of observation elevation angle  $\theta_s$ , which changes between  $0^\circ : 1^\circ : 360^\circ$ . The observation plane includes the specular reflection direction so the field is maximum for the co-polarized cases. The angle  $\theta_s$  is  $220^\circ$  and  $320^\circ$  for the specular reflection. The RCS level is low for the cross-polarized cases.

CPU time comparisons in seconds between the methods for flat square plates with different wavelengths are given in Table 7.1. It is observed that the matrix filling is faster in sinc based algorithms than those of the rooftop and SuperNEC. The mathematical properties of the sinc function is used in the formulations and matrix can be filled in less time by using the approximate functions given in (5.22) and (5.24). The matrix dimensions for the corresponding plate size are given in Table 7.2. The dimensions of the main matrices change, because discretization number changes in terms of the basis function and its step size. While the size of the main matrices increases, this difference in filling time also increases. If the linear matrix system is solved by using LU decomposition method, the overall time takes nearly two times of those of the SuperNEC for those of the sinc based. If an iterative solver is used by solving linear system equation, the overall time is decreased drastically. It is observed clearly that the use of the TFQMR increases the decrease in overall cpu time while the dimension of the problem increases when compared in terms of the LU decomposition. The overall time is decreased nearly the half of the time of that of SuperNEC. The overall CPU time of sinc based algorithms is faster than those of the well-known rooftop based Galerkin MoM formulation although their matrix dimensions are nearly the same. The  $4\lambda \times 4\lambda$  square flat plate scattering problem cannot be solved in hours with the optimum commercial code SuperNEC. Because of the dimension of the problem with these discretization (15 discretization for each wavelength) is out of the limit of the SuperNEC conditions. SuperNEC requires segments to be about a tenth of wavelength in length. Therefore, the sinc based algorithms can obtain the scattering results within hours. The sinc based algorithms fill the matrix in a shorter time and they can solve in less overall CPU time when compared to SuperNEC and rooftop.

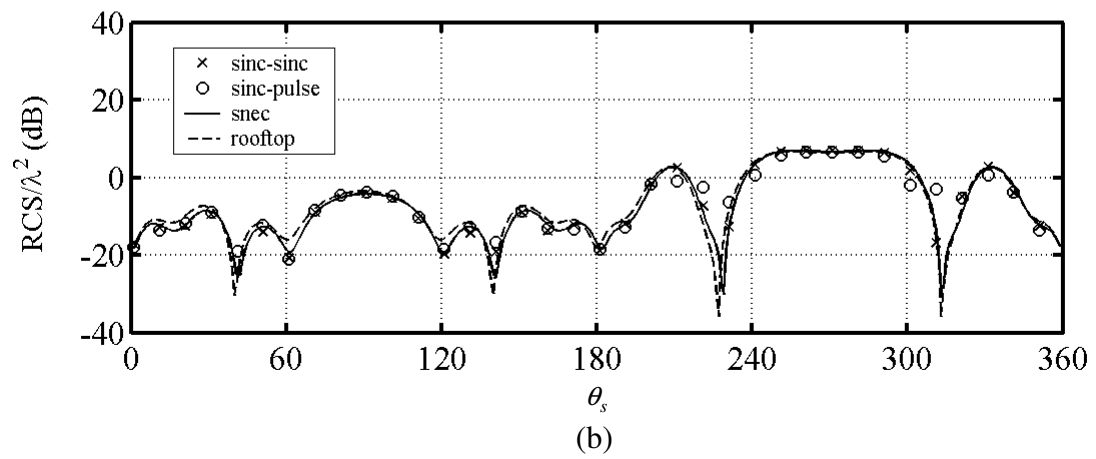
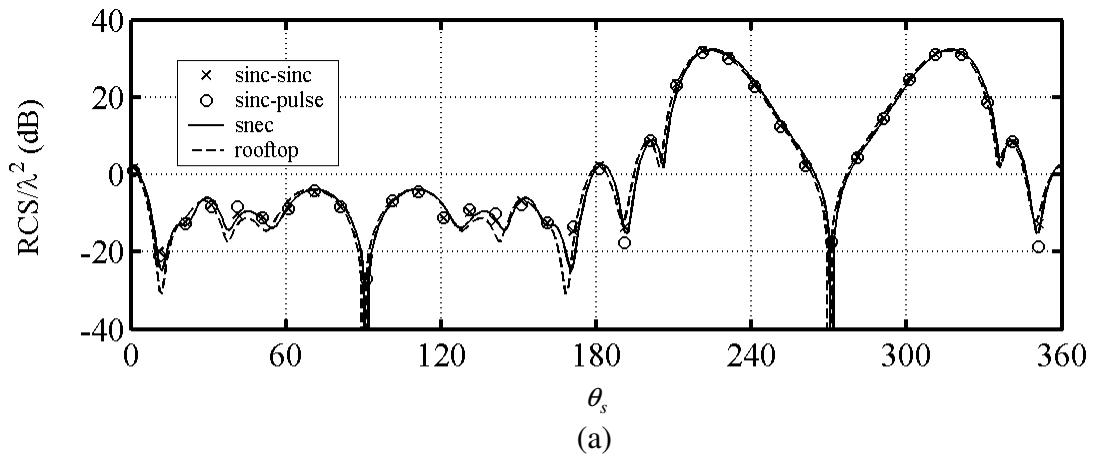


Figure 7.9. Bistatic scattering solutions of the  $4\lambda \times 4\lambda$  square flat plate ( $g_1$ ) at  $\varphi_{in} = 60^\circ$  and  $\theta_i = 45^\circ$ ,  $\varphi_s = 60^\circ$  while  $\theta_s = 0^\circ : 360^\circ$ . (a) co-polarized (vertical-vertical), (b) cross-polarized case (vertical-horizontal).

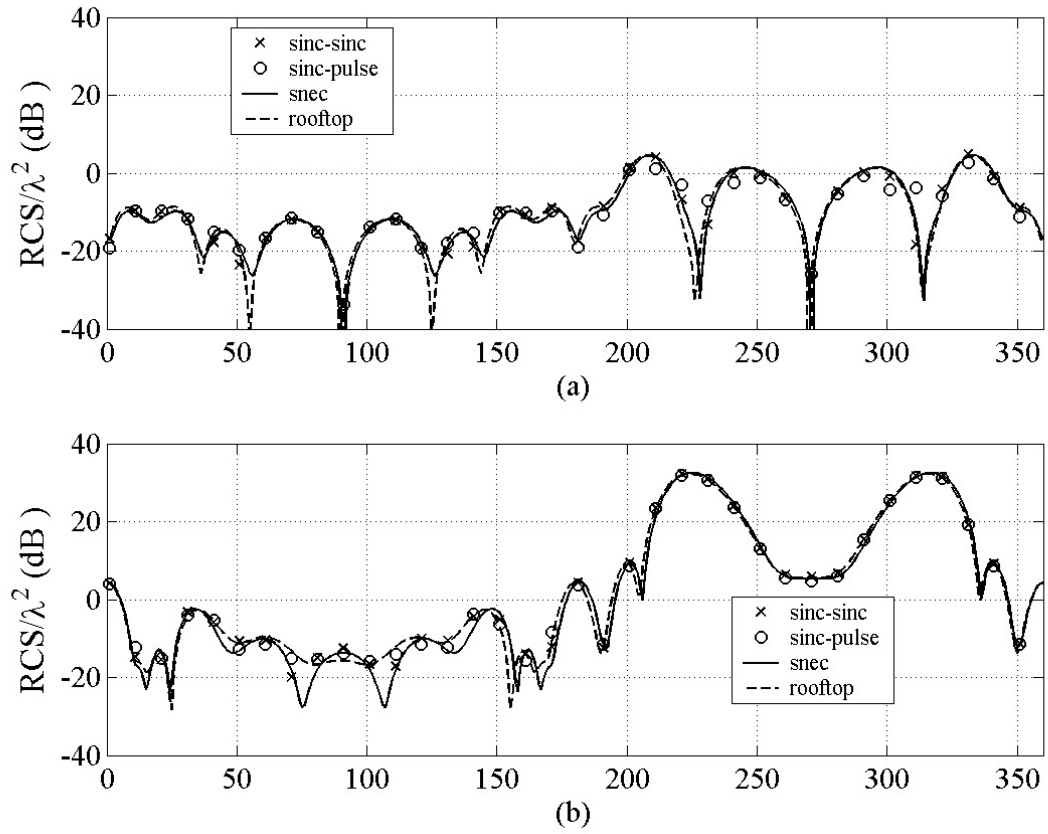


Figure 7.10. Bistatic scattering solutions of the  $4\lambda \times 4\lambda$  square flat plate ( $g_1$ ) at  $\varphi_{in} = 60^\circ$  and  $\theta_i = 45^\circ$ ,  $\varphi_s = 60^\circ$  while  $\theta_s = 0^\circ : 360^\circ$ . (a) cross-polarized (horizontal-vertical), (b) co-polarized case (horizontal-horizontal).

Table 7.1. CPU time comparisons of the MoM based formulations in seconds.

Dimension ( $a=b$ )	Sinc-sinc			Sinc-pulse			SNEC			Rooflop			
	Fill	Overall		Fill	Overall		Fill	Overall		Fill	Overall		
		LU	TFQMR		LU	TFQMR		LU	TFQMR		LU	TFQMR	
1 $\lambda$	0.06	1.6	2.7	0.09	1	2.3	3.6	0.8	1.7	-	1.61	161.7	164.1
2 $\lambda$	1.03	53.5	16	1.01	9.42	54	17	10.4	38.4	-	6.8	665	632
3 $\lambda$	7	590.1	96	7	32	552	90	46	350	-	1389	2001	1500
3.6 $\lambda$	15	1750	275	10.9	40	1759	270	91.2	534.8	-	1985	3646	2168
4 $\lambda$	25	6068	559	17	44	6081	600	*	*	-	2452	8059	2795

\*Out of memory, exceeds 3GB RAM.

-SuperNEC uses LU factorization in solving the system matrix.

Table 7.2. Matrix dimensions of the problems  $((N + K) \times (N + K))$

	Sinc-sinc	Sinc-pulse	SNEC	Rooftop
$1\lambda$	448 x 448	420 x 420	480 x 480	420 x 420
$2\lambda$	1798 x 1798	1740 x 1740	1860 x 1860	1740 x 1740
$3\lambda$	4048 x 4048	3960 x 3960	4140 x 4140	3960 x 3960
$3.6\lambda$	5830 x 5830	5724 x 5724	5940 x 5940	5724 x 5724
$4\lambda$	7198 x 7198	7080 x 7080	7320 x 7320	7080 x 7080

## 7.2. Error Analysis in the MoM Matrix Elements

The approximation of the integral of Sinc functions with Green's function is used by calculating the matrix elements in MoM. The approximated integral is shown in the below equation

$$\underbrace{\int_{-\infty}^{\infty} \int_{-\infty}^{\infty} \text{sinc}(2W_x u - L) \text{sinc}(2W_y v - M) G(u, v) du dv}_{I_1} = \underbrace{\frac{1}{4W_x W_y} G(|L|t_x, |M|t_y)}_{I_2} + \text{error} \quad (7.1)$$

where  $L = p(o) - p(s)$ ,  $M = q(o) - q(s)$  and  $t_x = t_y = 1/(2W)$ . The bandwidths of the sinc functions in  $x$  and  $y$  directions are given as  $w_x$  and  $w_y$  respectively so it is given  $w_x = w_y = w$  in (7.1). The error is calculated with the difference of the integrals between  $I_1$  and  $I_2$ . The relative error is the ratio of this difference to the exact value of  $I_2$ . For  $|L| < 2$  and  $|M| < 2$ , the double integral are evaluated numerically without any problem. The approximated value shown in (7.1) is used for  $|L| \geq 2$  and  $|M| \geq 2$ .

The MoM matrix elements are computed by using the analytical properties of the sinc functions given in (7.1). The approximated sinc integrals in the equations that constitute the matrix coefficients are therefore evaluated with an error. The relative error given in the Table 7.3 is calculated by using the difference between actual and approximated value of the integral given in equation (7.1) according to the distance

between source and observation points. Numerical integration technique, Simpson rule with 5000 subdivisions is used to evaluate the left hand side integral equation  $I_1$  given in (7.1) over the interval  $[-0.1 \ 0.1]$ . The numerical solutions for different  $L$  and  $M$  values are given in Table 7.3. The bandwidth of the sinc function is taken  $w_x = w_y = W$  and changes between 250 and 1000 where  $L$  and  $M$  increase which are the difference between observation and source points at  $x$  and  $y$  directions respectively. One can observe from Table 7.3 that the relative error in the computed matrix decreases while  $L$  and  $M$  increase, the observation and source points are getting far from each other. As can be seen from Table 7.3 that the relative error in the computed matrix elements decreases while  $W$  increases. The relative error values for  $L=2$  and  $M=3$  are same while the bandwidth of the sinc function increases. The relative error decreases while  $L$  and  $M$  increases for the bandwidths greater and equal than 500. In summary, for  $L > 1$  and  $M > 1$  the approximate integral equation of the sinc function shown in (7.1) as  $I_2$  can be used in obtaining matrix elements for the bandwidths greater and equal to 500.

Table 7.3. Relative error in the computed matrix elements (%).

$W^{(1)}$ \ L, M	2, 2	2, 3	3, 2	3, 3
250	0.103	0.070	0.070	0.093
300	0.098	0.071	0.071	0.077
500	0.095	0.071	0.071	0.061
750	0.095	0.071	0.071	0.059
1000	0.095	0.071	0.071	0.058

<sup>(1)</sup>  $\lambda = 0.015m, t_x = t_y = 1/(2W)$ .

### 7.3. Arbitrary Flat Plate Geometries

The flat arbitrary geometries are given in Figure 7.11. The plates are illuminated with a plane wave and their bistatic scattering results are given at different observation angles.

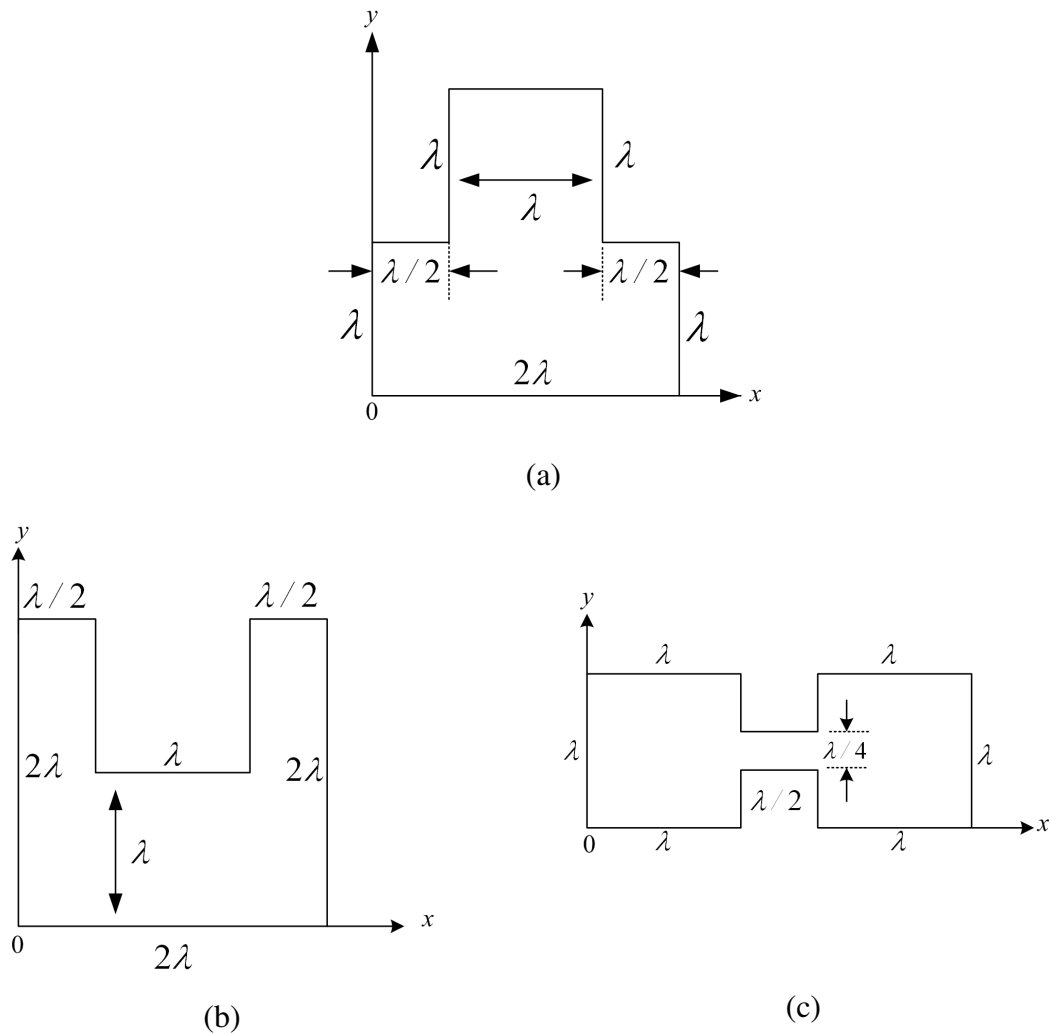


Figure 7.11. Arbitrary flat plate geometries. (a)  $g_2$ , (b)  $g_3$ , (c)  $g_4$ .

In the Figures 7.12 and 7.13, the incident azimuth and elevation angles are given as  $\varphi_m = 30^\circ$  and  $\theta_i = 45^\circ$  for the geometry shown in Figure 7.11(a). Also the observation plane is defined as  $\varphi_s = 30^\circ$  and the scattering results are obtained for the variational observation angles  $\theta_s = 0^\circ:360^\circ$ . It is seen from Figures 7.12 and 7.13 that they are similar with those of SuperNEC and rooftop solutions. The scattering results are in good agreement nearly at all observation angles. In this case, the observation plane has the



specular reflection direction. The RCS level is high like in Figures (7.9) and (7.10) for co polarized cases.

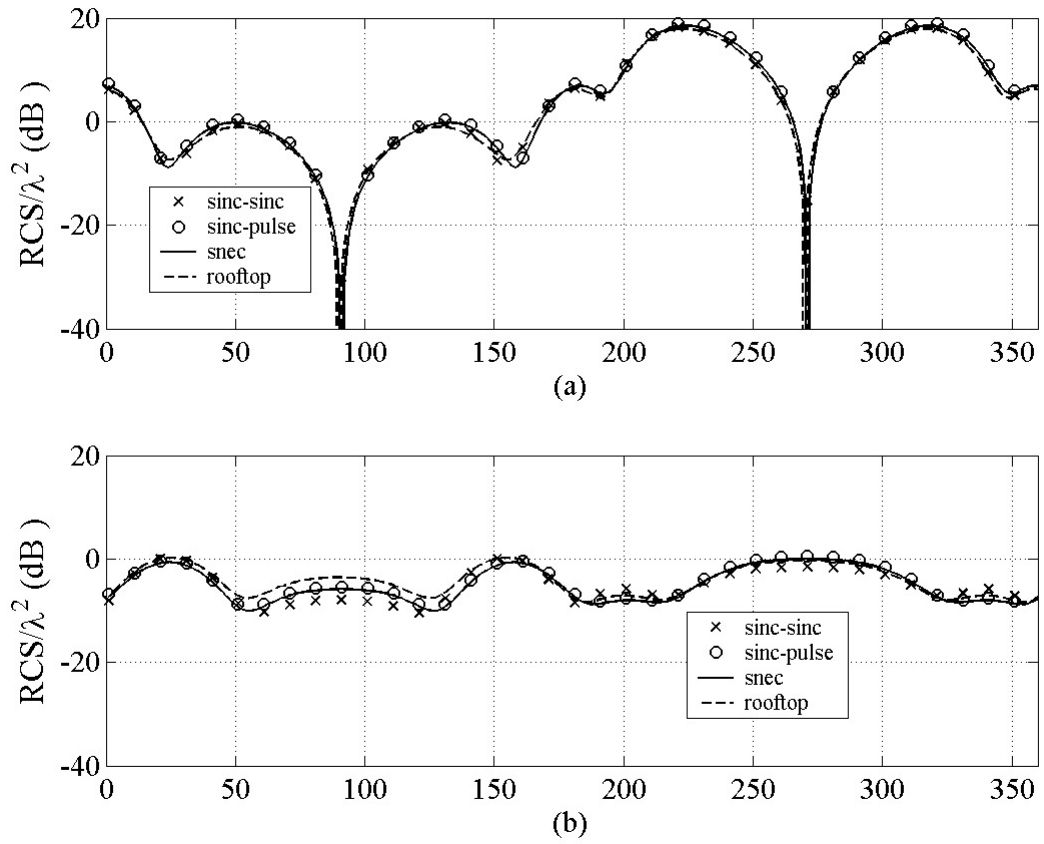


Figure 7.12. Bistatic scattering of the arbitrary geometry  $g_2$  for  $\varphi_{in} = 30^\circ$  and  $\theta_i = 45^\circ$ ,  $\varphi_s = 30^\circ$  while  $\theta_s = 0^\circ:360^\circ$ . (a) co-polarized (vertical-vertical) results, (b) cross-polarized (vertical-horizontal) results.

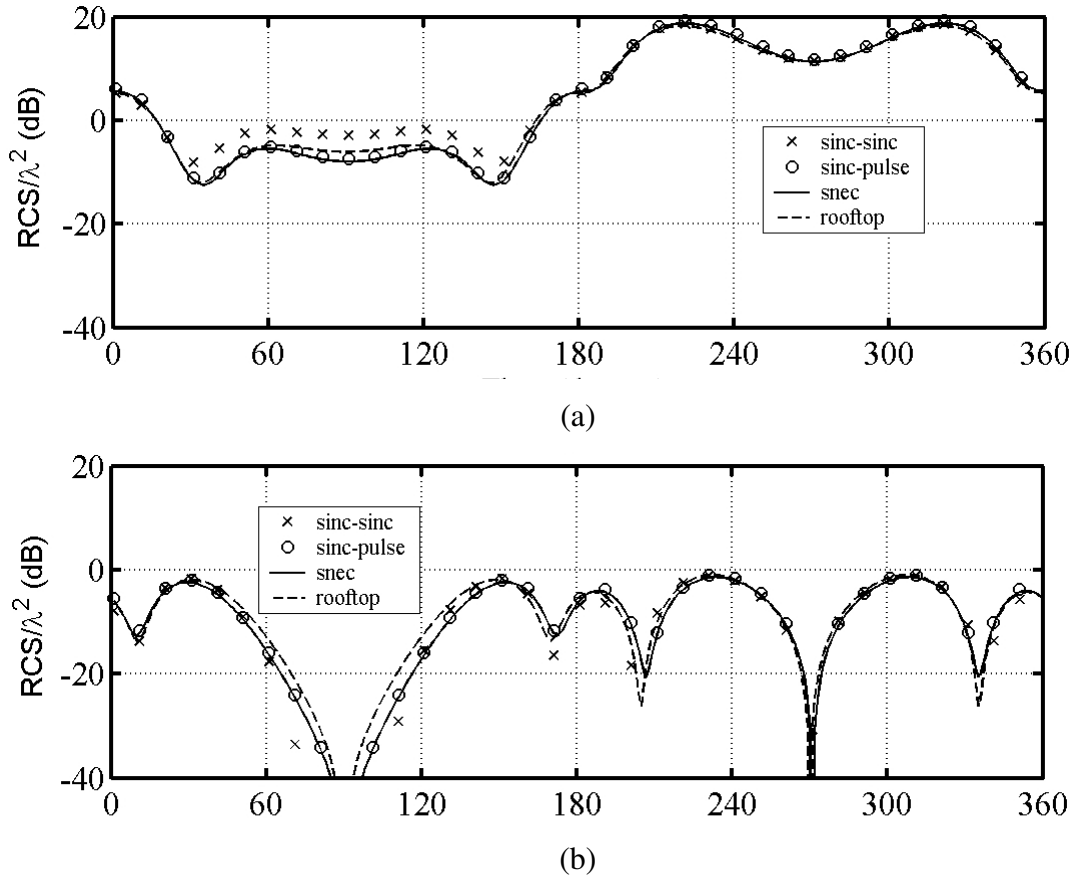


Figure 7.13. Bistatic scattering of the arbitrary geometry  $g_2$  for  $\varphi_m = 30^\circ$  and  $\theta_i = 45^\circ$ ,  $\varphi_s = 30^\circ$  while  $\theta_s = 0^\circ:360^\circ$ . (a)co-polarized (horizontal-horizontal) results, (b) cross-polarized (horizontal-vertical) results.

The bistatic scattering solutions of the geometry shown in Figure 7.11(b) are given in Figures 7.14. and 7.15. The RCS comparison is made for the incident angles given as  $\varphi_m = 60^\circ$  and  $\theta_i = 45^\circ$  while  $\varphi_s = 30^\circ$  and  $\varphi_s = 60^\circ$  cases. The results are again reasonably in good agreement with the SuperNEC and rooftop solutions. In part (a) of the figure, the nonspecular case is presented. Even though it does not include the specular reflection direction (the RCS level is low) the results show that it is again in good agreement. In the part (b) of the same figure, the specular observation plane is studied and it is seen that the results are again good even it presents cross-polarized components.

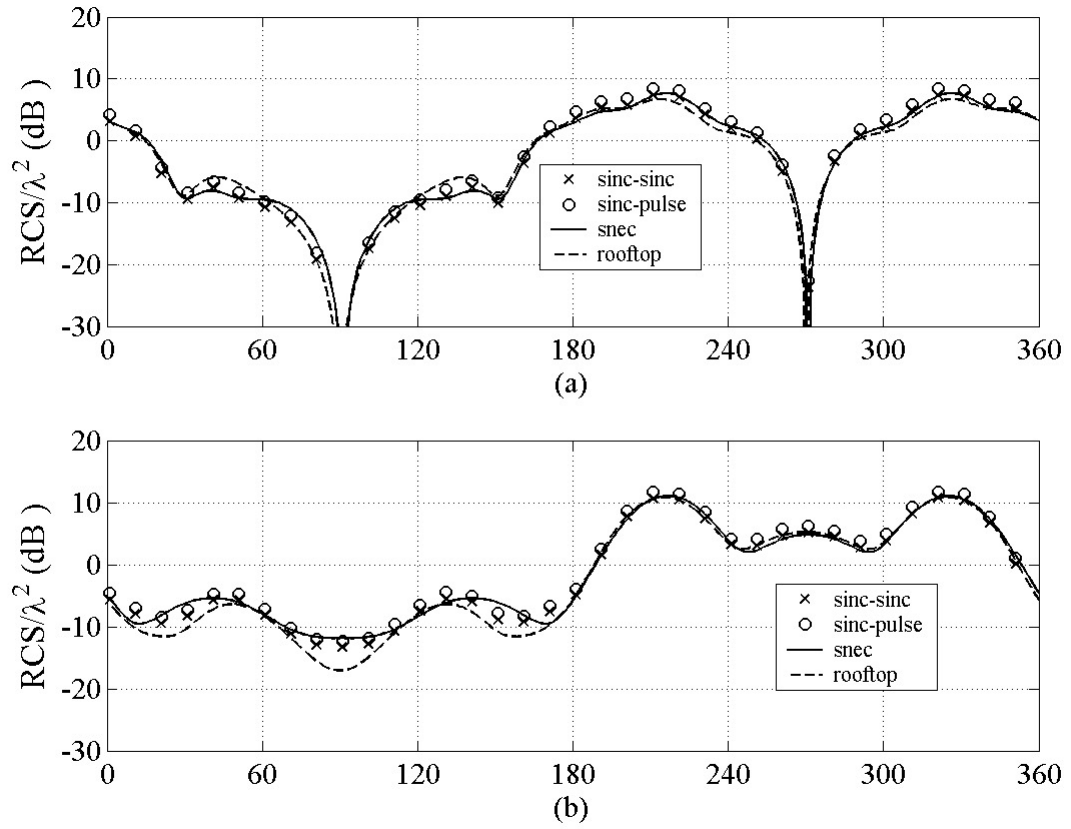


Figure 7.14. Compare of the RCS results for arbitrary geometry  $g_3$  for  $\varphi_{in} = 60^\circ$ ,  $\theta_i = 45^\circ$  while  $\theta_s = 0^\circ:360^\circ$ . (a) RCS VV co-polarized case  $\varphi_s = 30^\circ$ , (b) RCS VH cross-polarized case  $\varphi_s = 30^\circ$ .

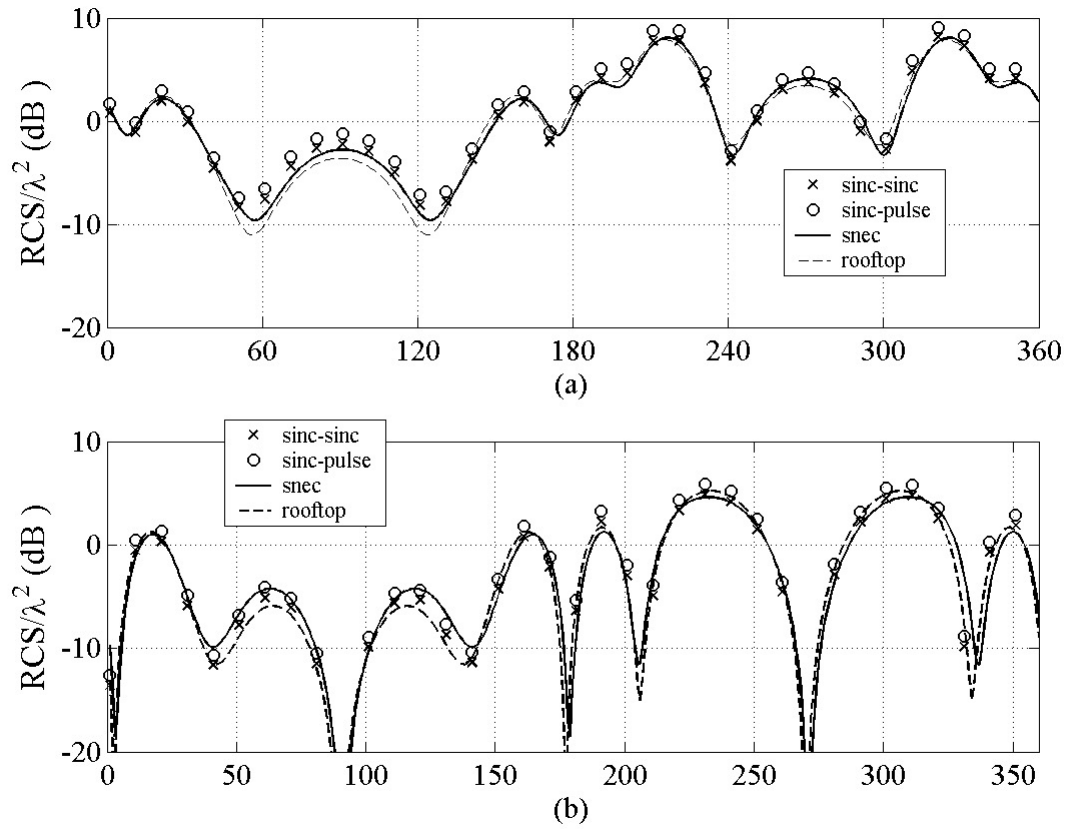


Figure 7.15. Compare of the RCS results for arbitrary geometry  $g_3$  for  $\varphi_{in} = 60^\circ$ ,  $\theta_i = 45^\circ$  while  $\theta_s = 0^\circ:360^\circ$ . (a) RCS HH co-polarized case  $\varphi_s = 30^\circ$ , (b) RCS HV cross-polarized case  $\varphi_s = 30^\circ$ .

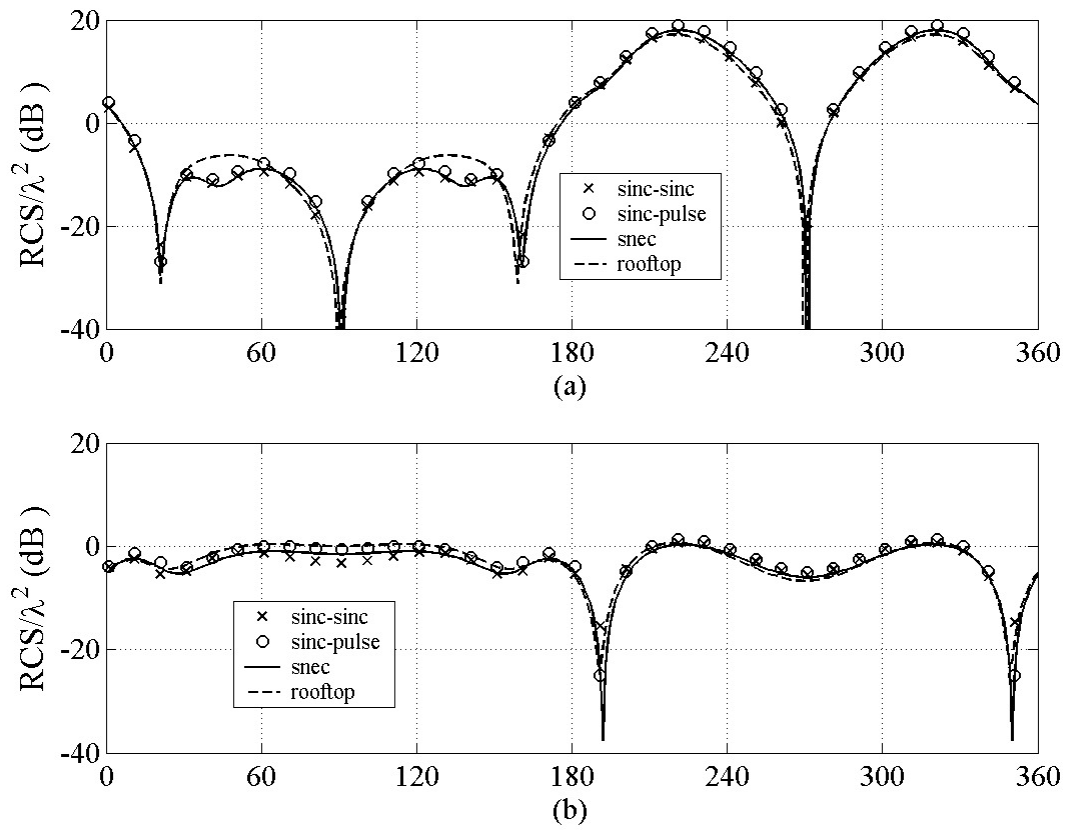


Figure 7.16. Compare of the RCS results for arbitrary geometry  $g_3$  for  $\phi_{in} = 60^\circ$ ,  $\theta_i = 45^\circ$  while  $\theta_s = 0^\circ:360^\circ$ . (a) RCS VV co-polarized case  $\phi_s = 60^\circ$ , (b) RCS VH cross-polarized case  $\phi_s = 60^\circ$ .

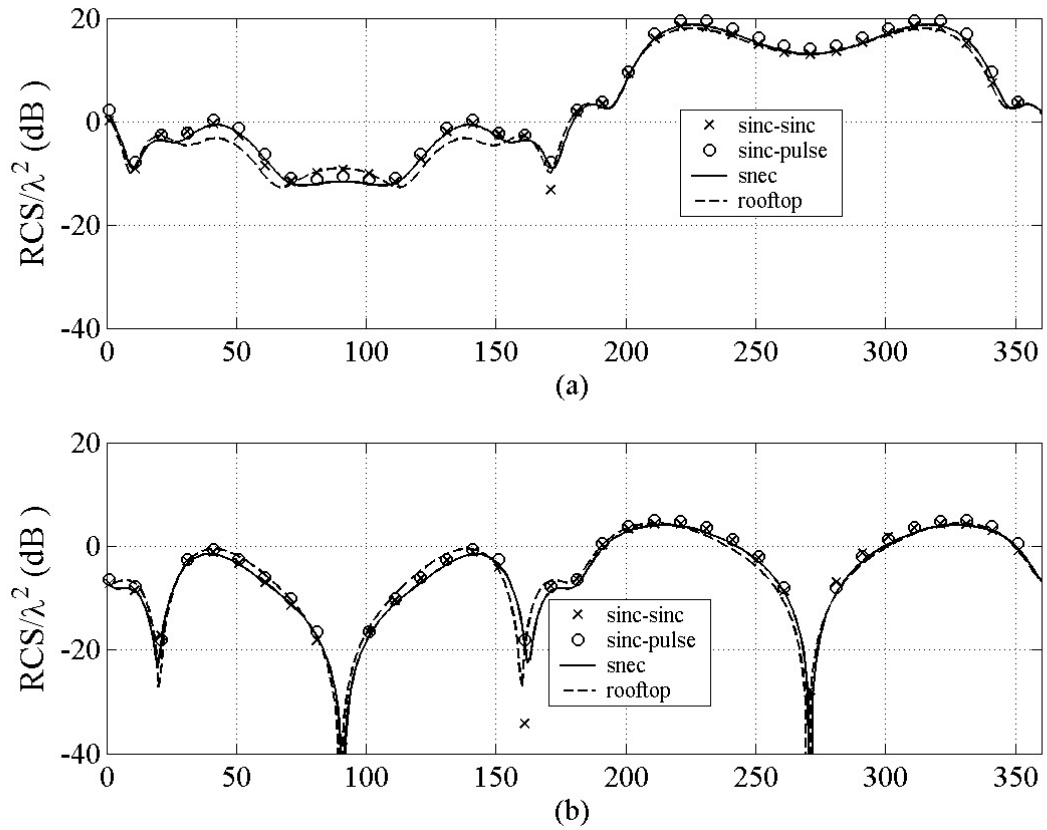


Figure 7.17. Compare of the RCS results for arbitrary geometry  $g_3$  for  $\varphi_{in} = 60^\circ$ ,  $\theta_i = 45^\circ$ ,  $\theta_s = 0^\circ:360^\circ$ . (a) RCS HH co-polarized case  $\varphi_s = 60^\circ$ , (b) RCS HV cross-polarized case  $\varphi_s = 60^\circ$ .

The bistatic scattering results of an arbitrary geometry given in Figure 7.11(c) illuminated with the incident angles  $\varphi_{in} = 0^\circ$  and  $\theta_i = 45^\circ$  shown in Figure 7.18. In the part (a) of the figure, the results are obtained for the plane including the specular direction and it is seen that the good agreement is obtained in the part (b) of the same figure, again the co-polarized results are presented and again the results are reasonably good even though the RCS level is lower.

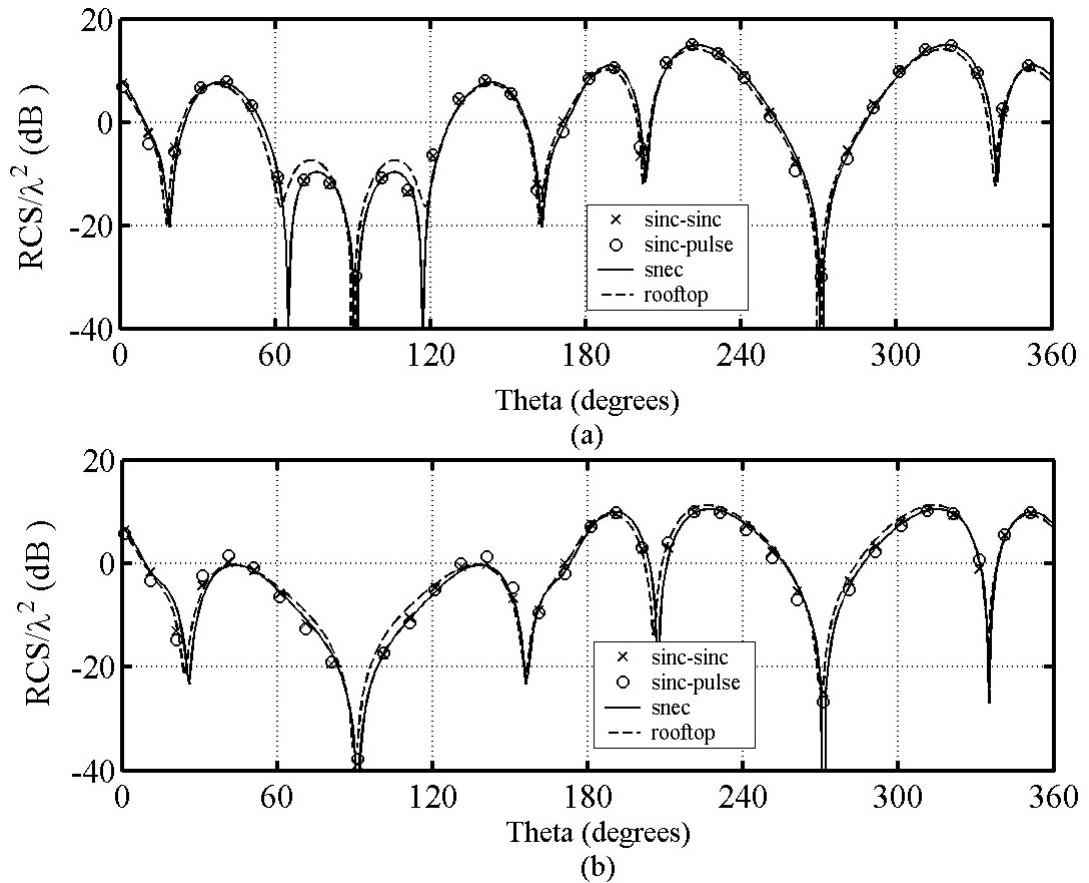


Figure 7.18. Bistatic scattering results of the arbitrary geometry  $g_4$   
 $\varphi_{in} = 0^\circ, \theta_i = 45^\circ, \theta_s = 0^\circ:360^\circ$  (a) co-polarized (vertical-vertical) at specular reflection direction  $\varphi_s = 0^\circ$ , (b) co-polarized (vertical-vertical) at nonspecular reflection direction  $\varphi_s = 30^\circ$ .

The bistatic scattering results obtained by sinc-based formulations are in good agreement with those of rooftop and SuperNEC. An error occurs in the approximated sinc integrals during obtaining matrix coefficients. However, this error stays under 0.061% for the bandwidth that is used in simulations. Additionally, less CPU time is spent in sinc-based formulation than those of the rooftop, while the coefficient matrix is filled. Large geometries can not be solved with SuperNEC on the personal computer because of the software limits, although they can be solved with developed fortran program including sinc formulation. Furthermore, overall CPU time of the program developed by sinc-based formulation is decreased by using iterative algorithms.

## CHAPTER 8

### CONCLUSIONS

Three dimensional electromagnetic scattering from flat arbitrary plates illuminated by a plane wave is numerically solved by using different sinc type basis functions in MoM. The sinc based formulations are obtained with Galerkin and non-Galerkin procedures. The formulation highly depends on the mathematical properties of the sinc functions. Easy implementation of the sinc functions provides fast and accurate results during simulations. The pseudocodes for sinc based algorithms are given in related chapters. Fortran computer language is used for programming. 15 discretizations per  $\lambda$  is taken in the simulations.

The effective rooftop based Galerkin algorithm is employed. Rooftop based formulation is well-known and mostly used in MoM. The unknown current densities are solved here with the subsectional basis functions such as triangular and pulse. The MoM matrix elements are evaluated numerically, not analytically as mentioned in [56]. The proposed sinc-sinc based results in the study are compared with those of the rooftop and SuperNEC in terms of accuracy and CPU time. 15 discretizations are used in the simulations. Current densities and bistatic scattering results of the rooftop based formulations at specular and nonspecular directions for flat plates are used for comparisons.

Sinc-sinc based MoM Galerkin formulation is developed with an effective algorithm. The formulation depends on the mathematical properties of the sinc functions such as convolution and interpolation. The accuracy of the program is tested with those of rooftop and the well-known software SuperNEC. Bistatic scattering results of the proposed sinc based solution method for specular reflection direction are compared with those of the well known MoM method for different observation elevation angles. Maximum field is obtained at the specular reflection direction for co-polarized cases. However, the RCS level is low for the cross-polarized cases. All results are in good agreement with those of the SuperNEC.

Sinc-pulse Galerkin and non-Galerkin MoM formulations are employed for flat geometries. In order to reduce the overflow problem at the edges, the pulse type basis



function is chosen perpendicular to the edge direction. Even the sinc-pulse based formulation is totally different from the sinc-sinc based formulation, their results are the same as those of the rooftop and SuperNEC. The RCS level obtained from pulse-sinc based formulation is the same as those of rooftop and SuperNEC.

Fortran is used in the numerical simulations. Our main goal is to obtain accurate bistatic scattering solutions in less CPU time. Using the mathematical properties of the sinc function in the formulation provides easy and fast computing, so the codes of the sinc based algorithms fill the main matrices quite faster than the other known ordinary methods. However, the overall running time is just slightly better than the rooftop MoM. Also our basis functions are in the sinc type and so their inclusion to the formulation is easier than the other complex basis functions like given in the equations (5.22) and (5.24). The overall CPU is decreased by using iterative solvers in solving MoM matrix elements. TFQMR method is used with preconditioning in solving linear matrix system and the overall CPU time is decreased when compared with those of SuperNEC and rooftop.

The relative error that occurred during the calculation of the MoM matrix elements is at a reasonable level. The error decreases appreciably while the bandwidth of the sinc function increases.

Linear algebraic equation system is solved iteratively using preconditioning, so the overall running time of the sinc based algorithms is reduced highly.

## REFERENCES

- [1] R. F. Harrington, Time Harmonic Electromagnetic Fields, IEEE Press, John Wiley and Sons, 2001.
- [2] R. F. Harrington, Field Computation by Moment Methods, New York, IEEE Press 1993.
- [3] A. F. Peterson, S. L. Ray, R. Mittra, Computational Methods for Electromagnetics, New York, IEEE Press, 1998.
- [4] C. A. Balanis, Advanced Engineering Electromagnetics, USA, John Wiley and Sons, 1989.
- [5] V. H. Rumsey, "Reaction Concept in Electromagnetic Theory", Physical Review, vol. 94, no.6, pp. 1483-1491, June 1954.
- [6] S. M. Rao, D. R. Wilton, A. W. Glisson, "Electromagnetic Scattering by arbitrary Shape", IEEE Trans. on Antennas Propagation, Vol. AP-30, no.3, pp. 409-418, 1982.
- [7] M. R. Barclay, Willard V. T. Rusch, "Moment-Method Analysis of Large, Axially Symmetric Reflector Antennas Using Entire-Domain Functions", IEEE Trans. on Antennas and Propagat., Vol.39, pp.491-496, 1991.
- [8] D. I. Kaklamani, A. Marsh, N. K. Uzunoglu, "Scalability of Parallel Processing Method of Moments technique in treating electrically large electromagnetic structures", Antennas and Propagat. Society International Symp., vol.2, pp. 1024-1027, 1995.
- [9] A. F. Peterson, D. R. Wilton, R. E. Jorgenson, "Variational Nature of Galerkin and Non-Galerkin Moment Method Solutions", IEEE Transactions on Antennas and Propagat., vol. 44, no.4, pp. 500-503, 1996.
- [10] Y. Saad, Iterative Methods by Sparse Linear Systems, Second Edition, SIAM, 2003.
- [11] R. Barrett, M. Berry, T. F. Chan, J. Demmel, J. M. Donato, J. Dongarra, V. Eijkhout R. Pozo, C. Romine, H. Van der Vorst, Templates for the solution of linear systems Building Blocks for iterative methods, second edition, <http://www.siam.org/books>.
- [12] A. Kas, E. L. Yip, "Preconditioned conjugate Gradient Methods for solving Electromagnetic Problems, IEEE Trans. on Antennas and Propagat., vol. AP-35, no.2, February 1987.
- [13] W. C. Chew, J. M. Jin, C. C. Lu, E. Michielssen, J. M. Song, "Fast Solution Methods in Electromagnetics", IEEE Trans. on Antennas and Propagat., vol.45,

no.3, pp.533-543, March 1997.

- [14] C. F. Smith, A. F. Peterson, R. Mittra, "The Biconjugate Gradient Method for Electromagnetic Scattering", *IEEE Trans. on Antennas and Propagat.* vol.38, no.6, June 1990.
- [15] R. W. Freund, N. M. Nachtigal , "QMR: A quasi-minimal residual method for non-Hermitian linear systems", *Numer. Math.*, 60(1991), pp.315-339.
- [16] C. F. Wang and J. M. Jin, "Efficient Computation of Electromagnetic Fields in Arbitrarily-Shaped, Inhomogeneous Dielectric Bodies Using Transpose-Free QMR and FFT", *IEEE Trans. on Microwave Theory and Techniques*, vol.46, no.5, May 1998, pp. 553-558.
- [17] J. von Hagen and W. Wiesbeck, "Physics-Based Preconditioner for Iterative Algorithms in MoM-Problems", *IEEE Trans. on Antennas and Propagat.*, vol.50, no.9, September 2002, pp. 1315-1316.
- [18] M. D. Garcia, E. Florez, A. Suarez, L. Gonzalez, G. Montero, "New Implementation of QMR-type algorithms", *Journal on Computers and Structures*, vol. 83, issue 28-30, November 2005, pp. 2414-2422.
- [19] L. Qing-bo, Z. Ping, S. Hui-ling, "Application of the TFQMR method to the analysis of PEC target scattering problem in a lossy half space", *International Conference on Electrical and Control Engineering*, 2010, pp. 3385-3388.
- [20] J. Lee, J. Zhang, Cai-Cheng Lu, "Incomplete LU preconditioning for large scale dense complex linear systems from electromagnetic wave scattering problems," *J. of Computational Physics*, vol.185, pp.158-175, 2003.
- [21] T. Malas and L. Gürel, "Incomplete LU preconditioning with the Multilevel Fast Multipole Algorithm", vol.29, no.4, June 2007.
- [22] T. Malas, O. Ergul, L. Gurel, "Effective preconditioner for large Integral-equation problem", *IEEE Trans. on Antennas and Propagat.*, 2007 EuCAP the Second European Conference, pp.1-5.
- [23] O. Ergül, L. Gürel, "Fast and Accurate Solutions of Large-scale Scattering Problems with Parallel Multilevel Fast Multipole Algorithm", *IEEE Antennas and Propagat. Symp.* 2007, pp.3436-3439.
- [24] O. Ergül, L. Gürel, "Efficient Solution of the Electric-Field Integral Equation Using the Iterative LSQR Algorithm", vol.7, pp.36-39, 2008.
- [25] Robert L. Wagner, W. C. Chew, "A Study of Wavelets for the Solution of Electromagnetic Integral Equations", *IEEE Trans. on Antennas and Propagat.*, vol.43, pp. 802-810, 1995.
- [26] B. Z. Steinberg, Y. Leviatan, "On the Use of Wavelet Expansions in the Method of Moments, *IEEE Trans. on Antennas and Propagat.*, vol.41, pp. 610-619, 1993.

- [27] Y. Shifman, Y. Leviatan, "On the Use of Spatio-Temporal Wavelet Expansions for Transient Analysis of Wire Antennas and Scatterers", *IEEE Trans. on Antennas and Propagat.*, Vol.52, pp. 2305-2318, 2004.
- [28] F. Stenger, "Numerical Methods based on Whittaker Cardinal, or Sinc Functions", *SIAM Review*, vol. 23, no. 2, pp. 165-224, April 1981.
- [29] S. A. Johnson, M. L. Tracy, "Inverse scattering Solutions by a Sinc Basis, Multiple Source, Moment Method-Part I: Theory", *Ultrasonic Imaging*, vol. 5, no. 4, pp. 361-375, October 1983.
- [30] S. A. Johnson, M. L. Tracy, "Inverse scattering Solutions by a Sinc Basis, Multiple Source, Moment Method-Part II: Numerical Evaluations", *Ultrasonic Imaging*, vol. 5, no. 4, pp. 376-392, October 1983.
- [31] S. A. Johnson, M. L. Tracy, "Inverse scattering Solutions by a Sinc Basis, Multiple Source, Moment Method-Part III: Fast Algorithms", *Ultrasonic Imaging*, vol. 6, no. 1, pp. 103-116, January 1984.
- [32] T. Cavicchi, S. A. Johnson and W. D. O'Brien, "Application of the Sinc Basis Moment Method to the Reconstruction of Infinite Circular Cylinders", *IEEE Trans. on Ultrasonics, Ferroelectrics and Frequency Control*, vol. 35, no.1, pp. 22-33, January 1988.
- [33] F. Stenger, *Numerical Methods based on Sinc and Analytic Functions*, Springer Verlag, New York, 1993.
- [34] A. Saadatmandi, M. Razzaghi, M. Dehghan, "Sinc collocation methods for the solution of Hallen's integral equation", *J. of Electromagn. Waves and Appl.*, Vol.19, pp. 245-256, 2005.
- [35] G. F. Herrmann, "Note on Interpolational Basis Functions in the Method of Moments", *IEEE Trans. on Antennas and Propagat.*, vol.38, no.1, pp.134-137, January 1990.
- [36] E. X. Huang and A. K. Fung, "An Application of Sampling Theorem to Moment Method Simulation in Surface Scattering", *J. of Electromagnetic Waves and Appl.*, vol.20, pp.531-546, 2006.
- [37] R. A. Ross, "Radar Cross Section of Rectangular Flat Plates as a function of aspect angle", *IEEE Trans. on Antennas and Propagat.*, vol. AP-14, no.8, pp. 329-335, May 1966.
- [38] R. A. Ross, "Bistatic Scattering from A Frustum", *IEEE Trans. on Antennas and Propagat.*, pp. 103-106, January 1969.
- [39] R. A. Ross, "Backscattering from square plates illuminated with vertical polarization", *IEEE Trans. on Antennas and Propagat.*, vol.54, no.1, January 2006.

- [40] R. A. Ross, "Forward Scattering at Grazing Incidence on Flat Plates", IEEE Trans. on Antennas and Propagat., vol.56, no.2, February 2008.
- [41] L. A. Polka, C. A. Balanis, "Non-principal plane scattering from perfectly conducting , flat , rectangular plates", Antennas and Propagat. Society International Symposium, 1989, AP-S Digest, vol.3, pp.1278-1281, 1989.
- [42] L. A. Polka, C. Birtcher, C. A. Balanis, "RCS Measurements of plate geometries with theoretical verification", Antennas and Propagat. Int. Symp. 1991, AP-S Digest, vol.2, pp. 1078-1081, 1991.
- [43] Taner Oğuzer, Fadil Kuyucuoglu, 'Tabakalı ortamda bulunan şeritten saçınımın sinc tipi fonksiyonlar kullanılarak moment metot çözümü', URSI 2006.
- [44] F. Fuyucuoglu, Z. Çay, T. Oğuzer, "Scattering from the PEC Flat Strip by Using the Method of Moments with Sinc type basis functions", Computational Electromagnetics, Sixth Int. Conference, April 2006.
- [45] F. Kuyucuoglu, T. Oğuzer, İ. Avgin, 'Scattering from the flat strip geometries in the layered medium by using the sinc based Method of Moments', Progress in Electromagnetics Research Symposium, July 2008, Cambridge, USA.
- [46] Taner Oguzer, Fadil Kuyucuoglu, "Moment Methods Solution by using Sinc-type Basis Functions for the Scattering from a Finite Number of Conducting Strip Gratings", Turk J. Elec. Engin., vol.16, pp.95-109, 2008, TUBITAK.
- [47] Taner Oğuzer, Fadıl Kuyucuoğlu, İbrahim Avgın, "Electromagnetic Scattering from layered strip geometries: the method of moments study with the sinc basis", Turk J. Elec. Engin., vol.19, no.2, 2011, TUBITAK.
- [48] M. Casaletti, S. Maci, G. Vecchi, "A Complete Set of Linear-Phase Basis Functions for Scatterers with flat faces and for planar apertures", vol.59, pp. 563-573, 2011.
- [49] C. J. Reddy, M. D. Deshpande, C. R. Cockrell and F. B. Beck, "Fast RCS Computation over a Frequency Band Using Method of Moments in Conjunction with Asymptotic Waveform Evaluation Technique", IEEE Trans. on Antennas and Propagat., vol. 46, no.8, pp. 1229-1233, August 1998.
- [50] D. Yan, S. Yufa and S. Yong, "Fast Analysis of Wideband Electromagnetic Scattering from multi-objects based on Characteristic basis function Method", 8<sup>th</sup> International Symp. On Antennas, Propagation and EM Theory, ISAPE 2008.
- [51] Y. Sun, Y. Du, Y. Shao, "Fast Computation of Wideband RCS using characteristic basis function method and asymptotic wavefom evaluation technique", vol.27, no.4, pp. 453-457, 1 July 2010.
- [52] R. J. Marhefka, O. Merih Büyükdura, Wataru Ebihara, *Radar Cross Section Studies*, The Ohio State University ElectroScience Laboratory, April 1986.

- [53] B. Ozbakis, T. Oguzer, A. Kustepeli, “Three dimensional Electromagnetic Scattering from the flat plates by using sinc-type Basis Functions in MoM,” Computational Electromagnetics International Workshop, CEM 2009, Izmir.
- [54] SuperNEC, Academic Licence 2.7, [www.supernec.com](http://www.supernec.com).
- [55] Olav Breinbjerg, ‘*Equivalent Edge Current Analysis of Electromagnetic Scattering by Plane Structures*’, Electromagnetics Institute Technical University of Denmark, March 1991.
- [56] B. Ozbakis, T. Oguzer, A. Kustepeli, “Electromagnetic Scattering from arbitrary flat plates: Analysis of the problem by using Method of Moments with different sinc type basis functions”, URSI GASS International Symposium, Istanbul 2011.
- [57] L. Alatan, M. I. Aksun, K. Mahadevan and M. Tuncay Birand, “Analytical Evaluation of the MoM Matrix Elements”, IEEE Trans. on Microwave Theory and Techniques, vol.44, no.4, April 1996, pp.519-525.
- [58] W. H. Press, S. A. Teukolsky, W. T. Vetterling, B. P.Flannery, Numerical Recipes in Fortran 77: The art of Scientific Computing, Cambridge University Press, 1992.
- [59] Karl S. Kunz and R. J. Luebbers, Finite Difference Time Domain Method for Electromagnetics, CRC Press USA, 1993.
- [60] Steven C. Chapra, Raymond P. Canale, Numerical Methods for Engineers, Mc Graw Hill, 2002.
- [61] Kendall Atkinson, Weimin Han, *Elementary Numerical Analysis*, John Wiley & Sons, Inc. , USA, 2004.
- [62] Merrill Skolnik, Radar Handbook, Mc Graw Hill, USA, 1990.
- [63] M. Abramowitz, I. A. Stegun, Handbook of Mathematical Functions, USA, 1972.

# APPENDIX A

## NUMERICAL DIFFERENTIATION

### A.1. First Order Derivative Approximations

Let  $f(x)$  is continuous on I (interval),  $h$  is a step size and  $0 < h < 1$ . Taylor expansion is applied to the function such that

$$f(x+h) = f(x) + hf'(x) + \frac{h^2}{2!} f''(x) + \dots \quad (\text{A.1})$$

$$f'(x) = \frac{f(x+h) - f(x)}{h} - \underbrace{\frac{hf''(x)}{2}}_{\text{remainder term}} \dots \quad (\text{A.2})$$

If the remainder terms are not taken then the approximated value of the first order derivative can be calculated with

$$f'(x) \cong \frac{f(x+h) - f(x)}{h}, \quad O(h) \text{ is the forward difference approximation.} \quad (\text{A.3})$$

Error occurs because of removing the remainder terms such as

$$\text{error} = \left| -\frac{h}{2} f''(\zeta) \right|, \quad x < \zeta < x+h. \quad (\text{A.4})$$

Backward difference can be calculated in a similar manner with (A.3) given below

$$\begin{aligned}
f(x-h) &= f(x) - hf'(x) + \frac{h^2}{2!} f''(x) + \dots \\
f'(x) &= \frac{f(x) - f(x-h)}{h} + \underbrace{\frac{h}{2} f''(x) + \dots}_{\text{ignore it}}
\end{aligned}
\tag{A.5}$$

and

$$f'(x) \cong \frac{f(x) - f(x-h)}{h}, \text{ backward difference,} \tag{A.6}$$

$$\text{error} = \left| \frac{h}{2} f''(\zeta) \right|, \quad x-h < \zeta < x. \tag{A.7}$$

By subtracting  $f(x-h)$  from  $f(x+h)$  the below central difference approximation is obtained.

$$f'(x) \cong \frac{f(x+h) - f(x-h)}{2h}, \text{ central difference} \tag{A.8}$$

## A.2. Second Order Derivative Approximation

The second order derivatives can be calculated approximately with the below formulations

$$y''(x) \cong \frac{y(x+2h) - 2y(x+h) + y(x)}{h^2}, \text{ forward difference} \tag{A.9}$$

$$y''(x) \cong \frac{y(x-2h) - 2y(x-h) + y(x)}{h^2}, \text{ backward difference} \tag{A.10}$$

$$y''(x) \cong \frac{y(x+h) - 2y(x) + y(x-h)}{h^2}, \text{ central difference.} \tag{A.11}$$



## APPENDIX B

### SINC FUNCTION

The normalized sinc function is defined on the real line [62],  $-\infty < x < \infty$ ,

$$\text{sinc}(x) = \begin{cases} \frac{\sin(\pi x)}{\pi x}, & x \neq 0 \\ 1, & x = 0 \end{cases}. \quad (\text{B.1})$$

The analytical properties of the sinc functions:

1. Sinc functions are complete orthogonal set of functions, such as

$$\int_{-\infty}^{\infty} \text{sinc}(2Wx-n)\text{sinc}(2Wx-m)dx = \begin{cases} \frac{1}{2W}, & n = m \\ 0, & n \neq m \end{cases}. \quad (\text{B.2})$$

2. The convolution of the two sinc functions are again gives a sinc function.

$$\int_{-\infty}^{\infty} \underbrace{\text{sinc}(2Wx'-n)}_{g_1(x')} \underbrace{\text{sinc}(2W(x-x')-m)}_{g_2(x-x')} dx' = \frac{1}{2W} \underbrace{\text{sinc}(2Wx-n+m)}_{g_3(x)} \quad (\text{B.3})$$

where (B3) can also be written as

$$g_1(x) * g_2(-x) = \frac{1}{2W} g_3(x). \quad (\text{B.4})$$

3. Sinc interpolation + error

$$\int_{-\infty}^{\infty} \text{sinc}(2Wx-m) g(x) dx = \frac{1}{2W} g\left(\frac{m}{2W}\right) + \text{error} \quad (\text{B.5})$$

$$\int_{-\infty}^{\infty} \int_{-\infty}^{\infty} \text{sinc}(2W_x x - m) \text{sinc}(2W_y y - n) g(x, y) dx dy = \frac{1}{4W_x W_y} g\left(\frac{m}{2W_x}, \frac{n}{2W_y}\right) + \text{error} \quad (\text{B.6})$$

## APPENDIX C

### SUBROUTINES

#### C1. LU Decomposition

SUBROUTINE DGEFAM (A,N,IPVT,INFO)

!input

!A is the matrix with (N,N) dimension

!N dimension of the matrix

!IPVT is the pivot vector

!INFO is the integer (default 0)

INTEGER LDA,N,IPVT(N),INFO

DOUBLE COMPLEX A(N,N)

INTEGER I,J,K,KP1,L,NM1

DOUBLE COMPLEX T

IPVT(N) = 1

INFO = 0

NM1 = N-1

IF (NM1 .LT. 1) GO TO 100

DO 90 K=1,NM1

    KP1 = K+1

    L = K

    DO 10 I=KP1,N

        IF (CDABS(A(I,K)) .GT. CDABS(A(L,K))) L = I

10 CONTINUE

    IPVT(K) = L

    IF (CDABS(A(L,K)) .EQ. 0.0D0) GO TO 70

    IF (L .EQ. K) GO TO 20

    T = A(L,K)

    A(L,K) = A(K,K)

    A(K,K) = T

```

20  CONTINUE
    T = 1.0D0/A(K,K)
    DO 30 I=KP1,N
        A(I,K) = T*A(I,K)
30  CONTINUE
    DO 60 J=KP1,N
        T = A(L,J)
        IF (L .EQ. K) GO TO 40
        A(L,J) = A(K,J)
        A(K,J) = T
40  CONTINUE
    DO 50 I=KP1,N
        A(I,J) = A(I,J)-T*A(I,K)
50  CONTINUE
60  CONTINUE
    GO TO 80
70  CONTINUE
    INFO = K
80  CONTINUE
90  CONTINUE
100 CONTINUE
    IPVT(N) = N
    IF (CDABS(A(N,N)) .EQ. 0.0D0) INFO = N
    RETURN
    END subroutine dgefam

```

SUBROUTINE DGESLM (A,N,IPVT,B)

!input

!A is the LU matrix with (N,N) dimension

!N dimension of the matrix

!IPVT is the pivot vector

!B is the right hand side vector for  $Ax=B$  with dimension N

!output

!B is the solution vector

INTEGER LDA,N,IPVT(N)

```

DOUBLE COMPLEX A(N,N),B(N)
INTEGER I,K,KB,KM1,KP1,L,NM1
DOUBLE COMPLEX T
IF (N .EQ. 1) GO TO 60
NM1 = N-1
DO 30 K=1,NM1
    KP1 = K+1
    L = IPVT(K)
    T = B(L)
    IF (L .EQ. K) GO TO 10
    B(L) = B(K)
    B(K) = T
10  CONTINUE
    DO 20 I=KP1,N
        B(I) = B(I)-T*A(I,K)
20  CONTINUE
30  CONTINUE
    DO 50 KB=1,NM1
        K = N+1-KB
        KM1 = K-1
        B(K) = B(K)/A(K,K)
        T = -B(K)
        DO 40 I=1,KM1
            B(I) = B(I)+T*A(I,K)
40  CONTINUE
50  CONTINUE
60  CONTINUE
    B(1) = B(1)/A(1,1)
    RETURN
END

```

## C2. Matrix Multiplication

```
SUBROUTINE MMUL (NA,NB,NC,L,M,N,A,B,C)
! *****PARAMETERS:
integer NB,N,NA,NC,L,M
DOUBLE complex A(NA,N),B(NB,L),C(NC,L)
! *****LOCAL VARIABLES:
INTEGER I,J,K
! *****SUBROUTINES CALLED:
! None
! *****PURPOSE:
!THIS SUBROUTINE COMPUTES THE MATRIX PRODUCT A*B AND STORES
THE
!RESULT IN THE ARRAY C. A IS M X N, B IS N X L, AND C IS
! M X L. THE ARRAY C MUST BE DISTINCT FROM BOTH A AND B.
! *****PARAMETER DESCRIPTION:
! ON INPUT:
! NA ROW DIMENSION OF THE ARRAY CONTAINING A AS DECLARED
! IN THE CALLING PROGRAM DIMENSION STATEMENT;
!
! NB ROW DIMENSION OF THE ARRAY CONTAINING B AS DECLARED
! IN THE CALLING PROGRAM DIMENSION STATEMENT;
!
! NC ROW DIMENSION OF THE ARRAY CONTAINING C AS DECLARED
! IN THE CALLING PROGRAM DIMENSION STATEMENT;
!
! L NUMBER OF COLUMNS OF THE MATRICES B AND C;
! M NUMBER OF ROWS OF THE MATRICES A AND C;
!
! N NUMBER OF COLUMNS OF THE MATRIX A AND NUMBER OF
ROWS
! OF THE MATRIX B;
!
```

```

!   A   AN M X N MATRIX;
!
!   B   AN N X L MATRIX.
!
!   ON OUTPUT:
!
!   C   AN M X L ARRAY CONTAINING A*B.
!
      DO 40 J=1,L
        DO 10 I=1,M
          C(I,J)=0.0D0
10      CONTINUE
        DO 30 K=1,N
          DO 20 I=1,M
            C(I,J)=C(I,J)+A(I,K)*B(K,J)
20      CONTINUE
30      CONTINUE
40      CONTINUE
      RETURN
!
!   LAST CARD OF MMUL
!
      END

```

### **C3. Inverse of the Matrix**

SUBROUTINE GAUJOR (N,A)

! GAUJOR COMPUTES THE INVERS OF THE MATRIX A(N,N) WITH THE HELP  
OF

! GAUSS-JORDAN-ALGORITHM, ....!

! COMMON /MATRIX/ ....

INTEGER IP(81)

```

real ZMAX,Z
COMPLEX A(N,N),HV(80),HR
DO 10 I=1,N
10 IP(I)=I
DO 100 J=1,N
ZMAX=CABS(A(J,J))
IR=J
IF (J.EQ.N) GOTO 200
JJ=J+1
DO 20 I=JJ,N
Z=CABS(A(I,J))
IF (Z.LE.ZMAX) GOTO 20
ZMAX=Z
IR=I
20 CONTINUE
! NOTATION FOR SINGULAR MATRIX
200 IF (ZMAX.LE.1.E-37) THEN
PRINT*,'ZMAX= ',ZMAX
PRINT*,'NOTATION ON MATRIX SINGULARITY%'
ENDIF
IF (ZMAX.LE.1.E-37) STOP 9999
IF (IR.LE.J) GOTO 40
DO 30 K=1,N
HR=A(J,K)
A(J,K)=A(IR,K)
30 A(IR,K)=HR
IHI=IP(J)
IP(J)=IP(IR)
IP(IR)=IHI
40 HR=CMPLX(1.E0,0.E0)/A(J,J)
DO 50 I=1,N
50 A(I,J)=HR*A(I,J)
A(J,J)=HR
DO 70 K=1,N

```

```

      IF (K.EQ.J) GOTO 70
      DO 60 I=1,N
      IF (I.EQ.J) GOTO 60
      A(I,K)=A(I,K)-A(I,J)*A(J,K)
60 CONTINUE
      A(J,K)=-HR*A(J,K)
70 CONTINUE
100 CONTINUE
      ! COLUMN PERMUTATION
      DO 150 I=1,N
      DO 110 K=1,N
110 HV(IP(K))=A(I,K)
      DO 120 K=1,N
      A(I,K)=HV(K)
120 CONTINUE
150 CONTINUE
999 CONTINUE
      RETURN
      END

```

#### **C4.One Dimensional Integration**

```

SUBROUTINE SIMPSONBIR(CFF,XA,XB,p,CVAL)
IMPLICIT NONE
EXTERNAL CFF
complex SUMN,SUMY,PART1,PART2
complex CFF
complex CVAL
real XA,XB,NX,X1,X2,H
INTEGER IJ
integer nxx
integer p
NX=400

```



```

nxx=400;
H=(XB-XA)/(2*NX);
SUMN=(0,0); SUMY=(0,0);
  DO IJ=1,nxx-1
    X1=XA+(2*IJ)*H;
    SUMN=SUMN+CFF(X1,p);
  END DO
PART1=(2*H/3)*SUMN;
  DO IJ=1,nxx
    X2=XA+(2*IJ-1)*H;
    SUMY=SUMY+CFF(X2,p);
  END DO
PART2=(4*H/3)*SUMY;
CVAL=PART1+PART2+((H/3)*(CFF(XA,p)+CFF(XB,p)))
RETURN
END

```

## C5. Two Dimensional Integration

```

SUBROUTINE SIMPSONIKI(CE, YA, YB, XA, XB, uint,vint,CTV)
IMPLICIT NONE
external CE
  DOUBLE COMPLEX CE
  DOUBLE COMPLEX CTV
  DOUBLE COMPLEX
SUMNP,SUMYP,PART1N,PART2N,CVAL1,CVAL2,RES1,RES2
DOUBLE PRECISION YA,YB,NY,YY1,YY2,XA,XB,H,uint,vint
INTEGER IJ
integer nyy
nyy=150;
NY=150.d 0
H=(YB-YA)/(2*NY);
SUMNP=0; SUMYP=0;

```

```

DO IJ=1,nyy-1
  YY1=YA+(2*IJ)*H;
CALL SIMPSONBIR(CE,YY1,XA,XB,uint,vint,CVAL1)
  SUMNP=SUMNP+CVAL1;
END DO
PART1N=((2*H)/3)*SUMNP;
DO IJ=1,nyy
  YY2=YA+(2*IJ-1)*H;
CALL SIMPSONBIR(CE,YY2,XA,XB,uint,vint,CVAL2)
  SUMYP=SUMYP+CVAL2;
END DO
PART2N=(4*H/3)*SUMYP;
CALL SIMPSONBIR(CE,YA,XA,XB,uint,vint,RES1)
CALL SIMPSONBIR(CE,YB,XA,XB,uint,vint,RES2)
CTV=PART1N+PART2N+((H/3)*(RES1+RES2));
RETURN
END

SUBROUTINE SIMPSONBIR(CF,Y,XA,XB,uint,vint,CVAL)
IMPLICIT NONE
EXTERNAL CF
DOUBLE COMPLEX SUMN,SUMY,PART1,PART2
DOUBLE COMPLEX CF
DOUBLE COMPLEX CVAL
DOUBLE PRECISION XA,XB,Y,NX,X1,X2,H,uint,vint
INTEGER IJ
integer nxx
NX=150.D0
nxx=150;
H=(XB-XA)/(2*NX);
SUMN=0; SUMY=0;
  DO IJ=1,nxx-1
    X1=XA+(2*IJ)*H;
    SUMN=SUMN+CF(X1,Y,uint,vint);
  END DO

```

```
PART1=(2*H/3)*SUMN;  
DO IJ=1,nxx  
X2=XA+(2*IJ-1)*H;  
SUMY=SUMY+CF(X2,Y,uint,vint);  
END DO  
PART2=(4*H/3)*SUMY;  
CVAL=PART1+PART2+((H/3)*(CF(XA,Y,uint,vint)+CF(XB,Y,uint,vint)))  
RETURN  
END
```

## VITA

Başak Özbakiş was born on 03.09.1978 in Karabük. She has undergraduated from Electrical-Electronics Engineering Department of Dokuz Eylul University on July 2001. Then, she had a Master Degree about Electromagnetic Theory with Fractal Antennas from Electrical-Electronics Engineering of Izmir Institute of Technology on July 2004, while she has worked as a Research Asistant in the same department. She has worked as a Research Assistant for 10 years in this department. She studied for a Doctor degree about Computational Electromagnetics.